ENGINEERING TUMOR-TARGETED POLY(AMIDOAMINE) (PAMAM) DENDRIMERS FOR IMPROVED PENETRATION AND CELLULAR DELIVERY OF SHORT-INTERFERING RNA (siRNA) THROUGH SOLID TUMORS

by

CAROLYN LEIGH WAITE

A Dissertation submitted to the

Graduate School-New Brunswick

Rutgers, The State University of New Jersey

in partial fulfillment of the requirements

for the degree of

Doctor of Philosophy

Graduate Program in Chemical and Biochemical Engineering

written under the direction of

Charles M. Roth

and approved by

_____

_____

_____

_____

_____

New Brunswick, New Jersey

October, 2011

ABSTRACT OF THE DISSERTATION

Engineering tumor-targeted poly(amidoamine) (PAMAM) dendrimers for improved penetration and cellular delivery of short-interfering RNA (siRNA) through solid tumors

By CAROLYN LEIGH WAITE

Dissertation Director:
Charles M. Roth

Cancer remains the second leading cause of death in the United States, despite significant advances in anticancer research. The standard-of-care for the treatment of cancer includes surgery in conjunction with traditional chemotherapy drugs or radiation therapy. However, the inherent cytotoxicity of conventional chemotherapeutics often causes adverse side effects in patients. Nanoscale materials have found utility for drug delivery to tumors as they accumulate in the tumor vasculature , reducing the necessary drug dose to patients. They have also proven useful to deliver unconventional drugs, including short-interfering RNA (siRNA), which is being explored to silence oncogenes. However, the current lack of safe, efficient siRNA delivery systems limits its widespread clinical use.

The objective of this dissertation was to study the ability of poly(amidoamine) (PAMAM) dendrimers to facilitate the delivery of siRNA to malignant glioma on the cellular and tumor tissue levels. The intracellular delivery aspects of PAMAM-mediated siRNA delivery to malignant glioma cells were explored by employing partial surface amine acetylation of PAMAM dendrimers to reduce their net positive charge This work demonstrated the importance of endosomal buffering and the advantages of charge reduction on siRNA delivery.

The ability of PAMAM dendrimers to mediate tumor-targeted siRNA delivery to tumor tissue was also studied. Dendrimers were modified to display various numbers of RGD peptides, and the number of peptides present influenced the distribution of siRNA cargo throughout a three-dimensional tumor model of malignant glioma. A biophysical analysis was performed to elucidate the transport mechanisms governing the tumoral penetration of these bioconjugates, and cellular binding affinity was found to influence significantly the transport of the bioconjugate materials through solid tumors.

The results from this dissertation provide insights into the mechanisms governing siRNA delivery to cancer on both the cellular and tumor tissue levels. Design guidelines for tumor-targeted nanoscale siRNA delivery vectors were derived, and a methodology was developed to understand the mechanisms governing the penetration and transport of siRNA drugs throughout solid tumors. This work will help other researchers to design more effective drug delivery systems for anticancer applications, and it may impact the effect of siRNA and nanoscale materials on human disease.

ACKNOWLEDGEMENT

I have had a wonderful experience during my tenure here at Rutgers, one which would not have been the same without all of the people who I was so fortunate to interact with during the course of my studies.

First I must acknowledge my advisor, Dr. Charles Roth, for his guidance, support, and patience over the years. Charlie has given me the freedom to explore my research interests for my thesis work, and has allowed me to pursue other research opportunities outside of Rutgers, all of which have helped me develop into an independent researcher. Further, he has not left a single email unanswered or a single word unread of any manuscript, abstract, or presentation that I have written.

Secondly, I am grateful for the colleagues of mine who have always been patient teachers and were willing to lend an ear to discuss research. I thank Dr. Sumati Sundaram for holding my hand through my first baby steps as a graduate student—I admire her patience and work ethic. I thank Lavanya Peddada who has been my "partner in crime" throughout graduate school. Lavanya has been my peer in research from the beginning of my time at Rutgers, and has since become one of my closest friends. I was fortunate to have so many other colleagues in the Roth lab who not only made working in the lab more enjoyable, but who also patiently listened to countless practice talks and offered research guidance and advice. I thank Dominik Naczynski, Dr. Salah Hamed, Aina Andrianarijaona, and Dr. Hong Yang. I also thank the undergraduate students who have worked with me in the lab, especially Paul Gianella, for their dedication and enthusiasm towards our research. I thank Dr. Sarah Sparks for her help with polymer chemistry.

I was fortunate to have the guidance of many mentors throughout my time here from whom I learned, first hand, about the focus and dedication that it takes to be a successful researcher. I thank Dr. Vidya Iyer, Dr. Nadine Utz, Dr. Koki Lilova, and Dr. Brenda Remy for their scientific and career mentorship. I thank the faculty members at Rutgers who have guided me through my research including the members of my thesis committee, particularly Dr. Kathryn Uhrich and Dr. Prabhas Moghe, for their mentorship.

I am grateful for the many friends I have made at Rutgers who have made my time here memorable and enjoyable. There is a special bond that I have with my graduate school friends since we truly can only understand each other. I thank all of my friends at Rutgers, especially Daniel Duffield for our daily coffee chats, Matthew Metzger, and Dr. Michael Wininger.

DEDICATION

This work is dedicated to my family who has been a constant source of love and support throughout my life. I thank my dad, Timothy Waite, who encouraged me to study chemical engineering in the first place. I thank my mom, Cheryl Waite, for her unending support, and for listening to my daily trials and tribulations for the past 5 years. I thank my brother, LCpl David Waite, USMC, for making me a very proud sister.

Finally, I thank my newly-wed husband, Dr. Justin Federici. In addition to his constant love and support on a personal level, Justin, having completed his PhD just two years ago, has been able to support me as a fellow scientist. Justin has endured the first practice run of every presentation that I have given and has read through countless abstracts, manuscripts, and lines of computer code. Justin is a truly gifted engineer whose insights have helped me to improve my own work. His dedication to our long-distance relationship has made the last several years of traveling between New Jersey and Delaware or Washington DC seem effortless, and I am thrilled that we will now begin a new chapter of our lives together. Sweetheart, this is for you.

PRIOR PUBLICATIONS

Several sections of this dissertation have been published elsewhere, or are pending external publication. These publications are acknowledged below:

- Several sections of Chapter 1, the introduction, are being submitted to *Critical Reviews in Biomedical Engineering* for publication as part of a review article entitled, "Nanoscale drug delivery systems for enhanced drug penetration into solid tumors: current progress and opportunities." in summer, 2011.
- Chapter 2 has been published in its entirety and has the following citation: Waite, C.L., Sparks, S.M., Uhrich, K.E. & Roth, C.M. Acetylation of PAMAM dendrimers for cellular delivery of siRNA. *BMC Biotechnol* **9**, 38 (2009).
- Chapter 3 has been published in its entirety and has the following citation : Waite, C.L. & Roth, C.M. PAMAM-RGD Conjugates Enhance siRNA Delivery Through a Multicellular Spheroid Model of Malignant Glioma. *Bioconjugate Chemistry* **20**, 1908-1916 (2009).
- Chapter 4 has been submitted for publication in its entirety to *Biotechnology and Bioengineering* in March, 2011.
- Appendix 3 has been accepted for publication in *Macromolecular Bioscience* in May, 2011.

TABLE OF CONTENTS

ABSTRACT OF THE DISSERTATION ii

ACKNOWLEDGEMENT iv

DEDICATION vi

PRIOR PUBLICATIONS vii

LIST OF TABLES xii

LIST OF FIGURES xiii

CHAPTER 1 xiii

INTRODUCTION 1

1.1. RNA-Interference for the Treatment of Cancer 1

1.2. Synthetic polymers for the cellular delivery of nucleic acids 3

1.3. Tumor-targeted delivery of drugs and nucleic acids 5

1.3.1 Active tumor-targeting by RGD peptides 6

1.3.2. Multivalency in tumor-targeted drug delivery 7

1.4. Delivery of drugs and genes throughout solid tumor tissue 9

1.4.1. Tumor properties hindering nanoscale drug transport 10

1.4.1.1. Abnormal Vasculature 10

1.4.1.3. Stiff Extracellular Matrix (ECM) 12

1.4.2. *In vitro* methods to study the tumor distribution of drugs 13

1.4.2.1. In Vitro three-dimensional (3D) tumor models 13

1.4.2.2. Theoretical Modeling Approaches 16

1.4.3. Methods to improve the tumor distribution of drug and siRNA delivery molecules 17

1.5. Dissertation overview and approach 19

CHAPTER 2 21

ACETYLATION OF PAMAM DENDRIMERS FOR CELLULAR DELIVERY OF SIRNA 21

2.1. Background 22

2.2 METHODS 24

2.2.1 Materials 24

2.2.2 Acetylation of PAMAM dendrimers....25
2.2.3 PicoGreen assay for siRNA/PAMAM complexation....26
2.2.4 Dynamic light scattering and zeta potential....26
2.2.5 Heparin competition assay....27
2.2.6 Cell culture....27
2.2.7 MTS cytotoxicity assay....27
2.2.8 siRNA delivery assay....28
2.2.9 Flow cytometry....29
2.2.10 Confocal microscopy....29
2.2.11 pH titrations....29
2.2.12 Statistics....30
2.3 RESULTS....30
2.3.1 Partial acetylation of PAMAM dendrimers....30
2.3.2 PicoGreen dye exclusion....31
2.3.3 Complex size and zeta potential....32
2.3.4 Heparin induced polyplex dissociation....33
2.3.5 Cytotoxicity of acetylated dendrimers....34
2.3.6 siRNA induced silencing of GFP in U87-d1EGFP cells....35
2.3.7 Confocal imaging....37
2.3.8 Titration of acetylated dendrimers....38
2.4 DISCUSSION....39
CHAPTER 3....43
PAMAM-RGD CONJUGATES ENHANCE SIRNA DELIVERY THROUGH A MULTICELLULAR SPHEROID MODEL OF MALIGNANT GLIOMA....43
3.1 INTRODUCTION....44
3.2 EXPERIMENTAL PROCEDURES....45
3.2.1 Materials.....45
3.2.2 Conjugation of PAMAM dendrimers with RGD peptides.....46

3.2.3 UV spectrophotometry of PAMAM-RGD conjugates. 47
3.2.4 MALDI-TOF Mass Spectrometry. 48
3.2.5 PicoGreen assay for PAMAM/siRNA complexation. 48
3.2.6 Dynamic light scattering. 49
3.2.7 Cell culture. 49
3.2.8 Multicellular spheroid formation. 49
3.2.9 SiRNA delivery assay. 50
3.2.10 Flow cytometry. 51
3.2.11 Competitive cell adhesion assay. 52
3.2.12 Confocal microscopy of multicellular spheroids. 53
3.2.13 Image analysis of multicellular spheroid fluorescence. 53
3.2.14 Statistics. 53
3.3 RESULTS 54
3.3.1 Reaction and characterization of PAMAM-RGD conjugates. 54
3.3.2 Characterization of dendrimer/siRNA complexes. 56
3.3.3 siRNA delivery and GFP silencing in U87 cells. 58
3.3.4 Competitive binding cell adhesion assay. 60
3.3.5 siRNA delivery through multicellular glioma spheroids. 62
3.4 DISCUSSION 65
CHAPTER 4 69
BINDING AND TRANSPORT OF PAMAM-RGD IN A TUMOR SPHEROID MODEL: THE EFFECT OF RGD TARGETING LIGAND DENSITY 69
4.1 INTRODUCTION 70
4.2 MATERIALS AND METHODS 72
4.2.1 Materials. 72
4.2.2 Mathematical Model of Tumor Transport. 72
4.2.3 Cell Culture and Spheroid Formation. 74
4.2.4 Surface Plasmon Resonance Spectroscopy. 74

4.2.5 Fluorescent Labeling of PAMAM and PAMAM-RGD Conjugates. 76
4.2.6 Cellular Internalization Kinetic Measurements and Rate Constant Determination. 76
4.2.7 Statistics. 78
4.2.8 Model Assumptions and Limitations. 78
4.3 RESULTS 79
4.3.1 Binding affinity and kinetic measurements. 79
4.3.2 Cellular Internalization Dynamics. 82
4.3.3 Mathematical Tumor Spheroid Transport Model Results. 84
4.4 DISCUSSION 87
CHAPTER 5 92
DISSERTATION CONCLUSIONS AND FUTURE DIRECTIONS 92
5.1 Dissertation Summary 92
5.2 Future Directions 93
5.3 Overall Dissertation Conclusions 96
REFERENCES 99
APPENDIX 108
CURRICULUM VITAE 140

LIST OF TABLES

Table 2.1. Extent of primary amine acetylation as determined by ^{1}H NMR spectroscopy. 31

Table 2.2. Particle diameter and zeta potential of dendrimer/siRNA complexes 33

Table 3.1. Particle diameter of dendrimer/siRNA complexes 58

Table 4.1. Kinetic binding and internalization rate constants for PAMAM-RGD 83

LIST OF FIGURES

Figure 1.1. RNAi mechanism…… ……...3

Figure 1.2. Polycations for nucleic acid delivery…….5

Figure 1.3. Micrographs of normal and tumor vasculature……11

Figure 2.1. Acetylation of PAMAM dendrimers……30

Figure 2.2. Effect of amine acetylation on siRNA complexation……...32

Figure 2.3. Effect of amine acetylation on polyplex dissociation by heparin competition……34

Figure 2.4. Cytotoxicity of dendrimer/siRNA complexes and of acetylated dendrimers…….35

Figure 2.5. SiRNA-induced GFP silencing and intracellular Cy3-siRNA levels of AcPAMAM……..37

Figure 2.6. Confocal microscopy images of Cy-5 labeled oligonucleotides delivered to U-87-d1EGFP cells by AcPAMAM……38

Figure 2.7. pH titrations…….39

Figure 3.1 Crosslinking scheme for PAMAM-RGD……..55

Figure 3.2 UV characterization of PAMAM-RGDs……..55

Figure 3.3 RGD-PAMAM/siRNA complexation……..57

Figure 3.4. Cellular delivery of siRNA by RGD-PAMAM……60

Figure 3.5 Competitive binding curves for U87 cells binding to fibrinogen coated plates in the presence of RGD-containing antagonists……...62

Figure 3.6. Confocal images of U87 spheroids after treatment with dendrimer/siRNA complexes……..63

Figure 3.7. Time-Course confocal images of U87 GFP spheroids treated with dendrimer/Cy5-ODN complexes……...64

Figure 4.1. Transport mechanisms governing nanoparticle penetration through solid tumors…….....71

Figure 4.2. Representative SPR sensorgrams of binding interactions between monovalent cyclic RGD peptide and multivalent PAMAM-RGD conjugates with immobilized human integrin protein……..…80

Figure 4.3. Dissociation constants (KD) and kinetic rate constants (ka and kd) for PAMAM-RGD.....….82

Figure 4.4. Polymer concentration detected within U87 cells after constant polymer exposure for up to 48 hours, and corresponding model fits for cell internalization……..83

Figure 4.5 Model-predicted concentration profiles of PAMAM-RGD polymers as a function of distance from the spheroid center and time……..85

Figure 4.6 Model-predicted concentration profiles of PAMAM-RGD polymers as a function of time in the spheroid center……86

Figure 4.7 Comparison of time-dependent concentration profiles of PAMAM-RGD conjugates predicted in the theoretical diffusion model and observed experimentally in U87 tumor spheroids…….87

CHAPTER 1

INTRODUCTION

1.1. RNA-Interference for the Treatment of Cancer

Cancer is a disease caused by complex cellular genetic mutations resulting in malignant tumors. Despite years of research leading to the development of numerous successful anticancer therapies, cancer prevails as the second leading cause of death in the United States resulting in an estimated 565,650 disease-related deaths in 2008 [1]. There exists an unmet need for the development of novel, effective anticancer therapies to combat aggressive, lethal cancers. Since cancer is caused by alterations in oncogenes or tumor-suppressor genes [2], successful therapies should utilize knowledge of the genetic mutations involved in the development of cancer. Malignancies arise from several genetic mutations that occur in a multistep process resulting in tumors with a grossly abnormal, aggressive phenotype [3]. These genetic alterations might produce oncogenes that confer an enhanced cell growth or survival advantage or they might prevent the expression of tumor-suppressor genes that would normally prevent excessive cell growth or survival in healthy cells [2, 3]. Such genetic mutations produce malignant cells that exhibit the aberrant phenotypes described as the "hallmarks of cancer", which include self-sufficiency in growth signals, insensitivity to anti-growth signals, tumor invasion and metastasis, limitless replicative potential, sustained angiogenesis, and evasion of apoptosis [3].

As the identities of genes and proteins involved in malignancy become increasingly identified and characterized, one successful strategy has been to develop therapeutics targeted against specific oncogenes or their encoded proteins. These

therapies have traditionally been monoclonal antibodies or small molecules that interact with oncogenic proteins.

More recently, attention has been given to gene therapy techniques for the treatment of cancer. Gene therapy involves the introduction of exogenous genetic information into cells that can interfere with their gene expression by either introducing a new gene, or by silencing the expression of an existing gene. Research has led to the initiation of several clinical trials using gene therapy strategies, of which 65% are for the treatment of cancer in 2008 [4]. One promising strategy for the use of gene therapy for cancer treatment is to use either antisense oligonucleotides (AS ODNs) or short interfering RNAs (siRNAs) to silence the expression of oncogenes in malignant tumors.

The use of siRNAs to silence gene expression occurs by a mechanism known as RNA interference (RNAi). RNAi is a naturally occurring mechanism used by eukaryotic cells to regulate gene expression[5]. In RNAi, short double-stranded RNA molecules known as siRNAs are incorporated into a protein complex called the RNA-induced silencing complex (RISC) that is associated with a target messenger RNA (mRNA). The siRNA sequence binds to the target mRNA in a sequence specific manner resulting in target mRNA degradation and subsequent gene silencing (Figure 1.1). This powerful, endogenous mechanism can be exploited by engineering synthetic siRNA sequences and delivering them to cells to elicit a desired gene silencing response.

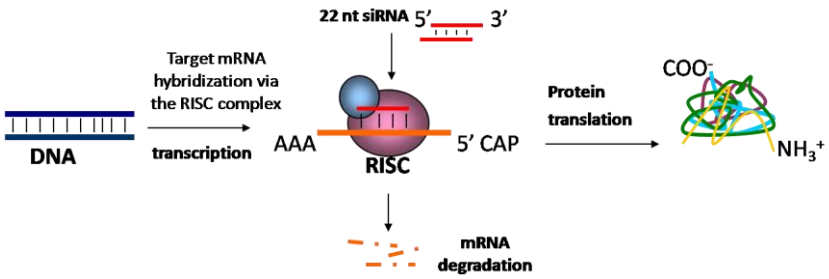

Figure 1.1. RNAi mechanism. siRNA molecules prevent protein translation by hybridizing to their target mRNA causing RNA degradation.

While RNAi is a promising strategy to attain gene silencing, several limitations prevent its widespread clinical development for the treatment of cancer including off-target gene silencing effects by siRNAs, stimulation of immune responses, and the lack of safe, effective siRNA delivery systems [5, 6]. In particular, significant research is ongoing toward the development of nucleic acid delivery systems designed to overcome several barriers to cellular delivery of RNA or DNA molecules including successful cellular entry and escape of the destructive endosomal/lysosomal pathway[7] . While viruses possess an extraordinary natural ability to deliver nucleic acids to cells, undesirable immune responses induced by viruses and their tendency to integrate at oncogenic sites within the genome hinder their widespread use in medicine. As a result, the development of non-viral delivery systems for nucleic acids is critical for gene therapy to become a reality.

1.2. Synthetic polymers for the cellular delivery of nucleic acids

A variety of molecules have been widely studied as vectors for nucleic acid (NA) delivery including liposomes [8], peptides [9], and cationic polymers [10, 11]. Delivery vectors must possess several properties to successfully deliver nucleic acids to cells including a cationic charge to promote electrostatic complexation with anionic NAs, an ability to

escape acidic endosomes either by disruption of the endosomal membrane or by pH buffering, and the presence of chemical functional groups to facilitate the conjugation of biological targeting ligands[12]. Cationic polymers can be windowed with pH sensitivity and/or functionalized with bioactive ligands and are thus particularly attractive molecules for NA delivery and have met with significant success in the literature for a diverse array of applications.

Cationic polyamines including polyethyleneimine (PEI)[13], poly-L-lysine, and poly(amidoamine) (PAMAM)[14, 15] have been widely studied for the delivery of NA molecules, including siRNA[16] (Figure 1.2). The high densities of cationic amine groups present on these polymers facilitate the efficient complexation and delivery of Nas into cells[7]. When amines with multiple pKa values including some in the pH range of 5 to 7 are present, they can assist with vector escape from acidic endosomal vesicles within cells by the "Proton Sponge Effect"[17]. Further, the primary amino groups can be chemically modified to alter and impart favorable properties onto these polymers for efficient NA delivery. For example, amine groups can be neutralized to reduce the amine-induced cytotoxicity of the materials by the addition of acetyl caps or other modifications[18-20]. Chains of poly(ethylene glycol) (PEG) can be attached to the polymer surface (also known as PEGylation) to reduce their inherent cytotoxicity and to promote stability of these materials in the bloodstream[21]. Further, the addition of biological targeting ligands can linked through primary amine groups to facilitate the tumor-targeted delivery of drug or NA cargo for anticancer applications[22].

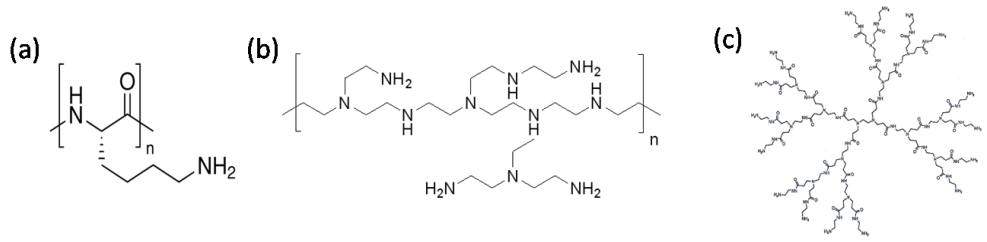

Figure 1.2. Polycations for nucleic acid delivery include (a) poly-L-lysine, (b) branched polyethylenimine (PEI), (c) Polyamidoamine (PAMAM) dendrimers.

Another class of materials that has found utility for NA delivery applications is represented by PEGylated polymeric micelles. Differing from the branched polyamines like PEI, polymeric micelles are amphiphilic molecules comprising of a hydrophobic polymer grafted to a hydrophilic PEG chain to impart their amphiphilic nature. Polymeric micelles self-assemble in aqueous solution to form PEG-shielded micelles with a hydrophobic corona. PEGylated micelles have been widely used for a variety of drug delivery applications[23], and the addition of cationic amine groups in the micelle core has rendered these constructs useful for NA delivery applications[24].

1.3. Tumor-targeted delivery of drugs and nucleic acids

Targeted delivery of therapeutic agents is of particular importance for cancer applications since it is important to deliver cytotoxic chemotherapy drugs or nucleic acids to malignant tumors and prevent their delivery to healthy cells. To this end, there are two mechanisms of tumor targeting: passive and active. Passive tumor targeting takes advantage of the enhanced permeation and retention (EPR) effect found in malignant tumors.[25] Tumors are known to have abnormal vascular linings with poorly aligned cells resulting in excessive vasculature leakage and large, accessible capillaries. As a result, nanosized polymeric macromolecules have been shown to selectively accumulate into

tumors by permeating into these pores. Furthermore, due to poor lymphatic drainage in tumors, the polymeric particles are retained within tumors for extended periods of time.

In addition to taking advantage of the inherent EPR effect found in tumors, polymeric particles are also useful for active tumor targeting. In contrast to passive targeting, active targeting employs the use of a chemical targeting ligand such as an antibody or peptide to bind to tumor-specific cell surface receptors. Some commonly used targeting ligands for cancer therapeutics include folic acid to target folate receptors that are overexpressed on various epithelial cancer cells[26], ransferring to facilitate drug transport across the blood-brain-barrier[27], and RGD peptides to facilitate integrin-mediated uptake of particles[28, 29]. In fact, a ransferring targeted, cyclodextrin based siRNA delivery system is currently in clinical trials for the treatment of cancer[30]. Similarly, integrin-targeting of therapeutic agents holds significant promise as an anticancer therapy due to the role of integrin receptors in tumor cell adhesion, growth, and angiogenesis.

1.3.1 Active tumor-targeting by RGD peptides

Integrin proteins are a family of heterodimeric cell-surface receptors with a large, extracellular domain containing one α and one β subunit. Expressed on epithelial cells, integrins play an important role in mediating cell adhesion to various extracellular matrix (ECM) proteins and also in mediating cell-cell adhesion. Several integrins are known to be grossly over-expressed on the surface of some cancer cells, where they promote tumorigenesis by potentiating tumor metastasis by facilitating cell invasion of the ECM [28,31] and by promoting tumor angiogenesis[32]. Specifically, the $\alpha_v\beta_3$ integrin is particularly known for its role in cancer progression and is overexpressed frequently in melanomas,

glioblastoma, ovarian, breast, and prostate cancers[28]. Integrin $\alpha_v\beta_3$ is a receptor for many ECM proteins, including fibronectin, vitronectin, fibrinogen, and thrombospondin that contain the tripeptide sequence Arginine-Glycine-Aspartic acid (RGD). One promising anticancer strategy is to interfere with this important integrin-ECM interaction to prevent angiogenesis of tumors and to promote cell death.

Several integrin antagonists have been developed, including small molecules, antibodies, and peptides that have shown significant success *in vitro* and *in vivo* to prevent cancer-related angiogenesis of tumor cells[28]. In particular, cyclic RGD-containing peptide sequences are the most widely studied integrin antagonists for cancer. Cyclic RGD peptides have a binding affinity to $\alpha_v\beta_3$ integrins an order of magnitude higher than their linear counterparts[33, 34]. Several studies have reported that cyclic RGD peptides induce apoptosis in malignant glioma cell lines and can detach glioma cells from their extracellular matrix protein ligands[35-37]. Further, *in vivo* studies using murine models have demonstrated that administration of RGD peptides increased survival of mice compared to those without any treatment[37]. Such promising preclinical studies led to Phase I and II clinical trials using Cilengitide, a cyclic RGD peptide drug, to treat patients with aggressive malignant glioma[38-40]. While efficacy trials are still ongoing, preliminary results indicate that Cilengitide is well-tolerated in patients, so it might hold significant promise as a treatment for advanced glioblastoma, specifically when used in combination with another standard of care such as chemotherapy or radiation therapy.

1.3.2. Multivalency in tumor-targeted drug delivery

In addition to selecting an appropriate tumor-targeting ligand for a drug delivery application, designing a delivery system that can display these ligands in a multivalent

array is an effective way to improve its tumor-targeting efficiency due to multivalent interactions with tumor cells. Multivalent binding, or the simultaneous binding of multiple ligands from one entity to multiple receptors on another, is an established mechanism that accounts for the strong binding interactions observed in many biological systems. Some well-known examples of multivalent binding in biology are the binding of oxygen to hemoglobin and the multivalent interactions between viruses and their host cells. Multivalent binding confers an energetically favorable binding advantage over monovalent interactions, resulting in a higher net binding affinity for ligands displayed in a multivalent array[41]. Researchers can take advantage of multivalent interactions in the design of drug delivery systems by incorporating multiple copies of targeting ligands from a molecular structure to promote multivalent binding to target cells. Multivalency has been built into various anticancer drug delivery systems including those targeting the folate receptor using multiple copies of folic acid[26, 42] as well as integrin targeting with multiple copies of RGD peptides. It is important to carefully engineer multivalency into drug delivery systems, as the optimal number of ligands presented from a nanoparticle scaffold is context-dependent. Due to potential steric interference between closely-spaced targeting ligands, it is important to optimize the presentation of multivalent ligands to promote favorable multivalent interactions between drug delivery systems and target cells.

Specifically, multivalent display of RGD peptides is known to have favorable tumor-targeting properties due to the promotion of integrin clustering[43], and has been widely used in the design of anticancer drug delivery vehicles. Multimeric RGD peptides have demonstrated improved tumor cell binding affinity and uptake compared to their

monomeric counterparts[44-47]. Multiple copies of RGD peptides have also been grafted onto nanoscale materials to facilitate the delivery of drugs or imaging agents into malignant tumors, imparting enhanced drug delivery to malignant tumor cells[48-51]. Thus, the use of multivalent RGD peptides represents a promising approach to designing effective anticancer therapies.

1.4. Delivery of drugs and genes throughout solid tumor tissue

Upon targeting a therapy to a solid tumor using passive or active tumor targeting techniques, it is necessary to facilitate penetration and subsequent tissue distribution of the drug to all regions of the malignant tumor. Limited penetration and poor spatial distribution of drugs throughout solid tumors represent significant barriers to their anticancer efficacy. Several conventional small-molecule chemotherapeutics including doxorubicin[52, 53], paclitaxel[54, 55], and other clinically relevant compounds[56] are known to exhibit poor distribution throughout solid tumors. These drugs remain localized to regions immediately surrounding blood vessels, leaving large regions of the tumor untouched by the therapy. Their poor tumor distribution may significantly impair their efficacy, possibly resulting in disease recurrence and the administration of high drug doses causing adverse effects in cancer patients. Improving the distribution of drugs in solid tumors is thought to improve their therapeutic index for the treatment of human disease[57].

With the increasing application of nanoscale materials for cancer drug delivery and imaging purposes, the importance of drug tumor penetration becomes more pronounced. As nanoscale materials are orders of magnitude larger than conventional chemotherapeutic compounds, their transport and diffusion through tumor tissue is even

more limited. On the other hand, nanomedicines can be engineered with functionalities to mediate more effective transport within tumors. While significant progress has been made to understand and improve the tumor transport of small molecule and antibody therapeutics[57, 58], much less work has been done to understand similar phenomena for nanoscale materials[59, 60]. The features of solid tumors that inhibit efficient drug penetration and distribution will be introduced here, followed by a summary of techniques used to study and improve the tumoral drug distribution of nanoscale materials, focusing on those used for the delivery of siRNA to solid tumors.

1.4.1. Tumor properties hindering nanoscale drug transport

Compared to healthy tissues, solid tumors have unique structural properties that make it particularly difficult for drug compounds to transport and distribute throughout malignant tissue. Several reviews have thoroughly discussed the architectural features of solid tumors that hinder drug transport [57-60], so only a brief overview of these features will be discussed here.

1.4.1.1. Abnormal Vasculature

One critical feature of cancerous cells enabling them to have an abnormal survival advantage is their ability to sustain angiogenesis, or to acquire their own blood supply[3]. For cells to survive, they should be within 100 μm of a blood vessel, providing them with critical oxygen and nutrients. In the development of healthy tissues, the formation of blood vessels is carefully regulated to ensure that there is an ample blood supply for all cells. Malignant tumors, however, are formed abnormally in the midst of healthy tissues, and therefore must acquire their own blood supply through dysregulated signaling pathways to progress to a large size[3]. As the acquisition of a blood supply is abnormal in

solid tumors, the structure of the tumor vasculature is poorly organized compared to healthy tissues (Figure 1.3). The blood vessels in solid tumors are more heterogeneous in distribution, size, and are more permeable than in healthy tissue[58].

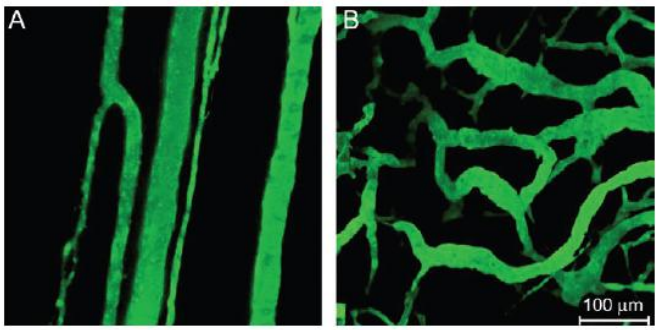

Figure 1.3. Micrographs of normal (A) and tumor (B) vasculature acquired from nude mice bearing tumors from human squamous cell carcinoma cells. This figure was reproduced from: Dreher, M.R. et al. Tumor Vascular Permeability, Accumulation, and Penetration of Macromolecular Drug Carriers. *Journal of the National Cancer Institute* 98, 335-344 (2006) with permission from Oxford University Press[61].

The abnormal tumor vasculature has conferred an advantage for the delivery of nanoscale therapeutics due to the well-known enhanced permeability and retention (EPR) effect. Tumor vasculature is excessively "leaky" compared to healthy vasculature, as a result of large pores in the blood vessels. Nanoscale therapeutics (on the order of 100nm) selectively accumulate in the leaky pores of tumors resulting in a size-dependent passive tumor-targeting known as the EPR effect[25]. While the abnormal tumor vasculature is advantageous for the selective tumor accumulation of nanoscale therapeutics, the ability of these materials to transport across vascular walls (extravasate) and subsequently diffuse into the surrounding tumor tissue poses a significant challenge for these emerging therapeutics.

1.4.1.2 Elevated Interstitial Fluid Pressure (IFP)

Another significant barrier to drug transport from blood vessels is the elevated interstitial fluid pressure (IFP) found in solid tumors. In healthy tissues, the IFP is carefully regulated so that the pressure gradient between the blood vessels and tissue is favorable for convective nutrient transport out of blood vessels and into the tissue. However, in the case of solid tumors, there is an elevated IFP resulting from abnormal blood vessel and extracellular architecture[62]. This high IFP in the tumor results in an unfavorable pressure gradient between the tissue and blood vessels, forcing the nutrients or anticancer drugs out of the high pressure tumor core and into the low pressure blood vessels. Several agents including antagonists of VEGF, PDGF, and TGFβ have been used to reduce the IFP within tumors, which has improved the convective tumoral transport and penetration of nanomedicines[62].

1.4.1.3. Stiff Extracellular Matrix (ECM)

Following extravasation from blood vessels, the transport of particles through the tumor extracellular space to reach malignant cells poses the next barrier to drug delivery. As the abnormal tumor vasculature results in a very low blood supply within tumors, there is little opportunity for convective transport of drugs within tumors, forcing drugs to be transported primarily by diffusion[63]. Diffusion through the tumor space is hindered by the complex structure of the extracellular matrix (ECM) in solid tumors. The extracellular space in solid tumors is comprised of fibrous macromolecular proteins including collagen and glycosaminoglycans (GAGs). In particular, the collagen content in solid tumors is significantly higher than in healthy tissues, resulting in a relatively dense and “stiff” tumoral extracellular space[59]. Small molecule drugs are able to diffuse

through this protein matrix due to their small size, however, the large size of nanoscale therapeutics impairs their ability to diffuse through this matrix, causing them to localize in regions immediately surrounding blood vessels[60]. Several researchers have successfully improved the transport of nanoscale therapeutics through the dense ECM by incorporating agents that can degrade or normalize ECM proteins[64-68] , representing a promising approach to improve the efficacy of tumor-targeted therapies.

1.4.2. *In vitro* methods to study the tumor distribution of drugs

Several experimental and theoretical approaches have been developed to better understand the distribution of drugs (both small molecule and macromolecular) throughout solid tumors. These methods have enabled researchers to visualize the distribution of drugs throughout tumors both *in vitro* and *in vivo*. Further, the use of mathematical models has enabled the quantification of physical transport parameters such as diffusion coefficients, providing a quantitative understanding of how drug design parameters impact their tumor transport. The available techniques for studying drug distribution *in vitro* will be introduced here, with a particular emphasis on how these methods have been applied to understanding the distribution of nanomedicines in solid tumors.

1.4.2.1 In Vitro three-dimensional (3D) tumor models

Three-dimensional tumor models have been widely used for studying anticancer medicines due to their ease of fabrication from commercially available cancer cell lines, and their ability to provide a more realistic model of the *in vivo* tumor microenvironment than cells cultured on conventional two-dimensional plates. Various types of 3D culture models exist to study tumors including multicellular layers, multicellular spheroids, and

collagen scaffold-based cultures, all of which have been thoroughly reviewed elsewhere [69-72]. While 3D cell culture models have been extensively used to study many aspects of solid tumors, they have proven particularly useful in understanding the tumoral transport of anticancer nanomedicines[73, 74].

Multicellular layers (MCLs) have been used to study the tumor penetration and transport of small molecule drugs. Their simple geometry makes them amenable to use in a diffusion chamber apparatus, enabling quantitative determination of drug diffusion coefficients across multiple layers of tumor cells. Specifically, MCL diffusion models have been used to study the diffusion kinetics of the small-molecule anticancer drugs tirapazamine[75], vinblastine[76], variety of anthracycline analogues including doxorubicin[77], and several other commonly used chemotherapeutic agents including paclitaxel and methotrexate[78]. The diffusion of doxorubicin through MCLs has also been described using a mathematical model, which may be a useful tool to predict drug penetration into tumors[79]. The kinetic information obtained for tirapazamine analogues using MCLs was found to be predictive of *in vivo* drug efficacy in a mouse xenograft model[75]. While MCLs have not been used specifically for nanoscale materials, the principle could be easily extended to these materials. An imaging technique using confocal microscopy to track nanoparticles through 3D tissue engineered cell culture models has been recently described[80], and may be applicable to studying nanoparticle distribution through MCLs. This relatively simple cell culture model coupled with effective imaging and mathematical modeling techniques may serve as a useful method to screen potential nanoparticle drug candidates for their antitumor efficacy prior to performing *in vivo* studies.

Multicellular spheroids are probably the most widely used 3D cell culture model for studying the penetration and transport of anticancer nanomedicines. There are several standard methods for generating spheroids including the hanging drop method[81], culturing cells on a non-adhesive substrate to promote the formation of multicellular bodies[82], or culturing cells in spinner flasks to form spheroids[83]. Some methodological improvements have been proposed to improve the growth and formation of spheroids, such as incorporating a transient polycation linker during the spheroid formation phase[84] which may aid in generating more consistent spheroids for drug screening applications, or by using a hydrogel micromold to control their shape and size[85]. Spheroids have been extensively used to study the penetration of nanoscale liposomes[86-89], gene and siRNA delivery vehicles[90-95], and other nanoparticles for drug delivery and imaging applications[66, 96-100]. Further, their spherical shape has made them particularly amenable for developing descriptive mathematical models describing drug transport of macromolecular[101-103] and nanoscale therapeutics[104]. Spheroids have already proven to be a critical tool in studying the penetration of nanoscale materials, and will likely continue as a valuable method to screen and understand the tumor transport of nanoparticle drugs.

Gel scaffolds (collagen or Matrigel) have also been used to replicate the architecture of solid tumors for drug penetration studies. One study found that collagen gels alone (without the use of any cells) could provide similar resistance to macromolecule penetration as observed in solid tumors[105]. Matrigel has also been used in an *in vitro* setting to represent the tumor ECM in conjunction with Caco-2 cells, and was found to be a reasonable model predicting the tumor penetration of small-molecule

thioxanthones[106]. Since gels are simple *in vitro* models that provide reasonable similarity to solid tumors, they might serve as a useful experimental tool for screening nanoscale drug compounds.

1.4.2.2. Mathematical Modeling Approaches

In conjunction with experimental techniques, mathematical modeling approaches have been utilized to better understand and predict drug penetration in solid tumors. Models describing drug transport on the cell and tissue level, as well as those extending transport to the whole-body scale have provided important insights into the properties and mechanisms governing drug transport in tumors.

Significant models describing antibody penetration into solid tumors has provided researchers with important design parameters for anticancer antibody therapeutics. Mathematical modeling approaches first identified a "binding-site barrier" to antibody transport in solid tumors wherein antibodies displaying a high binding affinity to tumor cells actually retard antibody penetration[107]. In this theory, high-affinity molecules bind rapidly to tumor cells, leaving very few unbound molecules free to transport deep within solid tumors. This theory was further proven experimentally when antibodies with a lower binding affinity to tumor cells exhibited more homogeneous penetration into guinea pig micrometastases[108] and colon cancer tumor spheroids[103] than antibodies with higher binding affinities. In addition to affinity, models have been developed describing the importance of other parameters such as antibody dosage[102], antigen turnover rate[101], and plasma clearance rate[109] on antibody penetration and retention into tumors. The knowledge gained from these models has enabled the prediction of antibody penetration based on the complex interplay between antibody molecular weight, size, and affinity[110].

These modeling approaches may serve very useful in predicting the antitumor activity of anticancer drugs prior to performing any extensive experiments. The knowledge gained from modeling antibody distribution has been applied to studying the tumor distribution of small-molecule drugs[79, 111] and nanoparticles[104, 112]. Large-scale pharmacokinetic modeling has also been employed to describe the whole-body distribution of macromolecular agents[113].

1.4.3. Methods to improve the tumor distribution of drug and siRNA delivery molecules

The transport properties governing tumor penetration of antibodies and small molecule therapeutics provide important guidelines that can be extended for the design of nanoscale therapeutics. The process of tumor penetration begins with convective transport through blood vessels and extravasation through vessel walls followed by diffusion through solid tumors. As blood vessel availability in solid tumors is limited, the primary mode of drug transport in tumors is diffusion[109].

The properties governing intratumoral transport include rates of free diffusion through the tumor interstitium, cell binding affinity, cell internalization and metabolism kinetics, and systemic clearance[103, 109]. Free diffusion within a tumor is inhibited by molecular crowding within the tumor interstitial space, by the binding of molecules or particles to the cell surface, and by cellular internalization. However, it is imperative that the therapeutic have some affinity to tumor cells to prevent it from diffusing through the tumor without accumulating at all. Thus, it is important to design drugs such that they strike a balance between efficient diffusion and cellular affinity, ensuring that the therapeutic will transport deep within the tumor, and accumulate in quantities sufficient

to elicit a therapeutic effect. The relative contributions of drug diffusion, cellular binding and internalization, and tumor clearance are known to govern the tumor penetration efficiency of antibody therapeutics[103]. Scaling analyses have suggested that if the rate of diffusion with binding is greater than both the systemic clearance rate and cell internalization rates, that there will be efficient antibody tumor transport[103]. Being mindful of these important scaling analyses will aid researchers in rationally designing antitumor therapeutics with favorable tumor penetration properties.

Several studies have investigated how drug architecture influences tumor penetration and retention. In addition to binding affinity, the tumor distribution of anticancer therapeutics is influenced by particle size, surface charge, and shape[59, 60]. As one example for antibodies, the accumulation of therapeutic proteins in HER2-overexpressing breast tumors was studied as a function of antibody size, affinity, and shielding by PEGylation[114]. In this study, the delicate interplay between size and affinity were found to be critical for tumor accumulation, and two design regimes were observed to elicit the highest tumor accumulation (small proteins with high affinity or large proteins with low affinity). For a class of small molecules (anthraquinones), the net molecular charge influenced drug distribution in tumor spheroids, presumably by altering their rate of cellular uptake[115]. These design guidelines that were initially derived for small molecules and antibodies have been extended to understanding and improving the tumor penetration of nanoscale materials.

Polycationic polymers have been widely used to deliver genes and antisense molecules to solid tumors by forming electrostatic nanoscale complexes with anionic nucleic acid molecules[12]. As it is necessary to maintain a net positive charge on nucleic acid delivery

vehicles[7], these charged complexes have been largely unable to penetrate into solid tumor models since they elicit undesirable interactions with charged cells or ECM proteins. A widely used gene delivery polymer, polyethyleneimine (PEI), was found to exhibit poor tissue penetration when delivering plasmid DNA to tumor spheroids[90]. In other cases, cationic polymers that successfully facilitated gene transfection in traditional monolayer cell culture, were significantly less efficient in delivering genes in a three-dimensional tumor model due to poor tissue penetration of the electrostatic complexes[90, 93, 116]. RGD peptides have also been used to improve the tumor penetration of anticancer agents[117, 118], and they may find utility for enabling the delivery of nanoscale therapeutics, including nucleic acids, homogeneously throughout solid tumors.

1.5. Dissertation overview and approach

The objective of this dissertation was to study the ability of PAMAM dendrimers to facilitate the tumor-targeted delivery of siRNA to malignant glioma cells and solid tumors. The intracellular delivery aspects of PAMAM-mediated siRNA delivery to malignant glioma tumor cells are explored in Chapter 2, where surface amine acetylation was employed to understand better the intracellular siRNA delivery mechanisms of PAMAM dendrimers. Next, RGD peptides were conjugated to PAMAM dendrimers, and these conjugates were used to facilitate targeted siRNA delivery of PAMAM/siRNA complexes to malignant glioma solid tumors. The number of RGD peptides displayed from a PAMAM scaffold was found to influence the ability of PAMAM to distribute siRNA hroughout a three-dimensional cell culture model of malignant glioma, as discussed in Chapter 3. The transport mechanisms involved in the efficient tumoral penetration and transport of PAMAM-RGD/siRNA complexes were further studied

through a combination of biophysical material characterization and theoretical modeling work, which is detailed in Chapter 4.

CHAPTER 2

ACETYLATION OF PAMAM DENDRIMERS FOR CELLULAR DELIVERY OF SIRNA

This chapter is published and has the following citation:

Waite, C.L., Sparks, S.M., Uhrich, K.E. & Roth, C.M. Acetylation of PAMAM dendrimers for cellular delivery of siRNA. *BMC Biotechnol* **9**, 38 (2009).

ABSTRACT

The advancement of gene silencing via RNA interference is limited by the lack of effective short interfering RNA (siRNA) delivery vectors. Rational design of polymeric carriers has been complicated by the fact that most chemical modifications affect multiple aspects of the delivery process. In this work, the extent of primary amine acetylation of generation 5 poly(amidoamine) (PAMAM) dendrimers was studied as a modification for the delivery of siRNA to U87 malignant glioma cells.

PAMAM dendrimers were reacted with acetic anhydride to attain partial acetylation of primary amines. Acetylated dendrimers were complexed with siRNA, and physical properties of the complexes were studied. The ability of acetylated dendrimers to deliver siRNA to U87 glioma cells was evaluated using flow cytometry, and their cytotoxicity was studied using the MTS assay. Dendrimers with up to 60% of primary amines acetylated formed ~200 nm complexes with siRNA. Increasing amine acetylation resulted in reduced polymer cytotoxicity to U87 cells, as well as enhanced dissociation of dendrimer/siRNA complexes.

Acetylation of dendrimers reduced the cellular delivery of siRNA which correlated with a reduction in the buffering capacity of dendrimers upon amine

acetylation. Primary amine acetylation of PAMAM dendrimers reduced their cytotoxicity to U87 cells, and promoted the release of siRNA from dendrimer/siRNA complexes. A modest fraction (approximately 20%) of primary amines of PAMAM can be modified while maintaining the siRNA delivery efficiency of unmodified PAMAM, but higher degrees of amine neutralization reduced the gene silencing efficiency of PAMAM/siRNA delivery vectors.

2.1. Background

Since its discovery in 1998, RNA interference (RNAi) has rapidly become a routine and powerful tool for use in basic research and has also gained momentum in development as a therapeutic[5, 6, 119]. While RNAi is an elegant, endogenous and conserved mechanism to selectively silence genes, inefficient delivery of exogenous short interfering RNA (siRNA) molecules to cells and tissues remains a barrier to its therapeutic development. As a result, the design of effective siRNA delivery systems is crucial for the clinical advancement of RNAi. Specifically, delivery vectors must be designed to effectively complex with nucleic acid molecules and aid in overcoming intracellular barriers such as endosomal escape and cytoplasmic vector dissociation.

A variety of molecules including polymers, lipids, and peptides have been studied for their effectiveness as delivery vectors for DNA and RNA molecules[7]. Successful delivery vectors must exhibit a combination of functional attributes. Polymeric carrier molecules should be cationic to complex with nucleic acids, possess a high buffering capacity, exhibit low cytotoxicity, and also contain chemically reactive groups that can be modified for the addition of targeting moieties or other groups [7, 10].

Highly branched, dendritic polymers including poly(amidoamine) (PAMAM) have recently attracted interest as nucleic acid delivery vectors. Previous work has demonstrated that dendrimers can bind to DNA and RNA molecules and mediate modest cellular delivery of these nucleic acids [14, 15, 120, 121]. Recently, some studies have evaluated the use of PAMAM dendrimers for successful delivery of siRNA or antisense molecules. Generation 5 dendrimers were found to have poor cellular delivery of siRNA to NIH 3T3 MDR cells compared to moderately effective delivery of antisense oligonucleotides[122]. Another study found that increasing the PAMAM dendrimer generation to seven to increase the number of primary amine groups significantly enhanced siRNA delivery efficiency, possibly by enhanced amine-induced pH buffering[123]. However, cytotoxicity of highly cationic dendrimers is a marked problem that hinders their widespread use in drug and gene delivery [120, 121].

Thus, it is desirable to exploit the potential of PAMAM dendrimers for nucleic acid delivery applications while reducing their cytotoxicity. The cytotoxicity of dendrimers can be reduced by conjugating hydrophilic polymers to the periphery of the dendrimer [124-126], conversion of a fraction of the cationic amine groups to uncharged moieties [127-129], or by modifying a neutrally charged dendrimer with a few cationic amino acid groups sufficient to facilitate nucleic acid complexation[130]. Since a wide variety of modifications exist to alter the properties of dendrimers, the development of structure-activity relationships will accelerate determination of the optimal dendrimer properties for a particular application [131-133].

In this study, the effect of primary amine acetylation of the cationic, dendrimeric polymer, PAMAM, on siRNA delivery was analyzed. Previous studies have shown that

neutralizing charges on the cationic polymer, polyethylenimine (PEI), by amine acetylation enhanced the transfection efficiency of plasmid DNA [19, 20]. This marked improvement in transfection efficiency correlated with decreased polymer/DNA interactions, thus promoting intracellular unpackaging of DNA from the polymer [20]. Additionally, amine acetylation of cationic polymers is attractive since it has been shown to reduce cytotoxicity in a variety of different cell lines [20, 129]. We studied dendrimer/siRNA interactions as well as the ability of acetylated dendrimers to deliver siRNA to cells and elicit a gene silencing effect. Additionally, we evaluated the tradeoff between reduced polymer/siRNA interactions and reduced endosomal buffering capacity. These design parameters are important in the rational modification of PAMAM dendrimers for siRNA delivery.

2.2 METHODS

2.2.1 Materials

A 22 nt anti-GFP siRNA sequence identified previously [134] as an effective inhibitor of pd1EGFP expression (sense strand: 5'-UUG UGG CCG UUU ACG UCG CCG U-3', antisense strand: 3'-UGA ACA CCG GCA AAU GCA GCG G-5') was utilized in this study. A scrambled siRNA sequence (targeted against firefly luciferase) was used as a negative control (sense strand: 5'-CUU ACG CUG AGU ACU UCG A dTdT-3', antisense strand: 5'- UCG AAG UAC UCA GCG UAA G dTdT-3'). The fluorescently labeled (5' Cy3 end modified on the sense strand) and unlabeled sequences were purchased from Integrated DNA Technologies (Coralville, IA, USA). The control siRNA sequence was purchased from Dharmacon (Lafayette, CO). The lyophilized powder was resuspended to a concentration of 20 μM (unlabeled siRNA) or 50 μM (Cy3

modified sequence) according to the manufacturer's protocol before use. Generation 5 PAMAM dendrimer was purchased as a 5 wt% solution in methanol from Dendritech (Midland, MI). Branched PEI of average molecular weight 25 kDa (Item 408727), acetic anhydride, triethylamine, heparin sodium salt, and deuterium oxide (D_2O) were purchased from Sigma. PicoGreen fluorescent dye was obtained from Molecular Probes (Eugene, OR, USA). MTS reagent was purchased from Promega (Madison, WI, USA). Unless otherwise stated, all cell culture products were obtained from Invitrogen (Carlsbad, CA, USA).

2.2.2 Acetylation of PAMAM dendrimers

The molar ratio between acetic anhydride and PAMAM dendrimer was adjusted to achieve 20, 40, 60, and 80% of primary amines capped by an acetyl group. A 1:1 stoichiometric ratio of primary amines: acetic anhydride was used to achieve the desired extent of acetylation. Partially acetylated dendrimers were prepared using the following procedure: To 15 mL of anhydrous methanol in a magnetically stirred round bottom flask, 5 mL of 5 wt% PAMAM (0.214 g) in methanol was added. Triethylamine (10% molar excess to acetic anhydride) was added to the flask and was stirred for 30 minutes. The appropriate amount of acetic anhydride was then added dropwise to the reaction mixture and the reaction was carried out overnight at room temperature under an argon atmosphere. The methanol was then removed by vacuum, and the polymer residue re-dissolved in distilled water. The polymer was then dialyzed against 1 L of phosphate buffered saline (PBS) for 8 hours followed by water overnight in a 10,000 kDa cutoff Slide-A-Lyzer Dialysis cassette (Pierce Biotechnology, Rockford, IL). The samples were then lyophilized and stored at -20ºC. Proton nuclear magnetic resonance (^{1}H NMR)

spectra were taken in D_2O using a Varian 400 MHz or 500 MHz spectrophotometer, using the solvent as reference signal. The extent of primary amine acetylation was determined using a previously described method[135].

2.2.3 PicoGreen assay for siRNA/PAMAM complexation

The complexes were prepared at various charge ratios by mixing equal volumes of PAMAM with siRNA in PBS. Charge ratios (N/P) were calculated as a ratio of the number of primary amines in the polymer, determined from ^{1}H NMR spectra, to the number of anionic phosphate groups in the siRNA. The samples were then vortexed and incubated at room temperature for 15 minutes to ensure complex formation. The complexes were prepared at a final siRNA concentration of 0.2 μg of siRNA/100 μL of solution. One hundred microliters of each complex were transferred to a 96-well (black-walled, clear-bottom, non-adsorbing) plate (Corning, NY, USA). A total of 100 μL of diluted PicoGreen dye (1:200 dilution in Tris-EDTA (TE) buffer) was added to each sample. Fluorescence measurements were made after a 30 minute incubation at room temperature using a DTX800 Multimode Detector (Beckman Coulter, CA, USA), at exitation and emission wavelengths of 485 and 535 nm, respectively. All measurements were corrected for background fluorescence from a solution containing only buffer and PicoGreen dye.

2.2.4 Dynamic light scattering and zeta potential

Dynamic light scattering (DLS) and Zeta Potential analyses were performed using a Malvern Instruments Zetasizer Nano ZS-90 instrument (Southboro, MA) with reproducibility being verified by collection and comparison of sequential measurements. Polymer/siRNA complexes (siRNA concentration = 100 nM, N/P=15) were prepared

using purified water (resistivity=18.5 MΩ-cm). DLS measurements were performed at a 90 ° scattering angle at 37 °C. Z-average sizes of three sequential measurements were collected and analyzed. Zeta potential measurements were collected at 25 °C, and the Z-average potentials following three sequential measurements were collected and analyzed.

2.2.5 Heparin competition assay

Complexes were prepared at a charge ratio of 10 as described above (final siRNA concentration of 0.2 μg in a total of 50 μL of solution) and were transferred to a 96-well (black-walled, clear-bottom, non-adsorbing) plate. A total of 100 μL of diluted PicoGreen dye was added to each well, followed by the addition of 50 μL of heparin solution prepared in TE buffer (pH=8). The plate was incubated for 60 minutes at 37ºC, and fluorescence measurements were then taken using the Multimode Detector plate reader. The percentage of siRNA released was calculated as described previously [136].

2.2.6 Cell culture

U-87 MG cells (ATCC HTB-14) were maintained in D-MEM medium supplemented with 10% fetal bovine serum (FBS), L-glutamine, sodium pyruvate, non-essential amino acids, and penicillin-streptomycin solution. A U-87 MG cell line containing a stably integrated destabilized EGFP (d1EGFP) transgene was produced by transfecting U-87 cells with the 4.9-kb pd1EGFP-N1 plasmid (BD Biosciences Clontech, Palo Alto, CA) and maintained under constant selective pressure by G418 (500 μg/mL). All cell lines were cultivated in a humidified atmosphere of 5% CO_2 at 37ºC.

2.2.7 MTS cytotoxicity assay

U-87 cells were plated at a density of 10^3 cells/well in a 96-well plate approximately 18 hours before the assay. Cells were exposed to 100 μL of dendrimers or

dendrimer/siRNA complexes at various concentrations in OptiMEM reduced serum medium (Invitrogen, Carlsbad, CA) for 4 hours. Twenty microliters of MTS reagent were added to each sample using a multi-channel pipette, and the plate was returned to the cell incubator for 2 hours. Absorbance measurements were subsequently recoreded at 490 nm using a Bio-Rad Model 680 microplate reader (Hercules, CA, USA). The values for treated samples were normalized to those for cells receiving a mock treatment of OptiMEM medium only (positive control).

2.2.8 siRNA delivery assay

U87 or U87-d1EGFP cells were plated at a density of 1.5 x 10^5 cells/well in 12 well plates ~18 hours prior to transfection. Prior to treatment of cells, PAMAM/siRNA complexes were prepared as described above in 200 μL of PBS. PolyFect (Qiagen), a commercially available dendrimeric transfection reagent, was used as a positive control. Transfections were also performed with a scrambled siRNA sequence not targeted against GFP to account for any non-specific GFP silencing effects. Eight hundred microliters of OptiMEM medium was mixed with each sample to obtain a final siRNA concentration of 100 nM. The serum-containing culture medium was aspirated from the cells, and each well was treated with 1 mL of the PAMAM/siRNA complexes in OptiMEM medium. After a 4 hour incubation period, the transfection mixture was replaced with serum-containing culture medium and maintained under normal growth conditions until the cells were assayed for fluorescence by flow cytometry either 24 or 48 hours after initial treatment. For cells being analyzed for GFP fluorescence, unlabeled siRNA was utilized. To determine intracellular siRNA levels, non-transformed U87 cells were treated with Cy3-labeled siRNA.

2.2.9 Flow cytometry

Cells were washed with PBS, detached with trypsin-EDTA, and collected in growth medium before they were pelleted by centrifugation for 3.5 min at 200 *g*, and resuspended in 150 μL PBS. Samples were maintained on ice before being subjected to flow cytometry analysis. Ten thousand cells were analyzed on a FACSCalibur two-laser, four-color flow cytometer (BD Biosciences) for GFP fluorescence (FL-1) or Cy3 fluorescence (FL-2). CellQuest software was used to acquire and analyze the results. Viable cells were gated according to their typical forward/side scatter characteristics.

2.2.10 Confocal microscopy

For confocal imaging, U87-d1EGFP cells were plated into 8-well Lab-Tek Chamber Slide chambers (Lab-Tek, Naperville, IL) at a cell density of 25,000 cells/well approximately 18 hours prior to transfection. For imaging purposes, complexes of PAMAM were prepared with a Cy5-labeled antisense oligonucleotide targeted against GFP[134] (ODN concentration = 100 nM) to prevent fluorescence interference between U-87-d1EGFP cells and Cy3-labeled siRNA. Transfections were performed in the same manner as for flow cytometry analysis. In some samples, 100 μM of chloroquine diphosphate, a buffering agent, was added to the transfection mixture. Imaging was performed at 63X magnification with a Leica LCSSB2 confocal microscope 24 hours after transfection.

2.2.11 pH titrations

Either PAMAM or PEI (~4.5 mg) was freshly dissolved into 5 mL of purified water in a 10 mL beaker and was magnetically stirred. pH measurements were taken

using a NMR tube micro pH probe (IQ Scientific, Carlsbad, CA). Using 1 N NaOH, solutions were adjusted to a pH of approximately 11.5. The polymer was then titrated by adding 5 μL aliquots of 1N HCl until a total of 100 μL of HCl had been added to the solution, at which point the pH had reached a constant value of pH ~ 2. Titrations were each performed in duplicate.

2.2.12 Statistics

All statistical comparisons among treatment groups were performed using a one way ANOVA test with Tukey's all-pairs post hoc comparison test.

2.3 RESULTS

2.3.1 Partial acetylation of PAMAM dendrimers

The primary amines of generation 5 (G5) PAMAM dendrimers were acetylated by reaction with prescribed amounts of acetic anhydride as depicted in Figure 2.1. ^{1}H NMR analysis of acetylated dendrimers was performed using a method similar to one described previously[135]. Briefly, the fraction of primary amine acetylation was determined by comparing the intensity of the peak at 1.87 ppm corresponding to $–CH_3$ protons of the acetyl group to the sum of all $–CH_2$- peaks. The observed extents of amine acetylation were very close to the theoretical maxima indicated by reaction stoichiometry (Table 2.1). The acetylated dendrimers are denoted by their experimentally determined acetylation levels as Ac_{20}, Ac_{40}, Ac_{60}, and Ac_{84}.

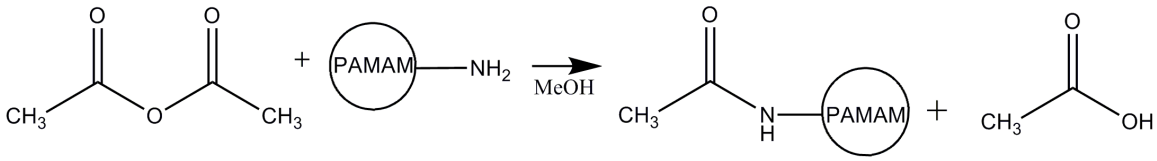

Figure 2.1. Acetylation of PAMAM dendrimers**.** Acetic anhydride reacts with primary amines of G5 PAMAM dendrimers to produce acetylated PAMAM.

Sample	(-CH_3/-CH_2-) ratio	Number of acetyl groups added	Percent of primary amine acetylation
Ac_{20}	0.041	27	21.1
Ac_{40}	0.075	50	39.1
Ac_{60}	0.115	76	59.4
Ac_{84}	0.160	107	83.6

Table 2.1. Extent of primary amine acetylation as determined by ^{1}H NMR spectroscopy.

2.3.2 PicoGreen dye exclusion

The ability of acetylated dendrimers to complex with siRNA as a function of polymer/siRNA charge ratio was evaluated. The amount of unbound siRNA in solutions of dendrimer/siRNA was determined by measuring the fluorescence of a commercially available dye, PicoGreen, that fluoresces upon binding to double-stranded DNA or RNA. The fluorescence intensity decreased when increasing amounts of polymer were added to a fixed amount of siRNA, indicating association of siRNA with the polymer (Figure 2.2). At N/P=1, differences in siRNA complexation ability could be discerned, with higher fractions of siRNA forming complexes with dendrimers possessing the greater primary amine levels. However, by N/P=10, almost complete complexation of siRNA was observed for unmodified dendrimer (G5), Ac_{20}, Ac_{40}, and Ac_{60}. In contrast, the binding curve for the Ac_{84} polymer was shifted markedly to the right, and little siRNA complexation was observed at N/P=10. Since the Ac_{84} dendrimer was not able to complex with siRNA at N/P=10, it was excluded from further studies.

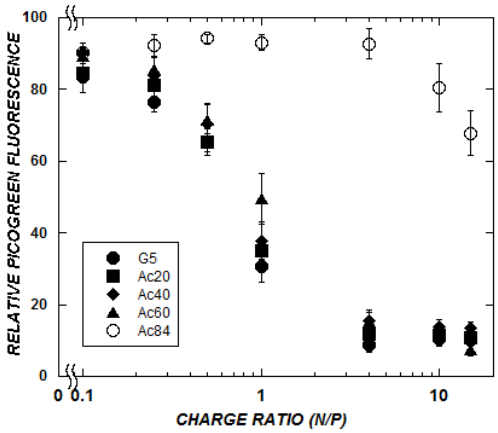

Figure 2.2. Effect of amine acetylation on siRNA complexation by PicoGreen dye exclusion. Complexes were prepared in PBS at a final siRNA concentration of 2 μg/mL. PicoGreen fluorescence correlates to unbound siRNA present in solution. Data represent mean ± SEM (*n*=3).

2.3.3 Complex size and zeta potential

Having demonstrated that acetylated dendrimers are able to complex with siRNA, the characteristics of these complexes were evaluated further by DLS and zeta potential measurements. Particle size analysis by DLS showed the formation of ~200 nm complexes between dendrimers and siRNA, regardless of acetylation extent (Table 2.2). Somewhat surprisingly, zeta potential measurements were approximately equal (~40 mV) for siRNA complexes with G_5, Ac_{20}, and Ac_{40} dendrimers. Though we do expect the surface charge of these complexes to become less cationic upon primary amine acetylation, this trend may not be reflected in zeta potential measurements as surface charge has been shown to be non-linearly correlated to zeta potential [137]. However, while the zeta potential of dendrimer/siRNA complexes at N/P=15 for G5, Ac_{20}, and Ac_{40} were approximately equal (~40 mV), the zeta potential did decrease somewhat for the Ac_{60}/siRNA complex (33 mV), indicating a modest change in the surface properties of this polyplex due to amine acetylation. This trend is consistent with the dye exclusion results (Figure 2.2).

Sample	Particle diameter (nm)	Zeta Potential (mV)
G5-siRNA	200.2 ± 28.1	40.2 ± 1.1
Ac_{20}-siRNA	226.2 ± 7.3	38.9 ± 0.9
Ac_{40}-siRNA	229.3 ± 8.4	39.7 ± 0.7
Ac_{60}-siRNA	173.7 ± 8.0	33.1 ± 0.8

Table 2.2. Particle diameter and zeta potential of dendrimer/siRNA complexes

2.3.4 Heparin induced polyplex dissociation

Previous work has shown that more effective cellular delivery of nucleic acids is achieved when polymers are able to easily release or unpackage their cargo nucleic acid following cellular entry [138]. To evaluate the effect of dendrimer amine acetylation on polyplex dissociation, dendrimer/siRNA complexes were challenged by exposure to heparin sulfate, an anionic competitive binding agent. Polyplexes were formed in solution at N/P=10 and exposed subsequently to either 20 μg/mL or 40 μg/mL of heparin sulfate. After 60 minutes of incubation, PicoGreen was used to measure the amount of siRNA released from dendrimer polyplexes. As expected, more siRNA was released from complexes with increasing heparin concentration (Figure 2.3). Upon addition of heparin, more siRNA was released from 25 kDa polyethylenimine (25K PEI), which was included as a well-studied reference, than from G5 dendrimer, indicating that 25K PEI allows greater polyplex dissociation than G5 dendrimer. Consistent with the decrease in cationic charge density conferred by primary amine acetylation, the amount of siRNA released increased with extent of primary amine acetylation. At high fractions (40 and 60%) of amine acetylation, the polyplex dissociation of acetylated dendrimers surpassed that of 25K PEI.

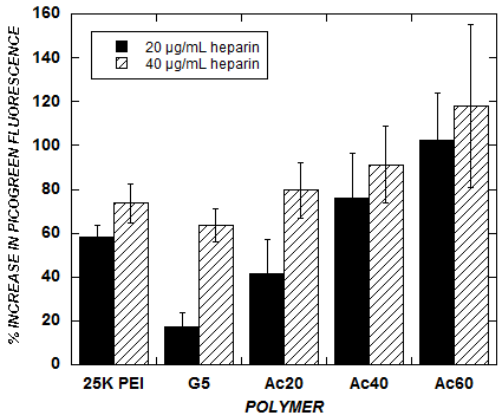

Figure 2.3. Effect of amine acetylation on polyplex dissociation by heparin competition. Complexes (N/P=10) were prepared in PBS at a final siRNA concentration of 2 µg/mL, and were exposed to heparin for 60 min at 37ºC. siRNA release from complexes was determined by PicoGreen fluorescence as in Figure 2. Data represent mean ± SEM (*n* =5).

2.3.5 Cytotoxicity of acetylated dendrimers

Primary amine acetylation of various cationic polymers has been shown to reduce their cytotoxicity [20, 129]. The cytotoxicity of acetylated dendrimers on a malignant glioma cell line, U87, was evaluated by treatment with either dendrimer/siRNA complexes (siRNA concentration = 100 nM) or with dendrimers in OptiMEM medium for 4 hours (0.005 mM or 0.01 mM). Subsequently, cells were analyzed for cell viability using the MTS assay. Cells exposed to OptiMEM medium alone were used as positive controls. Minimal cytotoxicity was observed from treatment with dendrimer/siRNA complexes at typical cell transfection conditions (Figure 2.4A). However, it is also important to evaluate the cytotoxicity of the native polymers without the presence of siRNA. In this case, a dose-dependent cytotoxicity was observed by increasing the dendrimer concentrations to higher concentrations than were used for cell transfections (Figure 2.4B). Additionally, a linear decrease in toxicity was observed upon reducing the number of primary amines by acetylation. This trend is consistent with previous work that

showed a linear decrease in cytotoxicity of a different cell type upon dendrimer amine acetylation [129].

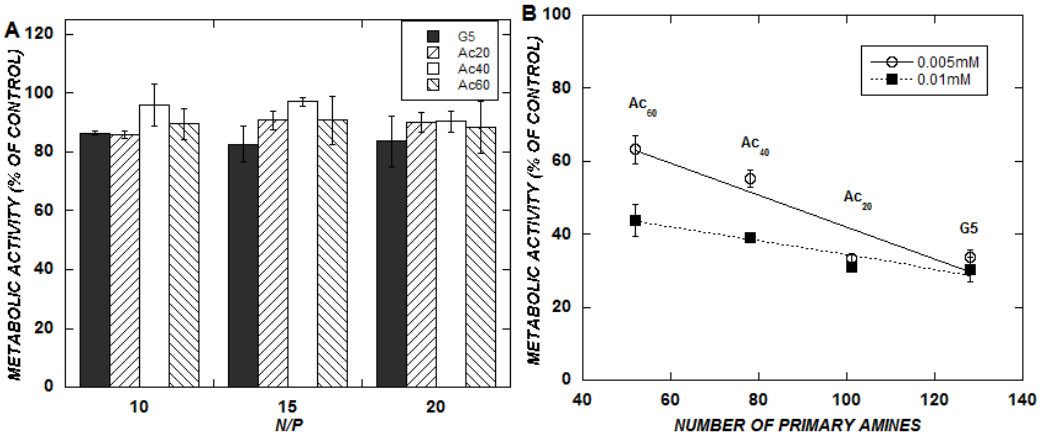

Figure 2.4. Cytotoxicity of dendrimer/siRNA complexes (A) and of acetylated dendrimers (B). U-87 cells were exposed to dendrimer/siRNA complexes (siRNA concentration = 100 nM) or to dendrimers (0.005 or 0.01 mM) for 4 hours in OptiMEM medium prior to MTS viability assay. MTS absorbance measurements were normalized to cells receiving a mock treatment of OptiMEM medium only (100%). The unmodified, generation 5 dendrimer has 128 primary amines. Data represent mean ± SEM (*n* =2 experiments, each measured in triplicate).

2.3.6 siRNA induced silencing of GFP in U87-d1EGFP cells

We tested the effectiveness of these polymers to deliver anti-d1EGFP siRNAs to U87 cells stably expressing the d1EGFP transgene. Cells were treated with dendrimer/siRNA complexes for 4 hours at several charge ratios within the range where all dendrimers (up to Ac_{60}) are able to complex the siRNA. After 24 and 48 hours, the d1EGFP fluorescence of cells was analyzed using flow cytometry. The fluorescence of polyplex treated cells was normalized to time-matched U87-d1EGFP cells that received a mock treatment of serum-free medium (positive control). SiRNAs delivered by unmodified G5 dendrimer produced significant gene silencing, manifest in reductions (up to 60% at a charge ratio of 20) of d1EGFP fluorescence after 24 hours (Figure 2.5a).

Upon primary amine acetylation of dendrimers, a significant decrease in GFP silencing efficiency was observed, particularly for the highest fractions of amine acetylation, 40% ($p = 0.0002$) and 60% ($p < 0.0001$) compared to unmodified dendrimer. The Ac_{20} material, with a modest fraction of amine modification, produced an insignificant change in GFP silencing ability as compared to the unmodified dendrimer ($p = 0.28$). For the G5 and Ac_{20} materials, an improved GFP silencing ability was observed upon increasing the N/P ratio of each dendrimer from 10 to 20. The extent and trends of GFP silencing using these polymers were maintained for 48 hours (data not shown). A low level of non-specific GFP silencing (~20%) was observed by all dendrimer/siRNA complexes delivering a scrambled siRNA sequence.

Having studied the ability of acetylated dendrimers to deliver siRNA to U87-d1EGFP cells to elicit a gene silencing response, we used fluorescently labeled (Cy3) siRNA to determine intracellular levels of siRNA delivered by the dendrimers. Previous work has shown that efficient gene silencing correlates to high intracellular nucleic acid levels [136]. A significant decrease in the intracellular fluorescence intensity of siRNA was observed with increasing fractions of amine acetylation ($p < 0.0001$ comparing Ac_{40} to G5 and $p < 0.0001$ comparing Ac_{60} to G5) (Figure 2.5B). This trend correlated closely to the decreased GFP silencing efficiency upon amine acetylation (Figure 2.5A).

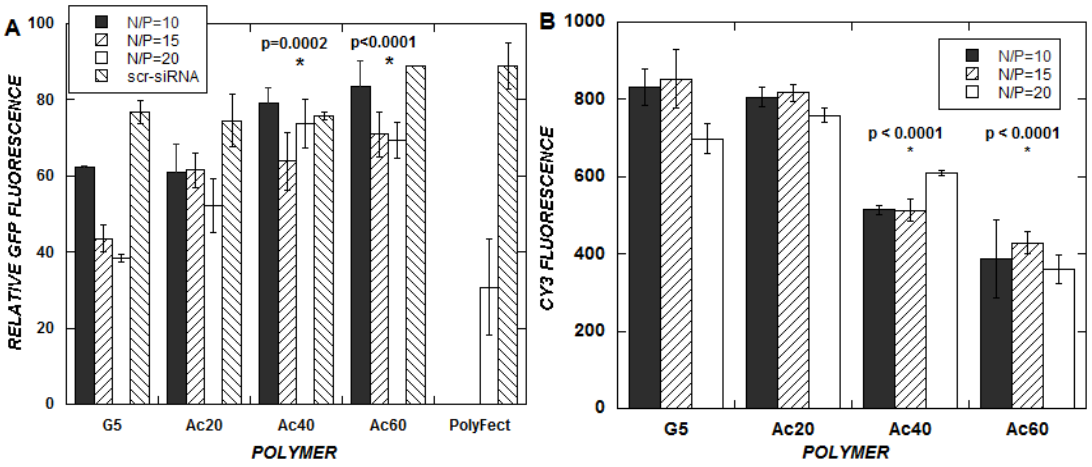

Figure 2.5. SiRNA-induced GFP silencing (A) and intracellular Cy3-siRNA levels (B). U-87-d1EGFP (A) or non-transformed U-87 cells (B) were treated with PAMAM/siRNA complexes at a final siRNA concentration of 100 nM for 4 hours under serum-free conditions. Cells were analyzed using flow cytometry for GFP fluorescence (A) or Cy3 fluorescence (B) 24 hours after the initial treatment. PolyFect (A) was used at 5:1 wt. ratio of PolyFect:siRNA. Data represent mean $\pm$ SEM (*n* =3) (A) or (*n* =1 experiment, measurements performed in triplicate) (B).

2.3.7 Confocal imaging

Confocal imaging was performed to compare the cellular distribution of nucleic acids delivered by acetylated dendrimers compared to unmodified dendrimers. As endosomal escape is a well-known barrier to efficient nucleic acid delivery[7, 10], some transfections were performed in the presence of chloroquine diphosphate, a buffering agent, to identify if pH buffering is a significant barrier to efficient siRNA delivery by acetylated dendrimers. Confocal imaging indicated that ODNs delivered by PAMAM dendrimers were sequestered into vesicles. Red ODN fluorescence appeared as isolated, punctate specks when delivered by G5 or Ac_{60} dendrimers (Figure 2.6 a and b, respectively), with somewhat greater cytoplasmic distribution observed for G5 delivery. These distributions contrast with that of Lipofectamine2000, a commercially available reagent, that evenly delivered ODN throughout the cell (Figure 2.6h). Further, the presence of chloroquine diphosphate during transfection significantly improved the

distribution of ODN when delievered by cationic dendrimers G5 (Figure 2.6e), Ac_{60} (Figure 2.6f), or 25K PEI (Figure 2.6g) as the ODN appeared to be more evenly distributed throughout the cell compared to treatment without chloroquine.

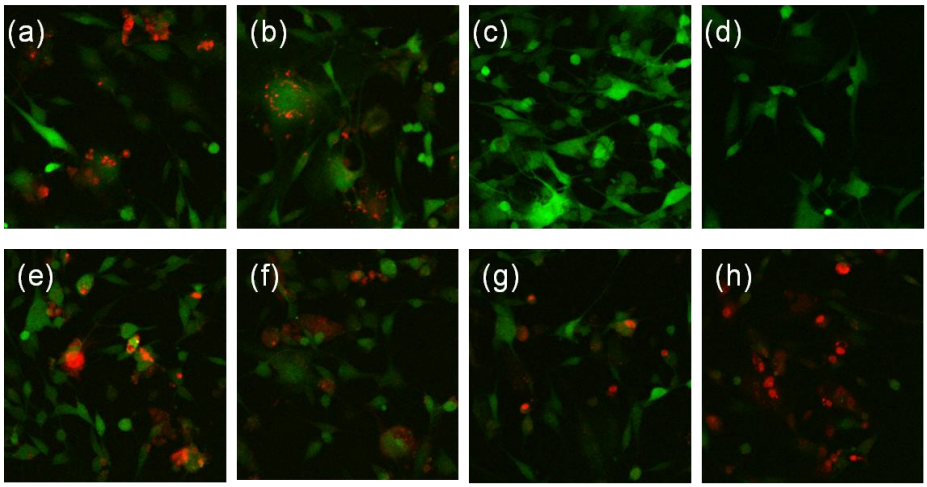

Figure 2.6. Confocal microscopy images of Cy-5 labeled oligonucleotides delivered to U-87-d1EGFP cells. U-87-d1EGFP cells were treated with polymer/Cy5-ODN complexes (N/P=15). Images show U-87-d1EGFP cells in green, and Cy5-ODN in red. Images represent cells transfected with: (a) G5 PAMAM; (b) Ac_{60} PAMAM; (c) 25K PEI; (d) OptiMEM medium only; (e) G5 PAMAM + 100μM chloroquine; (f) Ac_{60} PAMAM + 100 μm chloroquine; (g) 25K PEI + 100 μM chloroquine; and (h) Lipofectamine2000.

2.3.8 Titration of acetylated dendrimers

As the cellular distribution of ODN delivered by dendrimers was improved by the presence of chloroquine in the transfection medium, it is likely that endosomal escape is a significant barrier to efficient siRNA delivery for acetylated dendrimers. Hence, pH titrations were performed to compare the buffering capacity of acetylated dendrimers. Increasing the fraction of amine acetylation caused titration curves to shift, indicating a reduction in buffering capacity (Figure 2.7) upon addition of acid. This trend is consistent with previous work performed with acetylation of PEI [20]. Interestingly, the

titration curve showed that unmodified G5 PAMAM has a much lower buffering capacity than 25 kDa PEI. While PAMAM and PEI have similar numbers of amines per unit mass, approximately half of the PAMAM amines are secondary amines in the form of amide bonds that are not titratable.

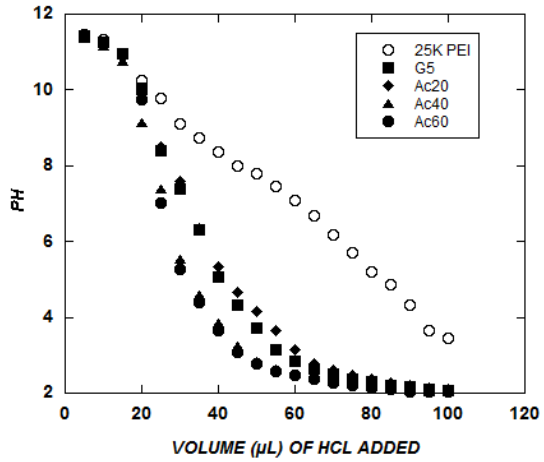

Figure 2.7. pH titrations. Polymers were freshly dissolved in 5 mL of PicoPure water prior to titration. Polymer solutions were first titrated to pH~11.5 using 1M NaOH. Five microliter aliquots of 1M HCl were added to polymer solutions and the pH was recorded.

2.4 DISCUSSION

One motivation behind amine acetylation of PAMAM dendrimers was to promote polymer-siRNA unpackaging in cells. That is, self-assembled vectors for siRNA delivery must associate strongly enough to remain intact during cellular binding and entry, yet must dissociate at some point within cells to release their cargo. Previous studies have identified vector unpackaging to be an important barrier to polymeric gene and siRNA delivery [20, 138, 139]. Specifically, correlations have been observed between the release of DNA in competitive displacement assays in vitro and transfection efficiency in cells [138]. Furthermore, others have found that gene transfection was improved by increasing fractions of amine acetylation of PEI, and this result was attributed to decreased polymer-

DNA interactions resulting in enhanced intracellular polyplex dissociation [20]. Previous work by our group has also reported a positive correlation between intracellular oligonucleotide levels (and gene silencing) and enhanced complex dissociation among various molecular weights of PEI [136].

To reduce PAMAM/siRNA interactions in this work, we employed partial amine acetylation of PAMAM dendrimers. The heparin competition assay showed that unmodified generation 5 PAMAM dendrimer (molecular weight ~ 28 kDa) exhibited less dissociation of siRNA than did 25 kDa PEI. Given that 25K PEI possesses a high charge density and exhibits strong association with oligonucleotides [136], the even greater resistance of G5 PAMAM to heparin dissociation can be interpreted as indicating a poor tendency of the dendrimer to dissociate from siRNA. As hypothesized, greater dissociation was observed upon primary amine acetylation of PAMAM, which surpassed that of 25 kDa PEI at a high fraction (60%) of primary amine acetylation. However, polyplex size analysis demonstrated that stable particles of high positive zeta potential were formed between acetylated dendrimers and siRNA, with a slight reduction in both at relatively high fraction (60%) of primary amine acetylation. This suggests that amine acetylation did not destabilize dendrimer/siRNA complexes, but rather facilitated the ease of dissociation of siRNA from the polymer complex in the face of an anionic competitor.

In addition to promoting polyplex dissociation by amine acetylation, we also expected to reduce cytotoxicity by partial charge neutralization. Cytotoxicity often correlates with a high charge density, and is a marked problem with highly cationic PAMAM dendrimers. Previous work has shown a reduction in cytotoxicity upon amine acetylation of cationic polymers [129]. Indeed, we observed a linear decrease in

cytotoxicity upon amine acetylation of PAMAM dendrimers. Thus, "tuning" of cationic polymer charge is a useful design principle in modulating both vector unpackaging and cytotoxicity.

Another important barrier to the cellular delivery of nucleic acids is their sequestration in acidic endosomes. Cationic polymers with titratable amines are thought to mediate endosomal escape by buffering in the pH range of 5-7, leading to osmotic pressure buildup and membrane permeability via the "proton sponge" effect [17]. In the current study, we found that primary amine acetylation somewhat decreased the pH buffering capacity of dendrimers by removing primary amine groups. This decrease in endosomal buffering capacity induced by amine acetylation is likely responsible for the decreased siRNA delivery, as the presence of a buffering agent appeared to improve cellular distribution of antisense molecules delivered by acetylated dendrimers.

It is important to note that acetylation of PEI was successful for delivery of plasmid DNA [19, 20] in contrast to the present study in which amine acetylation of PAMAM was employed for the delivery of siRNA. Since siRNAs are much shorter and thus less polyvalent than plasmid DNA, it is likely that siRNA will more easily dissociate from a cationic polymer than would a large, anionic plasmid DNA, making polyplex dissociation a potentially less critical step in the delivery process [11]. Further, it has been shown that the properties of polyplexes formed by dendrimers and RNA depend significantly on the size of the RNA molecule with more stable particles being formed with large RNA molecules due to cooperative multivalent interactions[100]. These differences between polymers and their interactions with different types of nucleic acids highlight the importance of developing a more comprehensive and quantitative

understanding of intracellular delivery mechanisms so that data from various delivery systems and studies can be interpreted and used to rationally design nucleic acid carriers .

In summary, cationic dendrimers are promising architectures for use as nucleic acid delivery vectors. Their highly organized, cationic structure with functionalizable amine groups provides them with molecular properties that are favorable for efficient nucleic acid delivery. Neutralizing a fraction of primary amines by acetylation in this study did, as expected, promote polyplex unpackaging *in vitro*. Additionally, a reduction in cytotoxicity was noticed upon acetylation. However, a reduction in pH buffering was also observed, possibly resulting in decreased siRNA delivery to tumor cells. The addition of a buffering agent chloroquine promoted favorable cellular distribution of nucleic acids delivered by dendrimers, indicating that endosomal escape is a substantial barrier to siRNA delivery by these polymers. Others efforts to modify PAMAM dendrimers for gene or siRNA delivery have also reported success in decreasing cytotoxicity but difficulties in achieving active nucleic acid delivery[128]. This observation demonstrates both the importance of endosomal buffering to siRNA delivery as well as the advantages of charge reduction including reduced cytotoxicity and enhanced vector dissociation. The next generation of dendrimers for siRNA delivery will need to integrate charge reduction of dendrimers without compromising their endosomal buffering capacity.

CHAPTER 3

PAMAM-RGD CONJUGATES ENHANCE SIRNA DELIVERY THROUGH A MULTICELLULAR SPHEROID MODEL OF MALIGNANT GLIOMA

This chapter is published and has the following citation:

Waite, C.L. & Roth, C.M. PAMAM-RGD Conjugates Enhance siRNA Delivery Through a Multicellular Spheroid Model of Malignant Glioma. *Bioconjugate Chemistry* **20**, 1908-1916 (2009)

ABSTRACT

Generation 5 poly(amidoamine) (PAMAM) dendrimers were modified by the addition of cyclic RGD targeting peptides and were evaluated for their ability to associate with siRNA and mediate siRNA delivery to U87 malignant glioma cells. PAMAM-RGD conjugates were able to complex with siRNA to form complexes of approximately 200 nm in size. Modest siRNA delivery was observed in U87 cells using either PAMAM or PAMAM-RGD conjugates. PAMAM-RGD conjugates prevented the adhesion of U87 cells to fibrinogen coated plates, in a manner that depends on the number of RGD ligands per dendrimer. The delivery of siRNA through three-dimensional multicellular spheroids of U87 cells was enhanced using PAMAM-RGD conjugates compared to the native PAMAM dendrimers, presumably by interfering with integrin-ECM contacts present in a three-dimensional tumor model.

3.1 INTRODUCTION

Gene silencing using RNA interference (RNAi) is a powerful platform technology being developed clinically for a variety of diseases including cancer, where it is typically considered as part of a multi-pronged approach [5, 140]. While RNAi holds promise as an anticancer therapeutic modality, the ability to efficiently and safely deliver siRNA molecules to cells is the main barrier limiting its widespread clinical use [12]. The use of synthetic, non-viral delivery vectors such as polymers and liposomes has shown promise in mediating cellular delivery of siRNA molecules [141]. Benefits of synthetic delivery vectors include their ability to be manufactured on a large-scale, low immunogenic response compared to their viral counterparts, and the ability to chemically tailor their structure for a particular application.

Poly(amidoamine) (PAMAM) dendrimers are a family of highly branched, synthetic polymers that have garnered interest as potential delivery vectors for nucleic acids, recently including siRNA. Several studies have demonstrated successful delivery of siRNA using PAMAM dendrimers or their derivatives [18, 122, 123, 127, 142, 143]. The branched architecture of dendrimers makes them particularly attractive for targeted delivery applications as they can present targeting ligands in a manner favorable to promote multivalent binding to target cellular receptors. Multivalent ligand presentation from PAMAM dendrimers has been demonstrated for various targeted systems including folic acid [42], mannose and glucose [144, 145].

Integrin proteins are a family of cell-surface receptors, several of which are known to be over-expressed on the surface of cancer cells. The $\alpha_v\beta_3$ integrin is particularly known for its role in cancer progression and is overexpressed in melanomas,

glioblastoma, ovarian, breast, and prostate cancers [28]. The high-affinity interaction between RGD peptides and cancer-related integrins has led to the widespread use of RGD peptide sequences as ligands for integrin-targeted drug and gene delivery applications [29]. Several examples of PAMAM dendrimer-RGD conjugates have been reported to enhance the delivery of imaging agents to target carcinoma cells [50, 146]. PAMAM-RGD conjugates have also been found to mediate cellular binding and adhesion [147, 148].

As significant promise has been shown for PAMAM-RGD conjugates in drug delivery and imaging applications, the goal of this study was to evaluate this bioconjugate for use as a siRNA delivery vector. Specifically, we sought to investigate the effects of extent of ligand functionalization (multivalency) on cellular delivery. To this end, the ability of dendrimers to deliver siRNA to malignant glioma cells with varying extents of RGD conjugation was evaluated. Furthermore, we hypothesized that the ligand presentation would have a greater impact on delivery in a three-dimensional tumor, where the interactions between the delivery vector, extracellular matrix and cells are more pronounced. To evaluate this hypothesis, the ability of PAMAM-RGD conjugates to interfere with cell-ECM interactions and to mediate siRNA delivery in a three-dimensional cell-culture model of malignant glioma was studied.

3.2 **EXPERIMENTAL PROCEDURES**

3.2.1 **Materials.**

A 22 nt siRNA sequence previously identified as an effective inhibitor of pd1EGFP expression [134] (sense strand: 5'-UUG UGG CCG UUU ACG UCG CCG U-3',

antisense strand: 3'-UGA ACA CCG GCA AAU GCA GCG G-5') and an irrelevant siRNA sequence (targeted against firefly luciferase; sense strand: 5'-CUU ACG CUG AGU ACU UCG A dTdT-3', antisense strand: 5'-UCG AAG UAC UCA GCG UAA G dTdT-3') were purchased from Dharmacon (Chicago, IL). A fluorescently labeled anti-GFP siRNA sequence (5' Cy3 end modified on the sense strand) was purchased from Integrated DNA Technologies (Coralville, IA, USA). A 20 nt phosphorothioated antisense oligonucleotide targeted against pd1EGFP with a fluorescent label was also purchased from Integrated DNA Technologies (5'- Cy5-TTG TGG CCG TTT ACG TCG CC -3'). The lyophilized powder was resuspended according to the manufacturer's protocol before use. Generation 5 PAMAM dendrimers with an ethylenediamine core and amine terminal groups were purchased as a 5 wt% solution in methanol from Dendritech (Midland, MI). Unless otherwise stated, all chemicals were purchased from Sigma, and all cell culture products were obtained from Invitrogen (Carlsbad, CA).

3.2.2 **Conjugation of PAMAM dendrimers with RGD peptides.**

Approximately 6 mg of dry generation 5 PAMAM dendrimers were obtained after the removal of methanol from the storage solution using rotary evaporation. The polymer residue was dissolved in ~2 mL of phosphate buffered saline (PBS) with 1 mM EDTA (reaction buffer). Various molar equivalents (6, 9, 12, or 15) of a Sulfo-LC-SPDP crosslinker (Pierce, Rockford, IL) were added to the polymer solution to yield SPDP-activated PAMAM after a 2 hour reaction at room temperature. Dialysis with a 10,000 MWCO Slide-A-Lyzer dialysis cassette (Pierce, Rockford, IL) was performed against 1 liter of reaction buffer overnight to remove any unreacted SPDP crosslinker. Following dialysis, 1.5 molar equivalents (to SPDP groups added) of cyclic RGDfC peptide

(Peptides International, Louisville, KY) were added to the SPDP-activated PAMAM dendrimers to yield PAMAM-RGD conjugates after an overnight reaction (Figure 2.1). Following conjugation, 10,000 MWCO dialysis was performed against reaction buffer followed by water to remove any unreacted RGD peptide. Purified PAMAM-RGD conjugates were lyophilized overnight to obtain a white powder.

3.2.3 **UV spectrophotometry of PAMAM-RGD conjugates.**

A series of PAMAM-RGD conjugates was characterized using UV spectrophotometry to determine the number of RGD peptides conjugated to each dendrimer. A disulfide reducing agent, DTT, was used to cleave the disulfide bond present in the SPDP crosslinker to release pyridine-2-thione (P2T), which has a UV absorbance at 343 nm. This analysis of pyridine-2-thione release was first performed on the intermediate product, PAMAM-SPDP and used to quantify the average number of SPDP groups added to each dendrimer. After removal of excess SPDP by dialysis, 50 μL of the PAMAM-SPDP solution was added to 450 μL of reaction buffer, and the absorbance of the solution at 343 nm was read using a Unicam UV 300 model UV spectrophotometer (Thermo Spectronics, Rockford, IL) (this reading indicated background absorbance). To the same sample, 5 μL of DTT (Pierce, Rockford, IL) (15 mg/mL) was added, and the absorbance at 343 nm was recorded after a 15 minute incubation at room temperature. The increase in UV absorbance observed after the addition of DTT corresponded to the addition of LC-SPDP groups to dendrimers. The average molar ratio of SPDP:PAMAM was calculated according to the manufacturer's protocol (Pierce, Rockford, IL). The same analysis was performed on the final PAMAM-RGD conjugate to confirm replacement of all SPDP groups with RGD peptides. After

the replacement of P2T groups by RGD peptides, an increase in UV absorbance at 343 nm was not observed.

3.2.4 **MALDI-TOF Mass Spectrometry.**

PAMAM-RGD conjugates were dissolved in water at a concentration of 1 mg/mL prior to MALDI-TOF MS analysis. A matrix solution of 2'-4'-6'-Trihydroxyacetophenone monohydrate (THAP) (10 mg/mL THAP in 50%ACN/(50% H_20 with 0.1% trifluoroacetic acid)) was used. The matrix solution and PAMAM dendrimers were mixed 1:1 by volume, and spotted on a 100-well stainless steel sample plate. MALDI-TOF MS analysis was performed in linear positive mode of a Voyager DE Pro instrument (Applied Biosystems) using 25 kV accelerating voltage, 95% grid voltage, 0.3% guide wire voltage, and a delay time of 700 ns. For each spectrum 75 shots were taken, and a minimum of 3 spectra were accumulated for each sample.

3.2.5 **PicoGreen assay for PAMAM/siRNA complexation.**

Complexes were prepared at various charge ratios by mixing equal volumes of PAMAM with siRNA in PBS. Charge ratios (N/P) were calculated as a ratio of the number of primary amines in the polymer to the number of anionic phosphate groups in the siRNA. The samples were then vortexed and incubated at room temperature for 15 minutes to ensure complex formation. The complexes were prepared at a final siRNA concentration of 0.2 μg of siRNA/100 μL of solution and varying polymer concentrations to reach the desired charge ratio. One hundred microliters of each complex were transferred to a 96-well (black-walled, clear-bottom, non-adsorbing) plate (Corning, NY, USA). A total of 100 μL of diluted PicoGreen dye (Molecular Probes, Eugene, OR) (1:200 dilution in Tris-EDTA (TE) buffer) was added to each sample. Fluorescence

measurements were made after a 30 minute incubation at room temperature using a DTX800 Multimode Detector (Beckman Coulter, CA), at exitation and emission wavelengths of 485 and 535 nm, respectively. All measurements were corrected for background fluorescence from a solution containing only buffer and PicoGreen dye.

3.2.6 **Dynamic light scattering.**

Dynamic light scattering (DLS) analysis was performed using a Malvern Instruments Zetasizer Nano ZS-90 instrument (Southboro, MA) with reproducibility being verified by collection and comparison of sequential measurements. Polymer/siRNA complexes (siRNA concentration = 100 nM, N/P=15) were prepared using purified water (resistivity=18.5 MΩ-cm). DLS measurements were performed at a 90 ° scattering angle at 37 °C. Z-average sizes of three sequential measurements were collected and analyzed approximately 30 minutes after the polymer/siRNA complexes were formed.

3.2.7 **Cell culture.**

U-87 MG cells (ATCC HTB-14) were maintained in D-MEM medium supplemented with 10% fetal bovine serum (FBS), L-glutamine, and penicillin-streptomycin solution. A U87 cell line containing a stably integrated destabilized EGFP (d1EGFP) transgene (U87-d1EGFP) was generated as described previously [18] and was maintained under constant selective pressure by G418 (500 ug/mL), and the growth medium was supplemented with sodium pyruvate and non-essential amino acids. All cell lines were cultivated in a humidified atmosphere of 5% CO_2 at 37ºC.

3.2.8 **Multicellular spheroid formation.**

Multicellular tumor spheroids (MCTS) were formed from the U87 or U87-d1EGFP malignant glioma cell lines using the hanging drop method as described

previously [81]. Cells from a confluent T-25 flask were detached using trypsin-EDTA and resuspended in 5mL of culture medium to a concentration of ~10^6 cells/mL. Twenty microliter droplets of this concentrated cell suspension were deposited into the lid of a petri dish. The bottom of the petri dish was filled with 2 mL of cell culture medium to facilitate moisture transfer. The lid containing the drops was inverted over the petri dish to form hanging drops. The petri dish was placed in the incubator for a period of 3 days, after which visible cell aggregates were formed in the hanging drops. The cell aggregates were harvested from the hanging drop suspension by adding ~2mL of culture medium to suspend the aggregates. The cell aggregates were individually transferred in 100 μL of culture medium to wells of a 96-well tissue culture plate that was base-coated with 2% agarose. After 24 hours on agarose, cell aggregates formed MCTS of diameters ranging from ~600-800 μm and were subjected to siRNA transfection and confocal imaging analysis.

3.2.9 **SiRNA delivery assay.**

U87-d1EGFP cells were plated at a density of 1.5 x 10^5 cells/well in 12 well plates ~18 hours prior to transfection. Prior to treatment of cells, PAMAM/siRNA complexes were prepared as described above in 200 μL of PBS (N/P=15). PolyFect (Qiagen, Valencia, CA), a commercially available dendrimer transfection reagent, was used as a positive control. Eight hundred microliters of OptiMEM medium was mixed with each sample to obtain a final siRNA concentration of 100 nM. The serum-containing culture medium was aspirated from the cells, and each well was treated with 1 mL of the PAMAM/siRNA complexes in OptiMEM medium. After a 4 hour incubation period, the transfection mixture was replaced with serum-containing culture medium and

maintained under normal growth conditions until the cells were assayed for fluorescence by flow cytometry at various time points after initial treatment. For cells being analyzed for GFP fluorescence, unlabeled siRNA was utilized. To determine intracellular siRNA uptake, non-transformed U87 cells were treated with a Cy-3 labeled siRNA.

To analyze siRNA delivery in multicellular tumor spheroids, a similar transfection protocol was performed as with cells on 12-well tissue culture plates. MCTS transfections were performed in 96-well plates that had been base-coated with 2% agarose. Transfections were performed in a total volume of 150 µL in OptiMEM medium. MCTS were exposed to a Cy3-labeled siRNA sequence to enable confocal imaging of siRNA localization throughout the spheroids at both 4 and 24 hours post-transfection. Spheroids generated from the U87-d1EGFP cell line were treated with a Cy5-labeled (red) antisense oligonucleotide (AON) targeted against d1EGFP so that the label and transgene fluorescence spectra would not overlap. U87-d1EGFP spheroids were imaged at 24, 48, and 72 hours after the initial treatment to evaluate both GFP silencing and localization of the AON with the various dendrimer/ODN formulations conjugates.

3.2.10 **Flow cytometry.**

Cells were washed with PBS, detached with trypsin-EDTA, and collected in growth medium, before they were pelleted by centrifugation for 3.5 min at 200 *g* and resuspended in 150 µL PBS. Samples were maintained on ice before being subjected to flow cytometry analysis. Ten thousand cells were analyzed on a FACSCalibur two-laser, four-color flow cytometer (BD Biosciences) for GFP fluorescence (FL-1) or Cy3

fluorescence (FL-2).CellQuest software was used to acquire and analyze the results. Viable cells were gated according to their typical forward/side scatter characteristics.

3.2.11 **Competitive cell adhesion assay.**

High-binding 96-well plates (Nunc Maxi SORP) were coated with fibrinogen protein by adding 100 μL/well of fibrinogen solution (100 μg/mL in PBS) overnight at 4ºC. The next day, the plate was blocked with 150 μL/well of bovine serum albumin (BSA) solution (10 mg/mL in PBS) for 1 hour at 37ºC. The plate was washed in triplicate with cold PBS. Ten microliters of test compounds (RGD-conjugated polymers) at various concentrations were added to wells of the fibrinogen-coated plate on ice in triplicate. Following the addition of test compounds, 90 μL of U87 cells in culture medium (330,000 cells/mL) were added to the plate, and mixed thoroughly with a multi-channel pipette. The plate was incubated at 37ºC for 3 hours until the cells attached to the plate. Non-adherent cells were washed from the plate with PBS, and adherent cells were fixed by the addition of 100 μL of 70% ethanol for 30 minutes at room temperature. Following one wash with PBS, 100 μL of PicoGreen dye in TE buffer were added to the plate for 30 minutes to detect adherent cells. PicoGreen fluorescence was measured using a DTX800 Multimode Detector (Beckman Coulter, CA), at excitation and emission wavelengths of 485 and 535 nm, respectively. PicoGreen fluorescence values of wells treated with a RGD-containing competitor was normalized to wells that received no competitor (maximum cells adhering). Data analysis and calculation of IC_{50} values was performed using GraphPad Prism 4 software (GraphPad Software, La Jolla, CA).

3.2.12 **Confocal microscopy of multicellular spheroids.**

Uptake and distribution of Cy3-labeled siRNA or Cy5-labeled AS ODN in U87 MCTS or U87–d1EGFP MCTS, respectively, were analyzed using confocal microscopy. Imaging was performed at various time points after siRNA transfection of spheroids using an Olympus IX81 model confocal microscope (Olympus, Center Valley, PA). Images of MCTS were performed directly on agarose-coated 96-well plates at 10X magnification. Z-stack imaging was performed to take image slices through spheroids at 20 μm intervals for a total depth of 100 μm. The following excitation and emission wavelengths were used to detect the fluorophores used in this study: GFP fluorescence (excitation= 482 nm, emission= 536 nm), Cy3 siRNA (excitation= 543 nm, emission=593 nm), and Cy5 AS ODN (excitation= 628 nm, emission= 692 nm).

3.2.13 **Image analysis of multicellular spheroid fluorescence.**

The fluorescence intensities of both the Cy5 and GFP channels of the confocal images of the U87-d1EGFP spheroids were quantified using ImageJ software [149].

3.2.14 **Statistics.**

All statistical comparisons among treatment groups were performed using a one way ANOVA test with Fisher's all-pairs post hoc comparison test. To compare among IC_{50} fits in the cell adhesion assay, a Monte Carlo procedure was employed. The standard error of measurement was used to randomly perturb individual experimental values around their means. Fits were then applied to the perturbed data and compared across groups. This procedure was repeated 10,000 times. If a particular group had a lower IC50 in at least 95% of Monte Carlo trials, then the fitted IC50 value was considered significant at the $p < 0.05$ level.

3.3 **RESULTS**

3.3.1 **Reaction and characterization of PAMAM-RGD conjugates.**

Generation 5 PAMAM dendrimers were conjugated with various amounts of a cyclic RGD targeting peptide, RGDfC, using a Sulfo-LC-SPDP crosslinker in a scheme depicted in Figure 3.1. The PAMAM-RGD conjugates were characterized using UV spectrophotometry at various stages during the crosslinking process. For this purpose, a disulfide reducing agent, DTT, was added to the conjugates to break the disulfide bond present in the SPDP crosslinker, enabling the release of pyridine-2-thione, a molecule that is UV active at 343 nm. PAMAM dendrimers were first reacted with various molar equivalents (6, 9, 12, or 15) of Sulfo-LC-SPDP to attain SPDP-activated PAMAM. After the addition of DTT, increasing amounts of pyridine-2-thione absorbance were detected with increasing SPDP:PAMAM ratios, as expected (Figure 3.2A). This information was used to calculate the average molar ratios of SPDP:PAMAM yielded in this reaction, ranging from approximately 2 to 10 SPDP:PAMAM. Following reaction with cyclic RGD peptides, the pyridine-2-thione absorbance decreased back to baseline, indicating complete replacement of pyridine-2-thione groups from the crosslinker with RGD peptides. The resulting PAMAM-RGD conjugates are denoted by their experimentally determined extents of RGD conjugation (rounded to whole numbers) as G5-2RGD, G5-3RGD, G5-7RGD, and G5-10RGD.

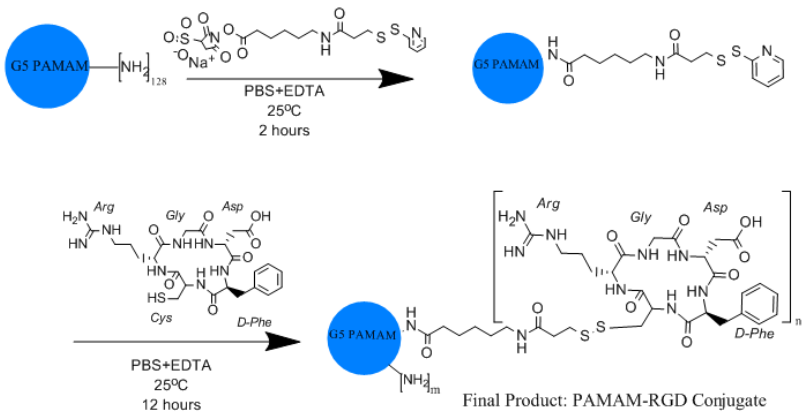

Figure 3.1. PAMAM dendrimers are reacted with Sulfo-LC-SPDP to yield SPDP-activated PAMAM intermediates. SPDP-activated PAMAM was reacted with cyclic RGD peptides to obtain final PAMAM-RGD conjugates.

A

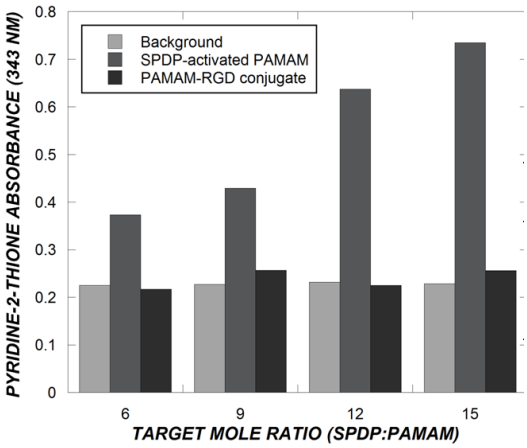

B

Theoretical Molar Ratios	Actual Ratios by DTT Release	Sample Name
6	2.12	G5-2RGD
9	3.21	G5-3RGD
12	7.07	G5-7RGD
15	9.65	G5-10RGD

Figure 3.2. UV detection of pyridine-2-thione release from SPDP-activated PAMAM and PAMAM-RGD conjugates after the addition of DTT (A). Experimentally determined extents of RGD conjugation and sample names(B).

PAMAM-RGD conjugates were further characterized using MALDI-TOF mass spectrometry to confirm conjugation of RGD peptides to the dendrimers. Several previous studies have successfully utilized MALDI-TOF MS to characterize PAMAM bioconjugates by observing an increase in molecular weight of dendrimers upon conjugation to other molecules [150, 151]. As expected, a shift to the right of MALDI MS curves correlated to increased extents of RGD conjugation, indicating an increase in the molecular weight of the conjugates (see Appendix). As MALDI MS has been shown to underestimate the actual molecular weight of high-generation dendrimers [150], it was not used to estimate the molecular weight of PAMAM-RGD conjugates, but as a tool to confirm successful crosslinking of RGD to PAMAM dendrimers. The molecular weight of the PAMAM-RGD conjugates was calculated instead from the RGD crosslinking extent determined using UV spectrophotometry as described above.

3.3.2 **Characterization of dendrimer/siRNA complexes.**

To facilitate siRNA delivery, cationic polymers such as PAMAM dendrimers should form electrostatic complexes with anionic siRNA molecules. The ability of PAMAM-RGD conjugates to complex with siRNA was evaluated using a dye exclusion assay. The amount of unbound siRNA in solutions of PAMAM/siRNA was determined by measuring the fluorescence of a commercially available dye, PicoGreen, that fluoresces upon binding to double stranded DNA or RNA. The fluorescence intensity of PicoGreen decreased following incubation of increasing amounts of polymer with added to a fixed amount of siRNA, indicating association of siRNA with the polymer (Figure 3.3). For all dendrimer conjugates tested, most of the PicoGreen fluorescence was quenched by N/P=10, indicating that the dendrimers had formed complexes with siRNA.

At lower charge ratios, however, it is possible to discern trends in siRNA complexation as a function of RGD crosslinking extent, with higher extents of RGD conjugation corresponding to somewhat less siRNA complexation. To ensure the presence of stable complexes, N/P = 15 was chosen for subsequent experiments.

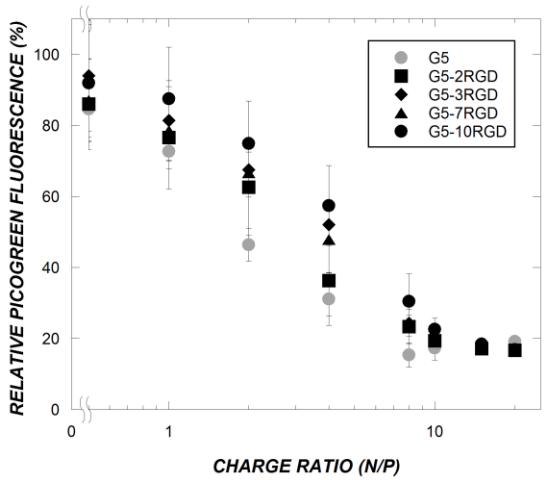

Figure 3.3. PAMAM/siRNA complexes were formed in PBS (final siRNA concentration= 2 μg/mL) and allowed to incubate for 15 minutes before measurement. Relative PicoGreen fluorescence corresponds to unbound siRNA present in solution. The data represent mean $\pm$ SEM ($n \geq 3$).

Having demonstrated the ability of PAMAM-RGD conjugates to complex with anionic siRNA, the characteristics of the siRNA/PAMAM complexes formed at N/P = 15 were evaluated further by dynamic light scattering (DLS) measurements. Particle size analysis by DLS showed the formation of ~200 nm complexes between dendrimers and siRNA, regardless of extent of RGD conjugation (Table 3.1).

Sample	Particle diameter (nm)
G5	192 ± 3
G5-2RGD	166 ± 36
G5-3RGD	187 ± 14
G5-7RGD	193 ± 14
G5-10RGD	182+5

Table 3.1. Particle diameter of dendrimer/siRNA complexes as determined by dynamic light scattering. The data represent mean ± standard deviation (n=3).

3.3.3 **siRNA delivery and GFP silencing in U87 cells.**

The ability of PAMAM-RGD conjugates to deliver siRNA to U87 cells and elicit a gene silencing response was evaluated. A fluorescently labeled siRNA sequence was delivered to U87 cells with PAMAM-RGD conjugates to evaluate siRNA uptake into cells, which was assayed using flow cytometry. Separately, but under the same conditions, a siRNA sequence targeted against the short half-life green fluorescent protein, d1EGFP, was delivered to U87–d1EGFP cells, and relative GFP expression was assayed using flow cytometry.

Significant intracellular siRNA levels were observed 24 hours after exposure of U87 cells to PAMAM-RGD/Cy3-siRNA complexes (Figure 3.4A). If cell binding is a limiting step in dendrimer-mediated siRNA delivery, intracellular siRNA levels would be expected to increase with increasing extent of RGD conjugation onto PAMAM dendrimers, as U87 cells express $\alpha_v\beta_3$ receptors for which cyclic RGD peptides have high binding affinities [152]. In this system, a statistically significant increase in siRNA delivery was not observed upon conjugation of dendrimers with RGD peptides ($p > 0.05$).

Having observed intracellular siRNA delivery by PAMAM-RGD conjugates, the ability of the system to deliver siRNA to elicit a GFP silencing response was evaluated by flow cytometry. Modest silencing (approximately 40%) of the GFP transgene was observed in U87-d1EGFP cells using unmodified G5 PAMAM dendrimers compared to control cells receiving no siRNA treatment. The extent of GFP silencing achieved was not significantly altered after the conjugation of RGD peptides to PAMAM dendrimers ($p > 0.05$) (Figure 3.4B). An irrelevant siRNA sequence not targeted against d1EGFP was used as a control and resulted in ~20% silencing relative to no siRNA treatment. As these values are rather low and not statistically different from each other ($p > 0.05$), it appears that, even with RGD modification, uptake of G5 PAMAM dendrimers is non-specific and does not result in intracellular trafficking sufficient for robust gene silencing [18]. A commercially available dendrimer-based transfection reagent, PolyFect, was used as a positive control in this experiment and elicited ~60% GFP knockdown, which was statistically greater than that induced when the irrelevant sequence was delivered with PolyFect (Figure 3.4B).

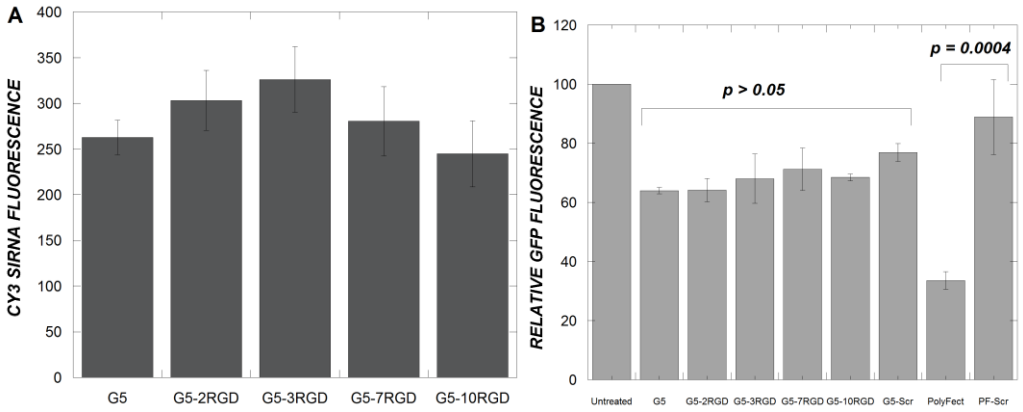

Figure 3.4. U87 cells (A) or U87–d1EGFP cells (B) were treated with PAMAM-RGD/siRNA complexes at a final siRNA concentration of 100 nM for 4 hours under serum-free conditions. Cells were analyzed using flow cytometry for Cy3 fluorescence (A) or GFP fluorescence (B) 24 hours after the initial treatment. A 5:1 wt ratio of PolyFect:siRNA was used (B). A scrambled siRNA sequence was delivered with PolyFect and G5 PAMAM dendrimer denoted by PF-Scr and G5-Scr, respectively. Data represent mean $\pm$ SEM.

3.3.4 **Competitive binding cell adhesion assay.**

Having observed that the addition of RGD peptides to PAMAM did not significantly alter the ability of PAMAM to deliver siRNA to U87 cells, probably due to significant non-specific cellular uptake of PAMAM/siRNA complexes, we sought to study whether active integrin targeting was occurring to any extent by the use of a cell adhesion assay. Here, the ability of PAMAM-RGD bioconjugates to bind specifically to $\alpha_v\beta_3$ integrin receptors on cells and prevent their adhesion to a fibrinogen-coated plate was evaluated. Polymers functionalized with various numbers of RGD peptides inhibited adhesion of U87 cells to fibrinogen protein in a concentration dependent manner (Figure 3.5A). In contrast, unmodified G5 PAMAM dendrimer did not prevent the adhesion of U87 cells to fibrinogen, demonstrating the specificity of this assay to integrin-RGD binding, and the lack of non-specific effects by PAMAM. This result indicated that in all PAMAM-RGD constructs, RGD was presented to the cells in a manner such that it binds

to $\alpha_v\beta_3$ integrin receptor proteins and is sufficient to prevent adhesion of U87 cells to the extracellular matrix protein, fibrinogen.

To discern trends in adhesion as a function of RGD conjugation extent, binding curves were fit to a competitive binding model to determine a concentration of RGD at which each dendrimer inhibited 50% of cells from adhering to the plate (IC_{50}) (Figure 3.5B). Fitted IC_{50} values were compared statistically using a Monte Carlo procedure described in the Methods. When a low number of RGD peptides was conjugated to the dendrimers (2 or 3), a significantly lower IC_{50} concentration (or a higher binding avidity) was achieved than with free RGD peptide ($p<0.05$). However, by increasing the number of peptides per dendrimer (7 or 10), a sharp increase in the IC_{50} value was observed, corresponding to a decreased net avidity of these PAMAM-RGD conjugates to the integrin protein compared to those conjugates containing just 2 or 3 RGD peptides ($p<0.05$). Further, a significant difference was observed between the IC_{50} values of dendrimers containing 7 or 10 RGDs ($p<0.05$). Using this assay, we found that three RGD peptides per dendrimer were optimal for preventing U87 adhesion to fibrinogen protein on a flat plate.

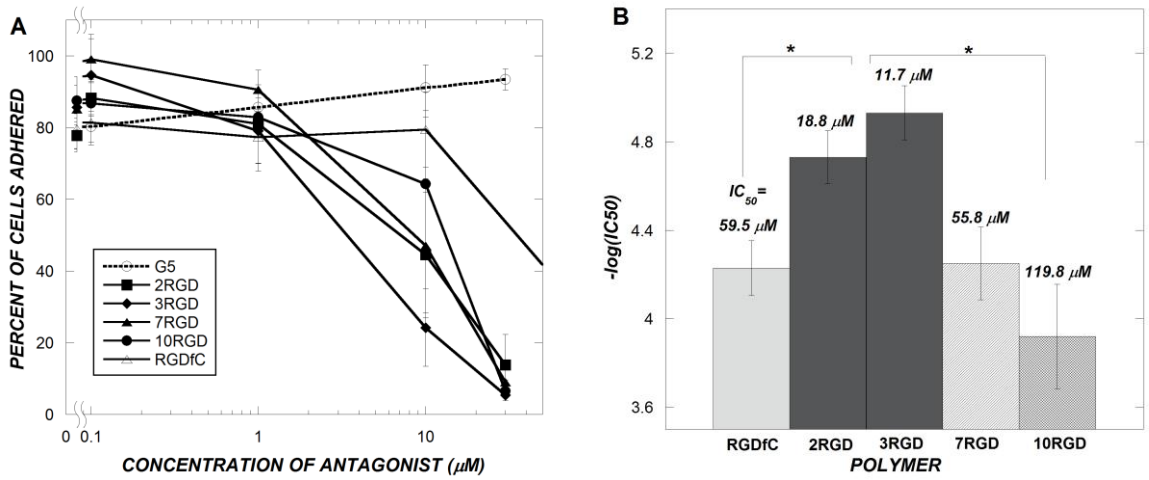

Figure 3.5. Competitive binding curves for U87 cells binding to fibrinogen coated plates in the presence of RGD-containing antagonists (A). Results of IC_{50} values obtained from binding curves for each antagonist used (B). Different colored bars represent statistically different IC_{50} values ($p<0.05$) as determined using a Monte Carlo curve fitting algorithm (B). Data represent mean $\pm$ SEM ($n \geq 3$) (A) or mean $IC_{50} \pm$ standard deviation (B).

3.3.5 **siRNA delivery through multicellular glioma spheroids.**

The strong effect of PAMAM-RGD on U87 cell adhesion suggests that these bioconjugates can interfere with integrin-ECM interactions, which would likely influence delivery in a three-dimensional tumor. To investigate this hypothesis, the ability of PAMAM-RGD to deliver siRNA through a three-dimensional multicellular tumor spheroid (MCTS) model of U87 cells was evaluated. As carcinoma cells cultured as 3D spheroids are known to secrete ECM proteins and feature active integrin-ECM interactions [72], we expected that PAMAM-RGD conjugates would be able to facilitate siRNA delivery through MCTS by interfering with integrin-ECM interactions formed by cells in three dimensions. To this end, cellular aggregates of U87 cells were formed using the hanging drop method, and aggregates were then transferred to agarose-coated tissue-culture plates to promote the formation of spheroids. U87 spheroids on agarose were treated with PAMAM-RGD/Cy3-siRNA complexes in a similar manner as for cells

cultured on standard 12-well tissue culture plates. PAMAM-RGD polymers containing either 3 or 10 RGDs were used for this study, as G5-3RGD was found to be optimal in the cell adhesion assay and G5-10RGD represents the highest extent of RGD conjugation used in this work. Confocal imaging was performed at four and twenty-four hours after transfection to evaluate the delivery and localization of Cy3-siRNA within U87 spheroids.

When delivered by G5 PAMAM dendrimers not containing RGD targeting ligands, siRNA fluorescence was observed primarily on the periphery of U87 spheroids (Figure 3.6). This result is consistent with previous studies on DNA delivery to MCTS using polyethylenimine (PEI), where poor tissue penetration using PEI/DNA complexes was observed [90]. However, when PAMAM-RGD conjugates were used, siRNA was delivered successfully throughout the spheroid volume, suggesting that tissue penetration was enhanced by the presence of RGD targeting ligands (Figure 3.6). Significant siRNA delivery to the center of spheroids was observed when using PAMAM-RGD conjugates containing either 3 or 10 RGD ligands.

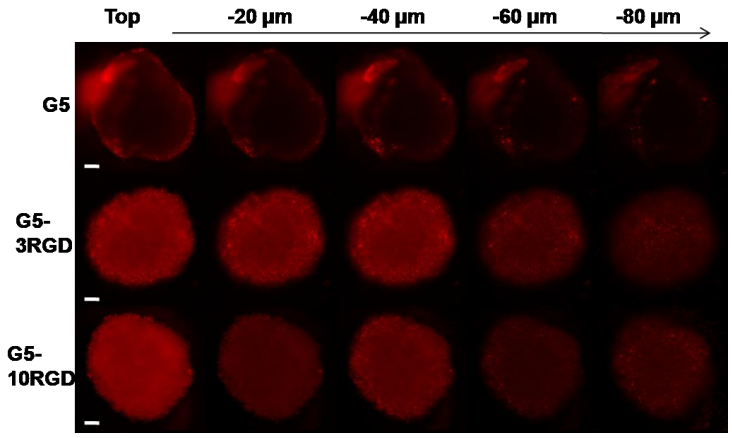

Figure 3.6. Confocal images of U87 spheroids 24 hours after treatment with dendrimer/siRNA complexes. Cy3 siRNA fluorescence is shown in red. Z-stack images were obtained starting at the top of the spheroid in 20 µm intervals for a total of 100 µm

into the spheroids. Images of each treatment were taken from three independent experiments with representative images shown here. The scale bar represents 100 μm.

Having observed the ability of PAMAM-RGD conjugates to enhance siRNA delivery through U87 MCTS, spheroids generated from U87–d1EGFP cells were used to study simultaneously the delivery of a fluorescently labeled antisense oligonucleotide (AON) and its target GFP silencing. Consistent with the Cy3-siRNA localization observed in U87 spheroids, AON fluorescence was observed primarily on the spheroid periphery when delivered by unmodified G5 PAMAM (Figure 3.7). When delivered by PAMAM-RGD conjugates, however, AON fluorescence was observed throughout the spheroid volume. A statistically significant increase in Cy5 AON fluorescence was observed in the interior of the spheroids when AON was delivered by dendrimers containing RGD peptides compared to the native dendrimers at both 48 ($p<0.002$) and 72 hours ($p<0.0001$) after treatment (Figure 3.7B). Despite the accumulation of AON within the MCTS, quantification of the GFP levels did not reveal significant gene silencing, consistent with the two-dimensional cell culture results (Figure 3.4B).

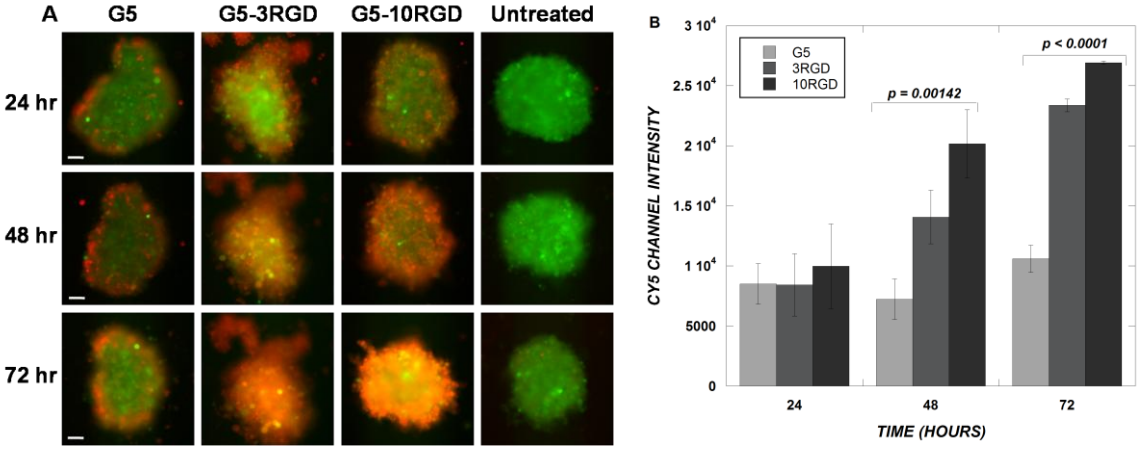

Figure 3.7. (A) Confocal images of U87 GFP spheroids treated with dendrimer/Cy5-ODN complexes. GFP fluorescence of U87 GFP cells is shown in green, and Cy5 ODN fluorescence is shown in red. All images shown are from a depth of 80 μm into each spheroid. The time points shown indicate the time post-transfection. The scale bar represents 100 μm. (B) Quantified intensities of Cy5 fluorescence. Data represent mean

channel intensities of five cross-sectional slices for each spheroid with three spheroids for each condition. Error bars represent mean ± standard deviation.

3.4 **DISCUSSION**

Integrins have proven to be promising targets for macromolecular drug and nucleic acid delivery systems for cancer. Several bioconjugate molecules containing RGD motifs have been successfully targeted to integrins to promote enhanced uptake and bioactivity in carcinoma cells. However, few studies have systematically evaluated how the number of RGD targeting ligands affects the bioactivity of targeted delivery systems. Hence, in this work, we conjugated cationic PAMAM dendrimers with various amounts of cyclic RGD targeting peptides to evaluate the ability of these bioconjugates to deliver siRNA to U87 glioma cells.

PAMAM dendrimers functionalized with varying levels of RGD peptides (2-10 RGDs/PAMAM) were able to deliver siRNA to U87 glioma cells, which express the $\alpha_v\beta_3$ integrin receptor, to elicit modest GFP silencing. However, contrary to our initial hypothesis, the attachment of RGD to PAMAM dendrimers did not enhance their ability to deliver siRNA to U87 glioma cells. This is likely due to the fact that non-specific uptake of PAMAM dendrimers, mediated by their high cationic charge density, was more considerable than integrin-mediated uptake mediated by the presence of RGD ligands. This result is consistent with other literature reports that have found poor active tumor cell targeting from cationic polymers such as PEI and PAMAM when a short crosslinker was used to conjugate a targeting peptide [122, 153, 154]. However, in addition to enhancing uptake of macromolecules into integrin-expressing cells, RGD targeting strategies can serve other purposes, such as interfering with integrin-mediated tumor cell adhesion to

ECM proteins [155]. This in turn may affect delivery of cargo in a tissue as opposed to a two-dimensional cell culture.

The integrin $\alpha_v\beta_3$ is intimately involved in tumor cell growth, proliferation, and angiogenesis. Thus, the ability to interfere specifically with the activity of this integrin could help to slow tumorigenesis in malignant glioma, and indeed a cyclic RGD peptide, Cilengitide, is undergoing clinical trials for glioma therapy [38, 39]. The PAMAM-RGD conjugates developed in this study inhibited the adhesion of U87 cells to the extracellular matrix protein, fibrinogen. A trend in inhibition of adhesion was observed as a function of RGD conjugation extent, with a maximum inhibition of cell adhesion observed with 3 RGD/PAMAM. Thus, a pronounced effect of RGD conjugation was observed in this cell adhesion model, contrasting the results obtained for siRNA delivery in which a trend was not observed as a function of RGD conjugation. Hence, the results of this assay support the ability of the PAMAM-RGD conjugates to perform active integrin binding.

MCTS models for cancer are garnering significant attention for anticancer drug screening as they mimic the microenvironment of tumors found *in vivo* more accurately than standard two-dimensional culture models [73, 82], and they have recently been shown to display angiogenic phenotypes akin to those observed in vivo [156]. Previous studies using spheroid cell culture models to evaluate nucleic acid delivery by synthetic polymers such as PEI or lipids have found that gene delivery using these carriers was confined to the outer layers of cells in spheroids due to poor penetration through the cell-matrix network [90]. However, one study reported that conjugating lactose targeting moieties onto a polymeric micelle delivery system enabled deeper penetration of siRNA into a spheroid

model of human hepatocarcinoma [91]. Further, the presence of ECM proteins was found to inhibit the transport of nanoparticles through tumor spheroids [104]. Since PAMAM-RGD conjugates were found to interfere with cell adhesion mediated by ECM , we hypothesized that using PAMAM-RGD conjugates would facilitate deeper penetration into a spheroid model of malignant glioma than unmodified PAMAM dendrimers via RGD modulation of cell-ECM interactions present in three-dimensional culture. As expected, PAMAM dendrimers conjugated with either 3 or 10 RGD peptides significantly improved the PAMAM-mediated delivery of siRNA to the spheroid interior compared to the native G5 dendrimer, suggesting that the addition of RGD peptides was able to overcome the poor tissue penetration of PAMAM dendrimers through spheroids. Notably, the PAMAM-RGD conjugates, in contrast to the G5 dendrimer, continued to penetrate into the MCTS throughout the 72 hour time course of the experiment, suggesting a dynamic interaction among bioconjugate, ECM and cell. However, despite the significant increases in tumor penetration, silencing levels of GFP remained insignificant. This outcome highlights the fact that cellular accumulation is not sufficient for efficient gene silencing. The siRNA must also be internalized by the cell and trafficked efficiently intracellularly, particularly with regards to endosomal escape. Modification of the dendrimers to enhance these steps is necessary for ultimate application to tumor oncogene silencing.

A major goal of this work was to study how the number of RGD peptides on a PAMAM dendrimer affects its ability to interfere with important cell-ECM interactions. Previous studies have found that controlling RGD ligand presentation from a nanoparticle platform can significantly impact the extent of integrin-targeting that is achieved [48, 157].

Here, three RGDs per dendrimer were found to exhibit the strongest integrin-binding response using a competitive binding cell adhesion assay, and a greater number of peptides per dendrimer did not provide any additional benefit. However, in contrast to the trend observed in the competitive binding cell adhesion assay, dendrimers displaying 10 RGD peptides yielded significantly greater delivery of oligonucleotides to U87 spheroids than did dendrimers containing 3 RGD peptides. The three-dimensional architecture of the spheroids likely confers a greater advantage to dendrimers with a greater RGD multivalency, allowing for multiple contacts with ECM molecules within the MCTS. The results of this study highlight the importance of screening novel chemical entities and drug delivery systems in three dimensions.

Taken together, these results suggest that RGD-conjugated dendrimers hold promise for siRNA delivery to solid tumors. Their ability to interfere with integrin-ECM interactions can potentially enable penetration into malignant tumors to improve siRNA delivery, and they may also interfere directly with tumor angiogenesis and integrin-mediated growth signaling by malignant cells. Such multifunctional delivery systems that can modify the biological processes of cancer cells and deliver a therapeutic cargo in concert represent a new venue for cancer therapy. Due to the architecture of dendrimers with many exterior functional groups, the concept can be extended easily to incorporation of conventional drugs and/or imaging agents. Such developments will amplify the impact of siRNA on human disease.

CHAPTER 4

BINDING AND TRANSPORT OF PAMAM-RGD IN A TUMOR SPHEROID MODEL: THE EFFECT OF RGD TARGETING LIGAND DENSITY

This chapter was submitted for publication in *Biotechnology and Bioengineering* in March, 2011.

ABSTRACT

The mechanisms governing the efficient tumor spheroid penetration and transport by poly(amidoamine) (PAMAM) dendrimers displaying varying numbers of cyclic RGD targeting peptides (2, 3, 7, or 10) were evaluated in this work. The cell-free binding affinities and cellular internalization kinetics of PAMAM-RGD conjugates to malignant glioma cells were determined experimentally, and the results were incorporated into a mathematical model to predict the transport of these materials through a multicellular tumor spheroid. The theoretical analysis demonstrated that greater RGD crosslinking may improve transport through tumor spheroids due to their decreased integrin-binding affinity. This study provides evidence that altering the density of tumor-targeting ligands from a drug delivery platform is a feasible way to optimize the tumor-penetration efficiency of an anticancer agent, and provides insight into the physicochemical mechanisms governing the relative effectiveness of these conjugates.

4.1 INTRODUCTION

The inability of anticancer drug molecules to penetrate through solid tumors presents a significant barrier to their efficacy. It is important that a drug molecule reaches all of the malignant cells in a tumor at a concentration sufficient to elicit a therapeutic effect. The distribution of both small molecule chemotherapy drugs and larger antibodies within tumors *in vivo* is confined to regions adjacent to blood vessels, leaving some regions untouched by the therapeutic compounds [57, 158].

Because of their tendency to accumulate in tumor beds due to the enhanced permeability and retention effect, the development of nanoscale anticancer therapeutics has yielded a wealth of promising results. Yet, it is important to improve the intratumoral distribution of these particles, as their relatively large size considerably slows their diffusion within tumors. Several studies have found that nanoscale drug and gene delivery systems comprised of polymers[90, 91, 94], peptides[93] , or liposomes[87 86] exhibit poor diffusion into multicellular tumor spheroids, an *in vitro* solid tumor model. The penetration of these macromolecules into tumors can be improved, however, by tuning their properties such as size and charge[86, 87], or by the incorporation of certain targeting ligands including glucosamine[99], lactose[91], or RGD peptides[92, 117].

Several studies have addressed the mechanisms governing the distribution of small molecule drugs [111] or antibody therapeutics [102, 103, 108, 158] in solid tumors, but significantly less work has been done to extend this understanding to nanoscale drug delivery systems. Some mechanisms governing nanoparticle transport through solid tumors are depicted in Figure 4.1. Reaction transport modeling has identified several important parameters that control the distribution of antibodies into solid tumors

including binding affinity, cell internalization kinetics, and rate of free diffusion [158]. A similar approach has been applied to describe the penetration of nanoparticles into tumor spheroids [104].

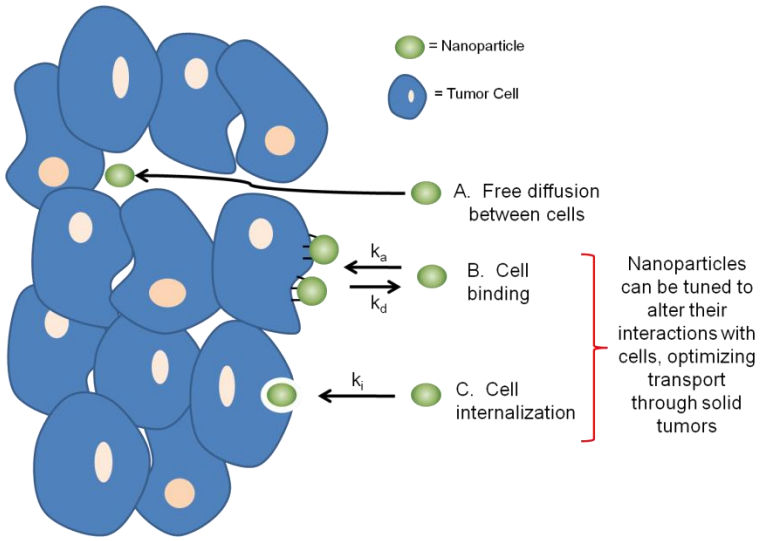

Figure 4.1. Transport mechanisms governing nanoparticle penetration through solid tumors. Nanoparticles are transported through tumors by (A) free diffusion in extracellular space, and can be inhibited by (B) cell binding and/or by (C) cell internalization. The structure of nanoparticles can be tuned to alter their interactions with cells and the tumor bed, thus optimizing their transport through solid tumors.

One benefit of utilizing synthetic drug delivery vehicles is the ability to chemically tune their structure to control properties such as particle size, charge, and the presentation of targeting groups. As these physical properties of a nanoparticle can alter their interactions with tumor tissue by changing their effective diffusion coefficient, cellular affinity, or rate of internalization, it is possible to exploit these properties to impart favorable penetration and distribution throughout solid tumors. Our previous work showed that conjugating cyclic (RGD) to a poly(amidoamine) (PAMAM) dendrimer enhances the penetration and delivery of short-interfering RNA (siRNA) through tumors in a manner that depends on the targeting ligand density[92]. In this work, we derive insights into how the density of RGD targeting ligands affects penetration into

tumor spheroids via a biophysical approach. The effects of targeting ligand density on integrin binding affinity and cell internalization kinetics were determined experimentally, and the experimentally determined parameters were used in a reaction-transport model to estimate the distribution of these materials through a solid tumor spheroid model, which is compared with experimental data.

4.2 MATERIALS AND METHODS

4.2.1 Materials.

All reagents, buffers, and sensor chips used in surface plasmon resonance experiments were purchased from GE Healthcare (Piscataway, NJ). Unless otherwise stated, all chemicals were purchased from Sigma, and all cell culture products were obtained from Invitrogen (Carlsbad, CA).

4.2.2 Mathematical Model of Tumor Transport.

A mathematical model similar to one previously developed [104] to describe the cell binding, internalization, and diffusion of nanoparticles in a three-dimensional tumor spheroid model was utilized in this work. A key distinction for this work is that PAMAM-RGD conjugates were assumed to enter cells additively via two pathways: (1) non-specific electrostatic interactions with cells, and (2) by receptor-mediated interactions between RGD targeting peptides and cell-surface integrin proteins. The subscripts 1 and 2 indicate these respective pathways. Entry from both pathways is by endocytosis but with distinct rates and numbers of binding sites. A system of partial differential equations (Equations 1-4) was utilized to describe the diffusion of PAMAM-RGD/siRNA complexes into a tumor spheroid model of malignant glioma:

$$\frac{dC}{dt} = \frac{1}{r^2}\frac{\partial}{\partial r}\left[Dr^2 \frac{\partial C}{\partial r} \right] - \left(k_{a1} C_{s1} + k_{a2} C_{s2} \right)\left(\frac{C}{\varepsilon} \right) + k_{d1} C_{b1} + k_{d2} C_{b2} \quad (1)$$

$$\frac{dC_{bj}}{dt} = k_{aj} C_{sj} \left(\frac{C}{\varepsilon} \right) - \left(k_{dj} + k_{ij} \right) C_{bj}; \;\; j = \{1,2\} \quad (2)$$

$$\frac{dC_{sj}}{dt} = -k_{aj} C_{sj} \left(\frac{C}{\varepsilon} \right) + \left(k_{dj} + k_{ij} \right) C_{bj}; \;\; j = \{1,2\} \quad (3)$$

$$\frac{dC_i}{dt} = k_{i1} C_{b1} + k_{i2} C_{b2} \quad (4)$$

In these equations, t is the time variable, r is the radial coordinate, $C(t,r)$ is the concentration of free particles in the spheroid volume, D is the effective diffusion coefficient of particles through the spheroid, ε is the average spheroid porosity, $C_{bj}(t,r)$ is the concentration of particles bound to pathway j (where j=1 denotes non-specific sites and j= 2 denotes integrins), $C_{sj}(t,r)$ is the concentration of available sites of type j per cell, C_i (t,r) is the concentration of internalized particles (summed over both pathways), and k_{a1}, k_{d1}, and k_{i1} are the non-specific and k_{a2}, k_{d2}, and k_{i2} are the integrin-specific association, dissociation, and internalization rate constants, respectively.

The following initial and boundary conditions were applied:

At t=0 (initial condition), $C(0,r) = C_{bj}(0,r) = C_i(0,r) = 0$, $C_{s2}=C_{integrins}(1-\varepsilon)$;

At r=R (spheroid surface), $C/C_o(t,R)$=1;

At r=0 (spheroid center), $\frac{\partial c}{\partial r} = \frac{\partial c_{bj}}{\partial r} = \frac{\partial c_{sj}}{\partial r} = \frac{\partial c_i}{\partial r} = 0, \;\; \forall t$;

The effective diffusion coefficient of particles through the spheroid, D, was estimated by comparing the model output to experimental data, an approach that has been taken by others to estimate the effective diffusion coefficients of particles through biological tissues[159]. The value was fixed at one sixth of the free diffusivity, with the latter calculated using the Stokes-Einstein relationship. The average spheroid porosity, ε,

was estimated from image analysis of the spheroid architecture, and was set to $\varepsilon = 0.09$ (See Appendix). The porosity estimation was used to account for the limited space available for free, unbound polymer, C, to exist within spheroids due to their complex architecture. The concentration of integrin proteins per cell ($C_{integrins}$) was estimated from a study reporting that ~$1.1x10^4$ β_3 integrin receptors per cell are expressed on the U87 cell line [160]. The number of non-specific binding sites per cell was assumed to be similar to one previously reported[104].

Equations 1-4 were solved numerically using the pdepe function within the MATLAB R2007b software package (The Math Works, Natick, MA).

4.2.3 Cell Culture and Spheroid Formation.

U-87 MG cells were maintained in D-MEM medium supplemented with 10% FBS, L-glutamine, and penicillin-streptomycin. Cells were cultivated in an environmental chamber at 37°C and 5% CO_2. Multicellular tumor spheroids were generated using the U87 cell line by the hanging drop method as described previously[92].

4.2.4 Surface Plasmon Resonance Spectroscopy.

The binding kinetics between PAMAM-RGD conjugates and the purified human integrin protein $\alpha_v\beta_3$ (Millipore, Billerica, MA) were determined using a Biacore 3000 surface plasmon resonance (SPR) instrument (GE Healthcare Life Sciences, Piscataway, NJ). The running buffer for all SPR experiments was HBS-EP (150 mM NaCl, 3 mM EDTA, 10 mM HEPES, 0.005% P20 surfactant, pH 7.4). Prior to immobilization onto a sensor chip, the integrin protein was desalted into Hepes buffered saline (HBS) using Amicon Ultra 30K MWCO centrifugal filters (Millipore, Billerica, MA) to remove the

Tris-containing salts in the formulation provided by the manufacturer. Integrin protein was immobilized onto a channel of the sensor chip surface (CM4 sensor chip) by amine coupling using a similar method as described previously [50]. The carboxyl groups on the sensor chip surface were activated by injecting 70 µl of a 1:1 v/v mixture of 0.2 M EDC and 0.05 M NHS. Protein coupling was achieved by injection of 70 µl of integrin protein (44.9 µg/mL in 10 mM acetate buffer at pH 4) across the activated surface.

Ethylenediamine at 1 M in water was then injected to deactivate residual NHS-esters on the sensor chip. The process yielded ~1.1 ng/mm^2 (~1100 RU) of integrin protein immobilized to the sensor chip surface. A reference surface was created by activating the carboxyl groups of a blank surface with EDC/NHS followed by blocking with ethylenediamine. PAMAM-RGD conjugates were diluted in running buffer at concentrations ranging from 20-200 nM. Carboxymethyl dextran sodium salt, 10 mg/mL in 0.015 M NaCl containing 0.02% NaN_3, was added at a concentration of 1 mg/mL to minimize non-specific binding of cationic dendrimers to the anionic dextran substrate on the sensor chip surface. The dendrimer conjugates were injected at a flowrate of 10 µL/min for 3 minutes across the integrin-conjugated active surface and the reference surface. Dissociation was monitored for 90 seconds following dendrimer injection.

Due to differences in size and affinity as compared to the dendrimers, it was necessary to acquire binding sensorgrams for the free cyclic RGD peptide (cRGDfC) using a protein surface with a higher level of integrin protein immobilization (~5 ng/mm^2) on a CM5 sensor chip, which contains a higher density of dextran substrate than the CM4 chip. The cyclic RGD peptide was dissolved in HBS-EP running buffer at

concentrations of 0.125 mM and 0.25 mM and was injected over the protein and reference surfaces at 10 μL/min for 3 minutes.

The final sensorgrams were obtained by subtracting the reference surface signal from the protein-conjugated surface signal. Regeneration of the surfaces was achieved by injection of 10 mM glycine-HCl, pH 2.5 at 100 μL/min for 30 seconds after each analyte injection. The data for all analytes were analyzed by simultaneously fitting all concentrations of analyte to a 1:1 Langmuir binding model using the BIAevaluation 4.1 software package.

4.2.5 Fluorescent Labeling of PAMAM and PAMAM-RGD Conjugates.

Generation 5 PAMAM dendrimers, and the PAMAM-RGD conjugates (G5-2RGD and G5-10RGD) previously synthesized[92] were fluorescently labeled with a green dye, DyLight488 using the manufacturer's protocol (Pierce Rockford, IL). Approximately 1 dye molecule was conjugated per dendrimers, as quantified by absorbance at 493 nm.

4.2.6 Cellular Internalization Kinetic Measurements and Rate Constant Determination.

The dynamics of cellular internalization by PAMAM dendrimers and by PAMAM- RGD conjugates were studied in a cellular internalization assay using a protocol similar to one described previously[99]. U87 cells were seeded at a density of 10^5 cells/mL (400 μL/well) onto 24-well tissue culture plates and were allowed to adhere overnight. Fluorescently labeled dendrimers (500 nM in culture media) were added to the cells and were harvested at various time points (4, 10, 24, or 48 hours). the cells were

washed three times with PBS prior to cell lysis with 200 μL of Triton-X in 0.1N NaOH. Cell lysates were stored frozen at -20ºC until analysis of lysates from all time points was performed simultaneously. The dendrimer concentrations detected at each time point were determined by measuring the DyLight fluorescence of each sample with a DTX800 Multimode Detector instrument (Beckman Coulter, CA, USA). The fluorescence values were converted to polymer concentrations using a standard curve of fluorescently-labeled dendrimers.

Equations describing a single cell that binds and internalizes nanoparticles were utilized in this work to parameterize the rate of cellular internalization of PAMAM-RGD conjugates (Equations 5-10)[161, 162]. Experimental cell internalization data were fit to Equation 8 to determine the rates of internalization of PAMAM-RGDs.

$$\frac{dN_{bj}}{dt} = C_0 \sum_{j=1}^{2} k_{aj} N_{sj} - \sum_{j=1}^{2} \left(k_{dj} + k_{ij} \right) N_{bj}; \;\; j = \{1,2\} \tag{5}$$

$$N_{rj} = R_{j0} - N_{bj}; \;\; j = \{1,2\} \tag{6}$$

$$\frac{dN_{ij}}{dt} = k_{ij} N_{bj}; \;\; j = \{1,2\} \tag{7}$$

The solution of Equations 5-7 yields:

$$N_t = \sum_{j=1}^{2} N_{ij} = \alpha_1 \left[k_{i1} t + \frac{\gamma_1 - k_{i1}}{\gamma_1} \left(1 - e^{-\gamma_1 t} \right) \right] + \alpha_2 \left[k_2 t + \frac{\gamma_2 - k_{i2}}{\gamma_2} \left(1 - e^{-\gamma_2 t} \right) \right] \tag{8}$$

$$\alpha_j = \frac{k_{aj} R_{j0} C_0}{\gamma_j}; \;\; j = \{1,2\} \tag{9}$$

$$\gamma_j = k_{aj} C_0 + k_{dj} + k_{ij}; \;\; j = \{1,2\} \tag{10}$$

Where $N_{bj}(t)$ is the number of bound particles, C_0 is the initial concentration of particles, $N_{sj}(t)$ is the number of available binding sites on the cells, R_{j0} is the initial

number of available binding sites on the cells, and $N_{ij}(t)$ is the number of internalized particles for pathway *j*.

The magnitude of non-specific cell interactions by PAMAM-RGDs was assumed to be equal to that of unmodified PAMAM dendrimers (k_{a1}, k_{d1}, and k_{i1}), and was determined by fitting the cell internalization data of unmodified PAMAM to Equation 8 with $\alpha_2 = 0$. PAMAM-RGDs were then assigned additional integrin-specific rate constants (k_{a2}, k_{d2}, and k_{i2}). The integrin-specific association and dissociation rate constants for PAMAM-RGDs (k_{a2} and k_{d2}) were determined from surface plasmon resonance (SPR) biosensor experiments which measured the binding kinetics between PAMAM-RGDs and $\alpha_v\beta_3$ integrin proteins immobilized on a sensor chip. The rate of cellular internalization (k_{i2}) of PAMAM-RGD conjugates was determined by fitting cellular internalization data to Equation 8 using the curve fitting toolbox in the MATLAB R2007b software package (The Math Works, Natick, MA).

4.2.7 Statistics.

Statistical comparisons within the SPR biosensor data and for the cellular internalization kinetics were performed using a one-way ANOVA test with Tukey's all-pairs post hoc comparison test.

4.2.8 Model Assumptions and Limitations.

The following assumptions were made when using the theoretical transport model employed in this work:

1. The transport model was employed approximating the shape of the tumor spheroids as being strictly spherical. While the spheroids generated in this work were not

perfect spheres, spherical coordinates have been utilized in several previous studies describing drug transport in tumor spheroids [103, 104], and have provided a reasonable shape estimate of the spheroids to describe drug penetration in this model.

2. The modes of cell association and internalization were characterized as strictly integrin-mediated and non-specific; furthermore, they were assumed to be additive and independent. While additional distinctions might also be made (e.g. according to internalization pathway as clathrin mediated vs caveolin-mediated), only the given terms were used to avoid overfitting.

3. The mathematical expressions utilized to evaluate the cell internalization and SPR kinetic data assumed saturable binding between RGD peptides and integrin receptors based on constant total number of receptors [41]. The turnover rates of cellular receptors, especially adhesion receptors such as integrins, are typically low enough to support this assumption.

4. Constant spheroid porosity was assumed. While it is well known that tumors and tumor spheroids are complex, heterogeneous structures, our measurements did not reveal a consistent trend in porosity as a function of radial distance for the spheroids utilized in this work (see Appendix). Hence, we elected to assume a constant, average porosity value ($\varepsilon = 0.09$) rather than to utilize a complex mathematical function which may confound or skew the model predictions.

4.3 RESULTS

4.3.1 Binding affinity and kinetic measurements.

The binding interactions between PAMAM-RGD conjugates and $\alpha_v\beta_3$ human integrin proteins were studied using a surface plasmon resonance (SPR) biosensor

instrument. Sensorgrams were generated to compare the monovalent interactions between the free cyclic RGD peptide and the human integrin protein to the multivalent interactions observed when displaying multiple copies of the RGD peptide from a PAMAM dendrimer scaffold. As expected, PAMAM-RGD conjugates exhibited a greater extent of binding and a slower rate of dissociation from the integrin protein surface as compared to the monovalent RGD peptide (Figure 4.2). Similar trends have been observed by others studying multivalent presentation of small ligands from PAMAM dendrimer scaffolds [42, 50].

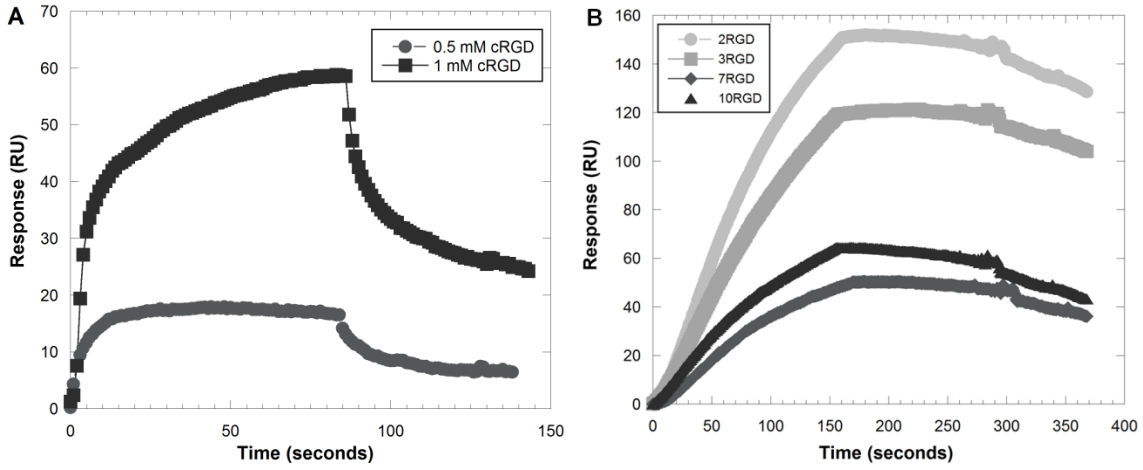

Figure 4.2. Representative SPR sensorgrams of binding interactions between monovalent cyclic RGD peptide (A) and multivalent PAMAM-RGD conjugates (B) with immobilized human integrin protein. The free RGD peptide was used at concentrations of 0.5 mM and 1 mM (A), and the PAMAM-RGD conjugates are shown at a concentration of 50 nM. The sensorgrams acquired for PAMAM-RGD and free RGD peptide were done on separate chip surfaces with differing amounts of immobilized integrin protein.

Further, the differences in binding affinities and kinetics between the multivalent PAMAM-RGD constructs displaying various numbers of the cRGD peptide (2, 3, 7, or 10) were compared. Kinetic association and dissociation rate constants (k_a and k_d) and the ratio of these constants, K_D, were determined for each polymer-peptide conjugate by

fitting the SPR sensorgram data to a Langmuir binding model (Figure 4.3). PAMAM-RGD conjugates displaying a low number of RGD peptides (2 or 3) were found to have a significantly higher binding affinity (lower K_D value) to the integrin protein than those displaying a high number of peptides (7 or 10) (Figure 4.3A). This trend is reflected in the more rapid rate of association (k_a) to the integrin protein surface for dendrimers with a low number of RGD peptides (2 or 3) than for dendrimers with a high number of peptides (7 or 10), which exhibit a slower rate of association to the protein surface (Figure 4.3B). Further, the K_D measured for PAMAM-RGD conjugates was lower than was measured for the free cRGD peptide, indicating a multivalent enhancement in affinity when conjugating cRGD onto a dendrimer scaffold (Figure 4.3A). This is consistent with previous reports demonstrating multivalent enhancement in the affinity of small molecules when they are displayed from the surface of PAMAM dendrimers[42, 50]. On the other hand, the decreased rate of association for PAMAM with higher numbers of RGD functionalized (7 or 10) suggests an interplay between avidity enhancement via multivalent binding and steric hindrance. Others have observed decreased association rates for multivalent ligands presented on nanoparticles[163] in SPR studies or decreased affinities in other binding assays[48, 164].

Unmodified G5 PAMAM dendrimers were used as a control material to evaluate non-specific binding interactions between dendrimers and the SPR sensor chip. Electrostatic interactions were observed between cationic PAMAM and the anionic dextran on the sensor chip surface. However, we were able to distinguish this non-specific response from the desired integrin-RGD interaction present with PAMAM-RGD

materials. A discussion of the studies performed to understand the electrostatic binding interactions between PAMAM and the sensor ship is provided in the Appendix.

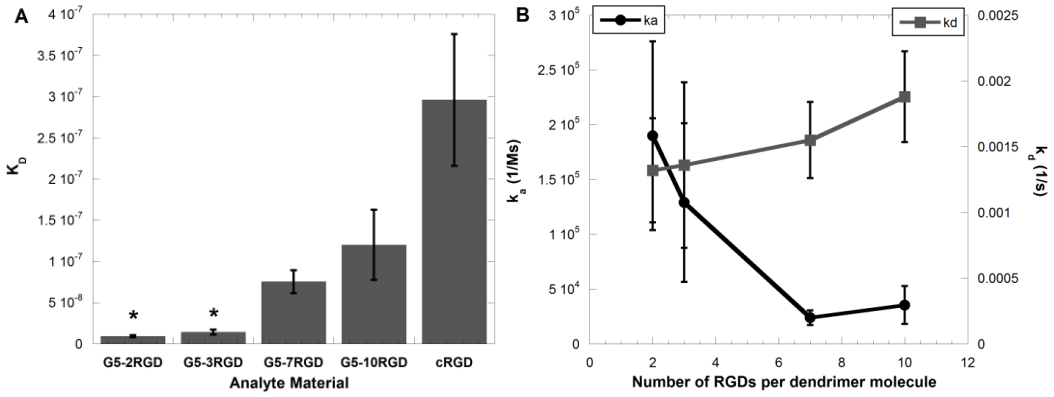

Figure 4.3. Dissociation constants (K_D) (A) and kinetic rate constants (k_a and k_d) (B) for PAMAM-RGD conjugates as determined from fitting SPR sensorgram data. Data represent average fitted values from 3 independent SPR experiments for 3 concentrations of each analyte, and error bars represent SEM. Statistically similar K_D values within the PAMAM-RGD conjugates are denoted with asterisks ($p<0.05$).

4.3.2 Cellular Internalization Dynamics.

The dynamics of cellular internalization of PAMAM and PAMAM-RGDs were evaluated by measuring the concentration of fluorescently labeled polymers internalized into U87 cells at various times over a 48 hour period. The uptake dynamics of unmodified PAMAM (G5) were compared to those of dendrimers displaying a low number (2) and high number (10) of RGD peptides. For all dendrimers studied, increasing concentration was detected within U87 cells over time, indicating cellular internalization of the polymers (Figure 4.4). Polymers displaying RGD targeting peptides (either 2 or 10) had significantly higher concentrations internalized into U87 cells ($p < 0.05$) than the unmodified parent polymer, with the polymer displaying 10

copies of the RGD peptide having the highest amount internalized after 48 hours (Figure 4.4).

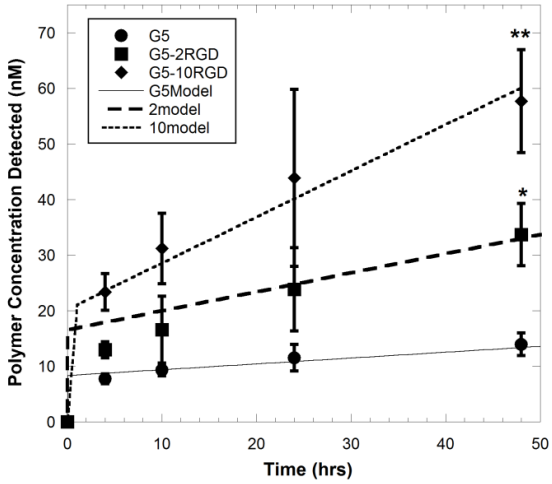

Figure 4.4. Polymer concentration detected within U87 cells after constant polymer exposure for up to 48 hours, and corresponding model fits for cell internalization. U87 cells were treated with 500 nM of fluorescently labeled dendrimers in culture medium, and cells were lysed at various time points to detect the concentration of polymers associated with the cells. Asterisks denote that all polymers were significantly different from one another by 48 h ($p < 0.05$). Data represent mean±SD (n=6).

The cellular internalization rates (k_{i1} and k_{i2}) for each polymer were determined by fitting internalization data to Equation 8 (Figure 4.4). The integrin-mediated rates of cellular internalization were about 2.5 (PAMAM-2RGD) to 5-fold (PAMAM-10RGD) more rapid than the non-specific rate (Table 4.1).

	Non-Specific Terms			***Specific integrin-mediated terms***		
	k_{a1} $((nm*hr)^{-1})$	k_{d1} (hr^{-1})	k_{i1} (hr^{-1})	k_{a2} $((nm*hr)^{-1})$	k_{d2} (hr^{-1})	k_{i2} (hr^{-1})
G5	0.184	8.93	0.0126	N/A	N/A	N/A
G5-2RGD	0.184	8.93	0.0126	0.684±0.31 (SPR)	4.77±1.42 (SPR)	0.0297±0.019
G5-3RGD	0.184	8.93	0.0126	0.465±0.26 (SPR)	4.91±2.27 (SPR)	0.0297±0.019
G5-7RGD	0.184	8.93	0.0126	0.086±0.024 (SPR)	5.57±1.04 (SPR)	0.0608±0.011
G5-10RGD	0.184	8.93	0.0126	0.127±0.062 (SPR)	9.13±1.11 (SPR)	0.0608±0.011

Table 4.1. Kinetic binding and internalization rate constants for PAMAM and PAMAM-RGD conjugates determined from fitting either SPR sensorgram curves or cell

internalization data. Non-specific terms (k_{a1}, k_{d1}, and k_{i1}) are from fitting the U87 internalization data for unmodified G5 dendrimer, and integrin-specific k_{a2} and k_{d2} terms are from SPR experiments (error is SEM). The integrin-specific internalization terms (k_{i2}) are from the U87 cell internalization data of PAMAM-RGDs (error is the 95% confidence interval).

4.3.3 Mathematical Model Results.

The experimentally determined parameters that represent the interactions between PAMAM-RGDs and U87 cells (k_a, k_d, and k_i) as well as those representing spheroid architecture (ε) were incorporated into a mathematical model of tumor transport and cell interaction to estimate the concentration profile of PAMAM-RGD particles throughout a 3-dimensional tumor spheroid. Concentration profiles calculated from the transport model predict that increasing the number of RGD peptides per PAMAM dendrimer (from 2 to 10) will result in a more homogeneous concentration profile of polymer particles across the cross-section of a spheroid (Figure 4.5). Polymers containing a low number of RGD peptides (2 or 3) show limited penetration throughout the spheroid according to the model, with a high concentration of material confined to the peripheral region of the spheroid. By increasing the number of RGD peptides to 7 or 10, a more homogeneous profile may be achieved, with a higher concentration of material being delivered to regions farther from the spheroid surface. Upon comparing the predicted concentrations of bound polymers to internalized ones, it is the differential binding to integrin receptors that likely causes the overall differences in polymer diffusion through the spheroid (Figure 4.6). As polymers with a low degree of RGD crosslinking (2RGD and 3RGD) exhibit a significantly higher integrin binding affinity than those with a high degree (7RGD and 10RGD), a higher concentration of the low crosslinking, high-affinity polymers binds to integrin leaving less polymer free to diffuse through the spheroid

(Figure 4.6A and B). As a result, free polymers with high RGD crosslinking are present at higher concentrations near the spheroid center (Figure 4.6B), and a higher concentration is internalized into tumor cells (Figure 4.6C).

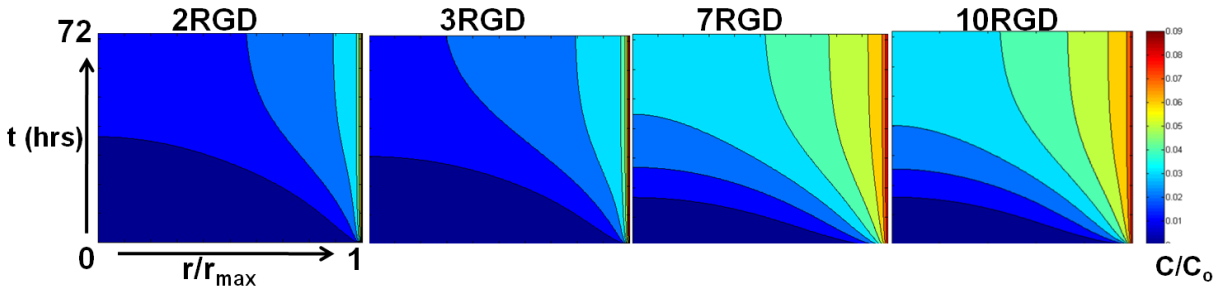

Figure 4.5. Model-predicted concentration profiles of PAMAM-RGD polymers as a function of distance from the spheroid center (r/r_{max}) and time (hours). Concentration profiles were calculated for PAMAM-RGD conjugates displaying 2, 3, 7, and 10 RGD peptides, and are reported as unbound concentrations, C, normalized by the initial polymer concentration exposed to the spheroids, C_{max}, of 100 nM.

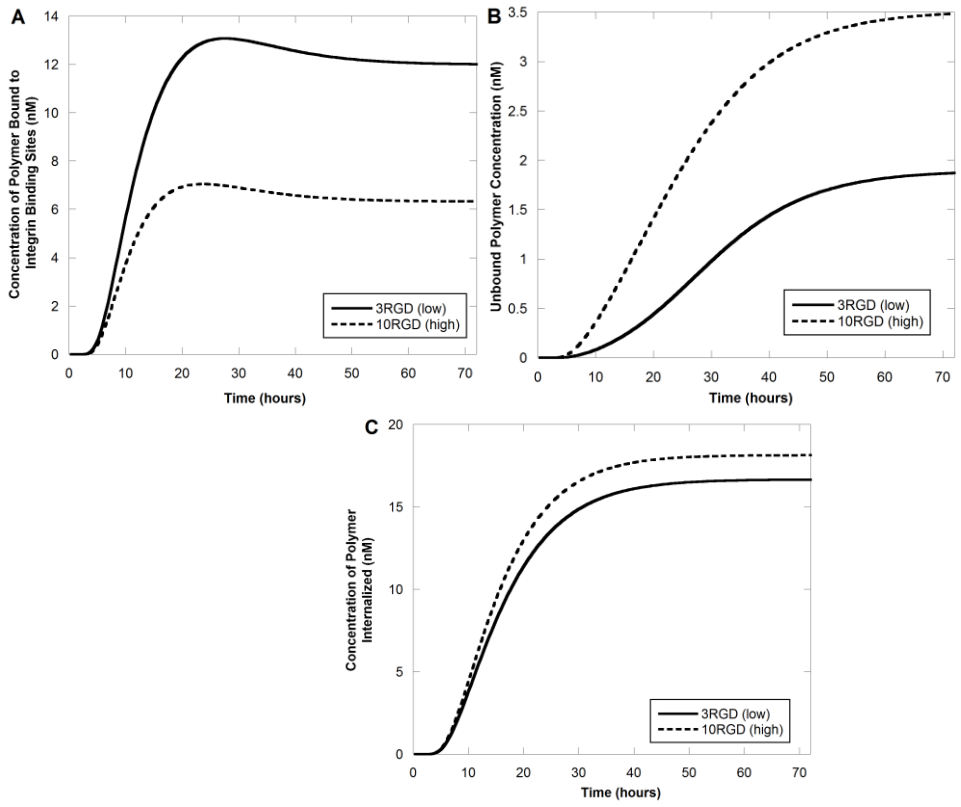

Figure 4.6. Model-predicted concentration profiles of PAMAM-RGD polymers as a function of time in the spheroid center. Concentration profiles showing the predicted concentrations of integrin-bound polymers (A), free polymers (B), and internalized polymers (C) are shown.

Further, in all simulations run, the predicted concentration of material increased in all regions of the spheroid as a function of time, as expected. These theoretical results are in good agreement with our previous experimental results that showed a significantly higher concentration of siRNA present in tumor spheroids when delivered by a PAMAM dendrimer displaying a high number (10) of RGD targeting peptides compared to one with a low number (3) of peptides (Figure 4.7).

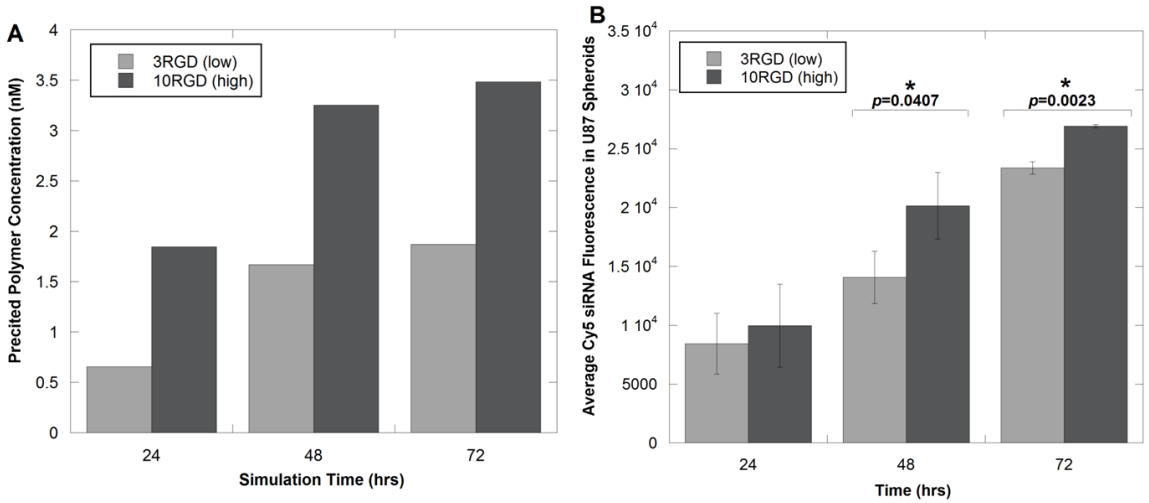

Figure 4.7. Comparison of time-dependent concentration profiles of PAMAM-RGD conjugates (A) predicted in the theoretical diffusion model with (B) average overall siRNA fluorescence intensity observed experimentally in U87 tumor spheroids (experimental data adapted from[92]). Asterisks in (B) indicate time points at which there was a statistically significant difference in fluorescence intensity between the 3RGD and 10RGD materials ($p<0.05$).

4.4 DISCUSSION

The inability of anticancer drugs and drug delivery systems to penetrate and distribute throughout solid tumors represents a major barrier to drug delivery. Mathematical modeling and scaling analyses have proven to be useful tools in describing the distribution of drugs or antibodies throughout solid tumors. Multicellular tumor spheroids (MCTS) have been a particularly useful experimental model for drug penetration studies, and their simple geometry lends itself well to use in theoretical models. Several previous studies have developed accurate and descriptive mathematical models describing the penetration of antibodies or nanoparticles through tumor spheroids [102, 104]. In this work, we employed a similar methodology, and extended it to evaluate the effect of targeting ligand density on distribution of PAMAM-RGD conjugates through MCTS of malignant glioma cells.

As the binding affinity of drugs is known to be an important parameter dictating their extent of tumor penetration, the binding affinities of a panel of PAMAM-RGD conjugates displaying between 2 and 10 RGD peptides to the immobilized human integrin $\alpha_v\beta_3$ protein were measured using a surface plasmon resonance (SPR) biosensor. Interestingly, dendrimers displaying a low number of RGD peptides (2 or 3) were found to have a significantly higher binding affinity to the immobilized integrin protein than dendrimers displaying a high number of peptides (7 or 10). This is in contrast to some previous studies where using a PAMAM dendrimer scaffold was found to promote multivalent interactions between folic acid and the folate receptor resulting in an increased binding avidity when numerous copies of folic acid were displayed [42]. These contrasting trends are likely due to the inherent differences between the ligand-receptor systems studied. The spacing between RGD peptides has proven to be a critically important parameter in achieving or hindering multivalent binding to integrin proteins or integrin-expressing cells[43, 46, 51, 165]. In some other studies, an optimal presentation of RGD peptides from a multivalent array was observed, where having too high a density of RGD peptides decreased the affinity to integrin-expressing cells, presumably due to steric hindrance[44, 48].

Previously, we developed a competitive binding cell adhesion assay to compare the abilities of PAMAM-RGD conjugates to inhibit the adhesion of U87 cells to the ECM protein, fibrinogen[92]. The results of this assay showed the same trends observed in the SPR experiments in this work, where dendrimers displaying low numbers of RGD peptides were more efficient at inhibiting adhesion of U87 cells to fibrinogen protein than were dendrimers displaying a high number of RGDs. This complementary assay

provides further support for the trends observed in the SPR experiments in this work. Taken together, the results suggest that an optimal presentation is strongly context-dependent and hence that new ligand-bearing conjugates should be evaluated experimentally.

In addition to binding affinity, rate of cellular internalization is another important parameter governing tumor penetration. Here, cellular internalization rates for fluorescently-labeled PAMAM-RGD conjugates were evaluated quantitatively. The addition of RGD peptides to PAMAM dendrimers significantly increased the amount of polymer that was internalized into U87 cells over a period of 48 hours, as expected. Presumably, this is due to the additional mode of cellular internalization (receptor-mediated) afforded by the introduction of RGD targeting peptides in addition to the non-specific electrostatic interactions known to exist between cationic PAMAM dendrimers and cells [166]. Increasing the extent of RGD crosslinking also increased the rate of cellular internalization somewhat, with dendrimers displaying 10 peptides internalizing twice as rapidly than those displaying 2 peptides.

It is notable that the effect of increasing RGD functionalization is different between the cell internalization and SPR binding measurements. There are several fundamental differences between the experimental conditions which might explain this apparent discrepancy. It is important to note the difference in time scales between the binding kinetics and cell internalization experiments; the binding kinetic SPR studies were evaluated on the order of ~5 minutes, whereas the cell internalization experiments were performed over a period of 48 hours. It is possible that steric hindrance might impede the initial attachment of dendrimers displaying many RGD peptides (which is

detected by the SPR instrument) and that a longer period of time (on the order of hours) may be required for multivalency to influence binding and cellular accumulation of these materials. Furthermore, SPR measurements utilize integrins rigidly immobilized on a sensor chip, which may restrict multivalent cooperativity. Cellular membranes, in contrast, are fluid, allowing dynamic clustering of receptors and facilitating multivalent interactions. Taken together, the combination of the binding kinetic and cell internalization experiments demonstrate that altering RGD ligand density has a pronounced impact on integrin binding kinetics, and impacts cell internalization dynamics to a lesser extent.

These experimentally determined binding affinity and cell internalization kinetic constants were incorporated into a reaction/transport model to describe polymer distribution through a tumor spheroid. The predicted concentration profiles for PAMAM-RGD conjugates showed that dendrimers with a high level of RGD modification (7 or 10) had a more homogeneous distribution throughout tumor spheroids than did polymers with a low level of RGD modification (2 or 3). These results are in good agreement with our previous study showing that PAMAM dendrimers with 10 RGD peptides were able to deliver significantly higher concentrations of siRNA to malignant glioma spheroids than were PAMAM dendrimers displaying just 3 RGD peptides[92]. Our previous work also indicated that PAMAM-RGD conjugates can interfere with the interactions between tumor cells and ECM proteins[92]. While not directly incorporated into the mathematical model developed here, the ability of PAMAM-RGD to break apart cell-ECM contacts may be another important mechanism involved in the efficient tumoral transport of these bioconjugates.

The present study provides insight into the mechanisms governing the efficient tumor penetration by PAMAM-RGD conjugates. Somewhat surprisingly, this work demonstrated that the addition of more than 2-3 RGD peptides to a dendrimer platform enhanced penetration through a tumor spheroid in spite of, or possibly due to, decreasing the binding affinity to cell-surface integrin proteins. It has been reported that low affinity antibodies have more homogeneous distributions through solid tumors than their high-affinity counterparts[102], and this study provides complementary evidence for similar behavior with tumor-targeted nanoscale materials. These results are promising for researchers working with synthetic drug delivery systems, demonstrating that a relatively minor architectural change such as varying targeting ligand density can significantly impact tumor penetration in a predictable manner. The methodology presented here can be applied by researchers working with a diverse set of targeting systems to predict and optimize the penetration of anticancer agents through solid tumors. This sort of quantitative approach can guide the rational design of effective anticancer therapies for the treatment of human disease.

CHAPTER 5

DISSERTATION CONCLUSIONS AND FUTURE DIRECTIONS

5.1 Dissertation Summary

In this work, PAMAM dendrimers were studied for their ability to facilitate the delivery of siRNA to malignant glioma on both the cellular and tumor tissue levels. First, the ability of PAMAM dendrimers to facilitate the intracellular delivery of siRNA was evaluated. To understand better the mechanisms governing PAMAM-mediated siRNA delivery on the cellular level, surface amine acetylation was employed to reduce the net positive charge of dendrimers (Chapter 2). Charge reduction of PAMAM dendrimers was found to decrease their strength of interactions with siRNA which may have facilitated improved intracellular siRNA release. The cytotoxitity of dendrimers was also decreased with amine acetylation. However, the removal of primary amines compromised the endosomal buffering capacity of PAMAM dendrimers, resulting in decreased siRNA transfection efficiency. This analysis demonstrated that while it is desirable to reduce the density of cationic amines to reduce cytotoxicity, care must be taken to maintain the desirable endosomal buffering properties of the amine groups to maintain efficient cellular siRNA delivery.

Having determined that it is necessary to maintain the highly cationic nature of PAMAM dendrimers to facilitate intracellular siRNA delivery, dendrimers were modified to display multiple copies of tumor-targeting RGD peptides from their surface to facilitate more efficient tumoral delivery of siRNA (Chapter 3). PAMAM-RGD conjugates were used to deliver siRNA to a three-dimensional spheroid cell culture model of malignant glioma, where the number of peptides displayed from the polymer surface

was found to influence the extent of siRNA penetration and delivery into tumor spheroids. In this work, displaying a higher number of RGD peptides (7 or 10) from PAMAM dendrimers elicited improved tumor penetration compared to a lower number of peptides (2 or 3). We also sought to better-understand the impact of RGD valency on the tumoral transport of PAMAM/siRNA complexes using a biophysical approach (Chapter 4). The biophysical interactions between PAMAM-RGD conjugates and malignant glioma cells and cell-surface integrin protein receptors were studied experimentally to determine kinetic binding and internalization rate constants. These kinetic parameters were incorporated within a mathematical model describing drug transport in tumor spheroids. This analysis revealed the importance of optimizing cellular binding affinity to improve particle transport through solid tumors, and provided a methodology for predicting the tumor-penetration efficiencies of tumor-targeted, nanoscale materials.

5.2 **Future Directions**

This dissertation provides insights into the mechanisms governing the efficient tumor penetration and delivery of siRNA by RGD-modified PAMAM dendrimers. The effect of targeting ligand density was studied extensively, and was found to have a pronounced impact on the transport efficiency of PAMAM-RGD through a tumor spheroid model of malignant glioma. Given this framework, some future directions of this work could be to determine a correlation between tumoral distribution of drugs and their anticancer efficacy, or to improve the PAMAM-RGD system such that it could be useful for *in vivo* siRNA delivery. Further, the insights derived in this work regarding the impact of targeting ligand density on tumor penetration and transport of nanoscale

materials can be applied to improve the tumor penetration abilities of other synthetic siRNA delivery systems.

In this work, siRNAs were fluorescently labeled to study their distribution through tumor spheroids. Given that we developed a panel of PAMAM-RGD conjugates that distribute siRNA throughout tumor spheroids with varying degrees of efficiency, it is important to quantify the extent to which better tumoral distribution correlates to enhanced siRNA-induced oncogene silencing. Thus, an important next step to this work would be to use the PAMAM-RGD conjugates to deliver a siRNA sequence targeted against an oncogene to evaluate the extent of oncogene silencing achieved with the delivery system. It would be interesting to use a more advanced imaging platform to study and quantify the extents of siRNA cell association, uptake, and corresponding gene silencing within the spheroids to understand how siRNA distribution correlates to gene silencing in three-dimensional tumors.

Further, as siRNA would likely be used clinically in conjunction with a chemotherapy drug, a co-treatment regimen using PAMAM-RGD conjugates to facilitate siRNA delivery along with a chemotherapy compound could be developed to improve the antitumor activity of this delivery system. We have performed some preliminary experiments (data not shown in this dissertation) demonstrating an additive effect between anti-STAT3 siRNA with the chemotherapy drug carmustine against malignant glioma cells. Thus, a logical extension of this work would be to optimize this therapeutically-relevant treatment regimen for the treatment of glioma using PAMAM-RGD conjugates to determine if this treatment regimen is able to retard the growth of glioma cells in a three-dimensional tumor model.

Another step in this work would be to study the tumoral distribution of siRNA in an *in vivo* solid tumor model, and to modify the PAMAM-based delivery system to impart favorable drug delivery to tumors *in vivo*. While the *in vitro* tumor spheroid model is a fairly reasonable cell culture representation of a solid tumor that captures some of the key features present in tumors, it is impossible to capture the complete tumor microenvironment without using an *in vivo* model. The PAMAM-RGD system studied in this dissertation provided reasonable siRNA delivery in a tumor spheroid model; however, it is unlikely that this system would be able to protect its siRNA cargo from degradation in the bloodstream *in vivo*. Most likely, the siRNA drug would not even reach the target tumor *in vivo* due to degradation of the complexes in the bloodstream. Hence, in order to use PAMAM-RGD for *in vivo* studies, it would be necessary to modify the PAMAM dendrimer scaffold.Incorporating PEG into the delivery system would likely improve the ability of PAMAM to protect siRNA in the presence of blood serum nucleases, and could improve its biodistribution to the solid tumor. Others have observed that PEGylation of PAMAM dendrimers can improve their ability to protect siRNA in the presence of blood serum *in vitro*,[167, 168] and PEGylated PAMAM dendrimers have been successfully used *in vivo* for gene delivery purposes.[169, 170] However, the incorporation of PEG may significantly impact the presentation of RGD targeting ligands from the dendrimer scaffold, so care would need to be taken to develop a system that incorporates the serum-protection of PEG while maintaining the RGD-integrin binding affinity that we found to be important for homogeneous tumor distribution.

It is important to note that the primary objective of this dissertation was not to develop a novel siRNA delivery system, but rather to understand the influence of

multivalent targeting ligand display on siRNA delivery to solid tumors. PAMAM dendrimers were used as a model siRNA delivery system due to their favorable branched architecture which is amenable to multivalent display of targeting ligands. While one future direction of this work could be to improve the PAMAM-RGD system for successful *in vivo* siRNA delivery, greater impact may be achieved if the design insights and guidelines derived in this work were applied to other, more promising siRNA delivery systems. Multivalent RGD targeting may be incorporated into polymeric micelle or liposomal systems that have already proven successful for *in vivo* drug and gene delivery applications, but which are limited by poor tumor penetration. Further, the concept of optimizing ligand density to influence the tumoral distribution of nanoscale materials may be applied to other ligand-receptor pairs including folate or epidermal growth factor receptor (EGFR) targeting to determine whether altering the presentation of these well-studied targeting ligands may improve their distribution throughout solid tumors. It may also be worthwhile to investigate the use of low-affinity targeting ligands to impart favorable tumor distribution properties of drug delivery systems.

5.3 **Overall Dissertation Conclusions and Contributions**

The work done in this dissertation studied the influence of PAMAM dendrimer architecture on its ability to mediate siRNA delivery to malignant glioma. On the cellular level, we found it important to maintain the majority of cationic amine groups on PAMAM to facilitate efficient endosomal escape and siRNA transfection efficiency. On the tumor tissue level, we found that altering the density of RGD ligands from PAMAM dendrimers is a facile, efficient means of controlling the efficiency of penetration and siRNA delivery to solid tumors. Specifically, the addition of more RGD peptides (7 or

10) from PAMAM dendrimers improved the penetration of the conjugates through a solid tumor model compared to dendrimers displaying a low number (2 or 3) of RGD peptides. By analyzing the transport of PAMAM-RGDs through tumor spheroids, we determined that the binding affinity of PAMAM-RGDs to integrin receptors primarily controls their penetration through spheroids. Dendrimer-RGD conjugates with a lower integrin binding affinity were found to diffuse more efficiently through malignant glioma spheroids.

Through this dissertation, we developed an experimental and theoretical framework for analyzing the penetration of nanoscale drug delivery vehicles through solid tumors, and developed design guidelines for tumor-targeted materials that may be useful to other researchers in this field. While there is significant evidence that the poor tumoral penetration of anticancer therpauetics may inhibit their efficacy *in vivo*, very few studies have attempted to overcome the poor tumor penetration of nanoscale materials. In this dissertation, the ability of tumor-targeted nanoscale delivery systems to penetrate into solid tumors was studied, and the impact of RGD targeting ligand density was quantified, where lower affinity nanoparticles were found to elicit favorable tumor distribution *in vitro*. To our knowledge, this is one of the first studies evaluting the impact of ligand density on tumor penetration of nanoscale materials. Through this work, a methodology has been presented to screen nanoscale materials for tumor penetration capabilities, and insights into how to rationally design tumor targeting systems have been derived. These insights can be applied to other targeted delivery systems, and may help other researchers to more efficiently design tumor-targeted drug delivery systems, or to improve the tumor penetration capabilities of existing systems. This work highlights the importance of tumor penetration on efficient drug delivery to solid tumors, and provides a

quantitative framework that may improve the efficacy of nanoscale anticancer therapeutics.

REFERENCES

1. Society, A.C. Cancer Facts & Figures 2008. (American Cancer Society, Atlanta; 2008).
2. Croce, C.M. Oncogenes and cancer. *N Engl J Med* **358**, 502-511 (2008).
3. Hanahan, D. & Weinberg, R.A. The hallmarks of cancer. *Cell* **100**, 57-70 (2000).
4. Edelstein, M. in The Journal of Gene Medicine (Wiley, 2008).
5. Aagaard, L. & Rossi, J.J. RNAi therapeutics: principles, prospects and challenges. *Adv Drug Deliv Rev* **59**, 75-86 (2007).
6. Kumar, L.D. & Clarke, A.R. Gene manipulation through the use of small interfering RNA (siRNA): From in vitro to in vivo applications. *Advanced Drug Delivery Reviews* **59**, 87-100 (2007).
7. Roth, C.M. & Sundaram, S. Engineering Synthetic Vectors For Improved DNA Delivery: Insights from Intracellular Pathways. *Annual Review of Biomedical Engineering* **6**, 397-426 (2004).
8. Torchilin, V.P. Recent advances with liposomes as pharmaceutical carriers. *Nat Rev Drug Discov* **4**, 145-160 (2005).
9. Lochmann, D., Jauk, E. & Zimmer, A. Drug delivery of oligonucleotides by peptides. *Eur J Pharm Biopharm* **58**, 237-251 (2004).
10. Thomas, M. & Klibanov, A.M. Non-viral gene therapy: polycation-mediated DNA delivery. *Appl Microbiol Biotechnol* **62**, 27-34 (2003).
11. Gary, D.J., Puri, N. & Won, Y.Y. Polymer-based siRNA delivery: perspectives on the fundamental and phenomenological distinctions from polymer-based DNA delivery. *J Control Release* **121**, 64-73 (2007).
12. Morille, M., Passirani, C., Vonarbourg, A., Clavreul, A. & Benoit, J.P. Progress in developing cationic vectors for non-viral systemic gene therapy against cancer. *Biomaterials* **29**, 3477-3496 (2008).
13. Lungwitz, U., Breunig, M., Blunk, T. & Gopferich, A. Polyethylenimine-based non-viral gene delivery systems. *Eur J Pharm Biopharm* **60**, 247-266 (2005).
14. Boas, U. & Heegaard, P.M.H. Dendrimers in drug research. *Chemical Society Reviews* **33**, 43-63 (2004).
15. Svenson, S. & Tomalia, D.A. Dendrimers in biomedical applications--reflections on the field. *Advanced Drug Delivery Reviews* **57**, 2106-2129 (2005).
16. Howard, K.A. Delivery of RNA interference therapeutics using polycation-based nanoparticles. *Advanced Drug Delivery Reviews* **61**, 710-720 (2009).
17. Behr, J.P. The proton sponge: A trick to enter cells the viruses did not exploit. *CHIMIA* **51**, 34-36 (1997).
18. Waite, C.L., Sparks, S.M., Uhrich, K.E. & Roth, C.M. Acetylation of PAMAM dendrimers for cellular delivery of siRNA. *BMC Biotechnol* **9**, 38 (2009).
19. Forrest, M.L., Meister, G., Koerber, J. & Pack, D. Partial Acetylation of Polyethylenimine Enhances In Vitro Gene Delivery. *Pharmaceutical Research* **21**, 365-371 (2004).
20. Gabrielson, N.P. & Pack, D.W. Acetylation of Polyethylenimine Enhances Gene Delivery via Weakened Polymer/DNA Interactions. *Biomacromolecules* **7**, 2427-2435 (2006).
21. Harris, J.M. & Chess, R.B. Effect of pegylation on pharmaceuticals. *Nat Rev Drug Discov* **2**, 214-221 (2003).
22. Danhier, F., Feron, O. & Préat, V. To exploit the tumor microenvironment: Passive and active tumor targeting of nanocarriers for anti-cancer drug delivery. *Journal of Controlled Release* **148**, 135-146 (2010).
23. Kataoka, K., Harada, A. & Nagasaki, Y. Block copolymer micelles for drug delivery: design, characterization and biological significance. *Advanced Drug Delivery Reviews* **47**, 113-131 (2001).
24. Nishiyama, N. & Kataoka, K. Current state, achievements, and future prospects of polymeric micelles as nanocarriers for drug and gene delivery. *Pharmacol Ther* **112**, 630-648 (2006).
25. Greish, K. Enhanced permeability and retention of macromolecular drugs in solid tumors: A royal gate for targeted anticancer nanomedicines. *Journal of Drug Targeting* **15**, 457-464 (2007).

26. Hilgenbrink, A.R. & Low, P.S. Folate receptor-mediated drug targeting: From therapeutics to diagnostics. *Journal of Pharmaceutical Sciences* **94**, 2135-2146 (2005).
27. Qian, Z.M., Li, H., Sun, H. & Ho, K. Targeted drug delivery via the transferrin receptor-mediated endocytosis pathway. *Pharmacol Rev* **54**, 561-587 (2002).
28. Cai, W. & Chen, X. Anti-angiogenic cancer therapy based on integrin alphavbeta3 antagonism. *Anticancer Agents Med Chem* **6**, 407-428 (2006).
29. Dunehoo, A.L. et al. Cell adhesion molecules for targeted drug delivery. *J Pharm Sci* **95**, 1856-1872 (2006).
30. Heidel, J.D. et al. Administration in non-human primates of escalating intravenous doses of targeted nanoparticles containing ribonucleotide reductase subunit M2 siRNA. *Proc Natl Acad Sci U S A* **104**, 5715-5721 (2007).
31. Rust, W.L., Carper, S.W. & Plopper, G.E. The Promise of Integrins as Effective Targets for Anticancer Agents. *J Biomed Biotechnol* **2**, 124-130 (2002).
32. Eliceiri, B.P. & Cheresh, D.A. The role of alphav integrins during angiogenesis: insights into potential mechanisms of action and clinical development. *J Clin Invest* **103**, 1227-1230 (1999).
33. Aumailley, M. et al. Arg-Gly-Asp constrained within cyclic pentapeptides. Strong and selective inhibitors of cell adhesion to vitronectin and laminin fragment P1. *FEBS Lett* **291**, 50-54 (1991).
34. Marinelli, L., Gottschalk, K.E., Meyer, A., Novellino, E. & Kessler, H. Human integrin alphavbeta5: homology modeling and ligand binding. *J Med Chem* **47**, 4166-4177 (2004).
35. Taga, T. et al. alpha v-Integrin antagonist EMD 121974 induces apoptosis in brain tumor cells growing on vitronectin and tenascin. *Int J Cancer* **98**, 690-697 (2002).
36. Mattern, R.H. et al. Glioma cell integrin expression and their interactions with integrin antagonists: Research Article. *Cancer Ther* **3A**, 325-340 (2005).
37. Chatterjee, S., Matsumura, A., Schradermeier, J. & Gillespie, G.Y. Human malignant glioma therapy using anti-alpha(v)beta3 integrin agents. *J Neurooncol* **46**, 135-144 (2000).
38. Eskens, F.A. et al. Phase I and pharmacokinetic study of continuous twice weekly intravenous administration of Cilengitide (EMD 121974), a novel inhibitor of the integrins alphavbeta3 and alphavbeta5 in patients with advanced solid tumours. *Eur J Cancer* **39**, 917-926 (2003).
39. Nabors, L.B. et al. Phase I and correlative biology study of cilengitide in patients with recurrent malignant glioma. *J Clin Oncol* **25**, 1651-1657 (2007).
40. Reardon, D.A. et al. Randomized phase II study of cilengitide, an integrin-targeting arginine-glycine-aspartic acid peptide, in recurrent glioblastoma multiforme. *J Clin Oncol* **26**, 5610-5617 (2008).
41. Mammen, M., Choi, S.-K. & Whitesides, G.M. Polyvalent Interactions in Biological Systems: Implications for Design and Use of Multivalent Ligands and Inhibitors. *Angewandte Chemie International Edition* **37**, 2754-2794 (1998).
42. Hong, S. et al. The binding avidity of a nanoparticle-based multivalent targeted drug delivery platform. *Chem Biol* **14**, 107-115 (2007).
43. Maheshwari, G., Brown, G., Lauffenburger, D.A., Wells, A. & Griffith, L.G. Cell adhesion and motility depend on nanoscale RGD clustering. *J Cell Sci* **113 (Pt 10)**, 1677-1686 (2000).
44. Garanger, E., Boturyn, D., Coll, J.L., Favrot, M.C. & Dumy, P. Multivalent RGD synthetic peptides as potent alphaVbeta3 integrin ligands. *Organic & Biomolecular Chemistry* **4**, 1958-1965 (2006).
45. Li, Z.B. et al. (64)Cu-labeled tetrameric and octameric RGD peptides for small-animal PET of tumor alpha(v)beta(3) integrin expression. *J Nucl Med* **48**, 1162-1171 (2007).
46. Liu, S. Radiolabeled cyclic RGD peptides as integrin alpha(v)beta(3)-targeted radiotracers: maximizing binding affinity via bivalency. *Bioconjugate Chemistry* **20**, 2199-2213 (2009).
47. Ye, Y., Bloch, S., Xu, B. & Achilefu, S. Design, synthesis, and evaluation of near infrared fluorescent multimeric RGD peptides for targeting tumors. *Journal of Medicinal Chemistry* **49**, 2268-2275 (2006).
48. Montet, X., Funovics, M., Montet-Abou, K., Weissleder, R. & Josephson, L. Multivalent effects of RGD peptides obtained by nanoparticle display. *J Med Chem* **49**, 6087-6093 (2006).
49. Rosca, E.V., Gillies, R.J. & Caplan, M.R. Glioblastoma targeting via integrins is concentration dependent. *Biotechnol Bioeng* **104**, 408-417 (2009).
50. Shukla, R. et al. Tumor angiogenic vasculature targeting with PAMAM dendrimer-RGD conjugates. *Chem Commun (Camb)*, 5739-5741 (2005).

51. Wang, L. et al. Improving tumor-targeting capability and pharmacokinetics of (99m)Tc-labeled cyclic RGD dimers with PEG(4) linkers. *Molecular Pharmaceutics* **6**, 231-245 (2009).
52. Primeau, A.J., Rendon, A., Hedley, D., Lilge, L. & Tannock, I.F. The Distribution of the Anticancer Drug Doxorubicin in Relation to Blood Vessels in Solid Tumors. *Clinical Cancer Research* **11**, 8782-8788 (2005).
53. Lankelma, J. et al. Doxorubicin Gradients in Human Breast Cancer. *Clinical Cancer Research* **5**, 1703-1707 (1999).
54. Kyle, A.H., Huxham, L.A., Yeoman, D.M. & Minchinton, A.I. Limited Tissue Penetration of Taxanes: A Mechanism for Resistance in Solid Tumors. *Clinical Cancer Research* **13**, 2804-2810 (2007).
55. Kuh, H.-J., Jang, S.H., Wientjes, M.G., Weaver, J.R. & Au, J.L.-S. Determinants of Paclitaxel Penetration and Accumulation in Human Solid Tumor. *Journal of Pharmacology and Experimental Therapeutics* **290**, 871-880 (1999).
56. Tannock, I.F., Lee, C.M., Tunggal, J.K., Cowan, D.S.M. & Egorin, M.J. Limited Penetration of Anticancer Drugs through Tumor Tissue. *Clinical Cancer Research* **8**, 878-884 (2002).
57. Minchinton, A.I. & Tannock, I.F. Drug penetration in solid tumours. *Nat Rev Cancer* **6**, 583-592 (2006).
58. Jang, S.H., Wientjes, M.G., Lu, D. & Au, J.L.S. Drug Delivery and Transport to Solid Tumors. *Pharmaceutical Research* **20**, 1337-1350 (2003).
59. Holback, H. & Yeo, Y. Intratumoral Drug Delivery with Nanoparticulate Carriers. *Pharm Res* (2011).
60. Jain, R.K. & Stylianopoulos, T. Delivering nanomedicine to solid tumors. *Nat Rev Clin Oncol* **7**, 653-664 (2010).
61. Dreher, M.R. et al. Tumor Vascular Permeability, Accumulation, and Penetration of Macromolecular Drug Carriers. *Journal of the National Cancer Institute* **98**, 335-344 (2006).
62. Heldin, C.-H., Rubin, K., Pietras, K. & Ostman, A. High interstitial fluid pressure- an obstacle in cancer therapy. *Nat Rev Cancer* **4**, 806-813 (2004).
63. Pluen, A. et al. Role of tumor–host interactions in interstitial diffusion of macromolecules: Cranial vs. subcutaneous tumors. *Proceedings of the National Academy of Sciences of the United States of America* **98**, 4628-4633 (2001).
64. Magzoub, M., Jin, S. & Verkman, A.S. Enhanced macromolecule diffusion deep in tumors after enzymatic digestion of extracellular matrix collagen and its associated proteoglycan decorin. *The FASEB Journal* **22**, 276-284 (2008).
65. Eikenes, L., Bruland, O.S., Brekken, C. & Davies Cde, L. Collagenase increases the transcapillary pressure gradient and improves the uptake and distribution of monoclonal antibodies in human osteosarcoma xenografts. *Cancer Res* **64**, 4768-4773 (2004).
66. Goodman, T.T., Olive, P.L. & Pun, S.H. Increased nanoparticle penetration in collagenase-treated multicellular spheroids. *Int J Nanomedicine* **2**, 265-274 (2007).
67. Netti, P.A., Berk, D.A., Swartz, M.A., Grodzinsky, A.J. & Jain, R.K. Role of extracellular matrix assembly in interstitial transport in solid tumors. *Cancer Res* **60**, 2497-2503 (2000).
68. Neeves, K.B., Sawyer, A.J., Foley, C.P., Saltzman, W.M. & Olbricht, W.L. Dilation and degradation of the brain extracellular matrix enhances penetration of infused polymer nanoparticles. *Brain Res* **1180**, 121-132 (2007).
69. Yamada, K.M. & Cukierman, E. Modeling tissue morphogenesis and cancer in 3D. *Cell* **130**, 601-610 (2007).
70. Kim, J.B. Three-dimensional tissue culture models in cancer biology. *Semin Cancer Biol* **15**, 365-377 (2005).
71. Burdett, E., Kasper, F.K., Mikos, A.G. & Ludwig, J.A. Engineering tumors: a tissue engineering perspective in cancer biology. *Tissue Eng Part B Rev* **16**, 351-359 (2010).
72. Sutherland, R.M. Cell and environment interactions in tumor microregions: the multicell spheroid model. *Science* **240**, 177-184 (1988).
73. Goodman, T.T., Ng, C.P. & Pun, S.H. 3-D tissue culture systems for the evaluation and optimization of nanoparticle-based drug carriers. *Bioconjug Chem* **19**, 1951-1959 (2008).
74. Fracasso, G. & Colombatti, M. Effect of therapeutic macromolecules in spheroids. *Crit Rev Oncol Hematol* **36**, 159-178 (2000).

75. Hicks, K.O. et al. Use of Three-Dimensional Tissue Cultures to Model Extravascular Transport and Predict In Vivo Activity of Hypoxia-Targeted Anticancer Drugs. *Journal of the National Cancer Institute* **98**, 1118-1128 (2006).
76. Modok, S., Hyde, P., Mellor, H.R., Roose, T. & Callaghan, R. Diffusivity and distribution of vinblastine in three-dimensional tumour tissue: Experimental and mathematical modelling. *European journal of cancer (Oxford, England : 1990)* **42**, 2404-2413 (2006).
77. Kyle, A.H., Huxham, L.A., Chiam, A.S.J., Sim, D.H. & Minchinton, A.I. Direct Assessment of Drug Penetration into Tissue Using a Novel Application of Three-Dimensional Cell Culture. *Cancer Research* **64**, 6304-6309 (2004).
78. Grantab, R., Sivananthan, S. & Tannock, I.F. The Penetration of Anticancer Drugs through Tumor Tissue as a Function of Cellular Adhesion and Packing Density of Tumor Cells. *Cancer Research* **66**, 1033-1039 (2006).
79. Evans, C.J. et al. A mathematical model of doxorubicin penetration through multicellular layers. *Journal of Theoretical Biology* **257**, 598-608 (2009).
80. Hearnden, V., MacNeil, S. & Battaglia, G. Tracking nanoparticles in three-dimensional tissue-engineered models using confocal laser scanning microscopy. *Methods Mol Biol* **695**, 41-51 (2011).
81. Del Duca, D., Werbowetski, T. & Del Maestro, R.F. Spheroid preparation from hanging drops: characterization of a model of brain tumor invasion. *J Neurooncol* **67**, 295-303 (2004).
82. Friedrich, J., Seidel, C., Ebner, R. & Kunz-Schughart, L.A. Spheroid-based drug screen: considerations and practical approach. *Nat Protoc* **4**, 309-324 (2009).
83. Sutherland, R.M., McCredie, J.A. & Inch, W.R. Growth of Multicell Spheroids in Tissue Culture as a Model of Nodular Carcinoma. *J Natl Cancer Inst* **46**, 113-120 (1971).
84. Ong, S.-M. et al. Engineering a scaffold-free 3D tumor model for in vitro drug penetration studies. *Biomaterials* **31**, 1180-1190 (2010).
85. Napolitano, A.P. et al. Scaffold-free three-dimensional cell culture utilizing micromolded nonadhesive hydrogels. *Biotechniques* **43**, 494, 496-500 (2007).
86. Kostarelos, K. et al. Engineering lipid vesicles of enhanced intratumoral transport capabilities: correlating liposome characteristics with penetration into human prostate tumor spheroids. *J Liposome Res* **15**, 15-27 (2005).
87. Kostarelos, K. et al. Binding and interstitial penetration of liposomes within avascular tumor spheroids. *International Journal of Cancer* **112**, 713-721 (2004).
88. Tsukioka, Y. et al. Pharmaceutical and biomedical differences between micellar doxorubicin (NK911) and liposomal doxorubicin (Doxil). *Jpn J Cancer Res* **93**, 1145-1153 (2002).
89. Du, J. et al. Dual-Targeting Topotecan Liposomes Modified with Tamoxifen and Wheat Germ Agglutinin Significantly Improve Drug Transport across the Blood−Brain Barrier and Survival of Brain Tumor-Bearing Animals. *Molecular Pharmaceutics* **6**, 905-917 (2009).
90. Mellor, H.R. et al. Optimising non-viral gene delivery in a tumour spheroid model. *J Gene Med* **8**, 1160-1170 (2006).
91. Oishi, M. et al. Enhanced growth inhibition of hepatic multicellular tumor spheroids by lactosylated poly(ethylene glycol)-siRNA conjugate formulated in PEGylated polyplexes. *ChemMedChem* **2**, 1290-1297 (2007).
92. Waite, C.L. & Roth, C.M. PAMAM-RGD conjugates enhance siRNA delivery through a multicellular spheroid model of malignant glioma. *Bioconjug Chem* **20**, 1908-1916 (2009).
93. Saleh, A.F. et al. Improved Tat-mediated plasmid DNA transfer by fusion to LK15 peptide. *Journal of Controlled Release* **143**, 233-242 (2010).
94. Han, M. et al. Transfection study using multicellular tumor spheroids for screening non-viral polymeric gene vectors with low cytotoxicity and high transfection efficiencies. *Journal of Controlled Release* **121**, 38-48 (2007).
95. Al-Abd, A.M. et al. Penetration and efficacy of VEGF siRNA using polyelectrolyte complex micelles in a human solid tumor model in-vitro. *Journal of Controlled Release* **137**, 130-135 (2009).
96. Grainger, S.J. et al. Pulsed ultrasound enhances nanoparticle penetration into breast cancer spheroids. *Mol Pharm* **7**, 2006-2019 (2010).

97. Bae, Y. et al. Preparation and biological characterization of polymeric micelle drug carriers with intracellular pH-triggered drug release property: tumor permeability, controlled subcellular drug distribution, and enhanced in vivo antitumor efficacy. *Bioconjug Chem* **16**, 122-130 (2005).
98. Kim, T.H., Mount, C.W., Gombotz, W.R. & Pun, S.H. The delivery of doxorubicin to 3-D multicellular spheroids and tumors in a murine xenograft model using tumor-penetrating triblock polymeric micelles. *Biomaterials* **31**, 7386-7397 (2010).
99. Dhanikula, R.S., Argaw, A., Bouchard, J.-F. & Hildgen, P. Methotrexate Loaded Polyether-Copolyester Dendrimers for the Treatment of Gliomas: Enhanced Efficacy and Intratumoral Transport Capability. *Molecular Pharmaceutics* **5**, 105-116 (2008).
100. Shen, X.C. et al. Importance of size-to-charge ratio in construction of stable and uniform nanoscale RNA/dendrimer complexes. *Org Biomol Chem* **5**, 3674-3681 (2007).
101. Ackerman, M.E., Pawlowski, D. & Wittrup, K.D. Effect of antigen turnover rate and expression level on antibody penetration into tumor spheroids. *Mol Cancer Ther* **7**, 2233-2240 (2008).
102. Graff, C.P. & Wittrup, K.D. Theoretical analysis of antibody targeting of tumor spheroids: importance of dosage for penetration, and affinity for retention. *Cancer Res* **63**, 1288-1296 (2003).
103. Thurber, G.M. & Wittrup, K.D. Quantitative spatiotemporal analysis of antibody fragment diffusion and endocytic consumption in tumor spheroids. *Cancer Res* **68**, 3334-3341 (2008).
104. Goodman, T.T., Chen, J., Matveev, K. & Pun, S.H. Spatio-temporal modeling of nanoparticle delivery to multicellular tumor spheroids. *Biotechnol Bioeng* **101**, 388-399 (2008).
105. Ramanujan, S. et al. Diffusion and Convection in Collagen Gels: Implications for Transport in the Tumor Interstitium. *Biophysical Journal* **83**, 1650-1660 (2002).
106. Marasanapalle, V., Li, X., Polin, L. & Jasti, B.R. Novel in vitro model barriers for evaluation of the permeability of antitumor compounds, thioxanthones. *Invest New Drugs* **24**, 111-116 (2006).
107. Fujimori, K., Covell, D.G., Fletcher, J.E. & Weinstein, J.N. A modeling analysis of monoclonal antibody percolation through tumors: a binding-site barrier. *J Nucl Med* **31**, 1191-1198 (1990).
108. Saga, T. et al. Targeting cancer micrometastases with monoclonal antibodies: a binding-site barrier. *Proc Natl Acad Sci U S A* **92**, 8999-9003 (1995).
109. Thurber, G.M., Zajic, S.C. & Wittrup, K.D. Theoretic criteria for antibody penetration into solid tumors and micrometastases. *J Nucl Med* **48**, 995-999 (2007).
110. Schmidt, M.M. & Wittrup, K.D. A modeling analysis of the effects of molecular size and binding affinity on tumor targeting. *Molecular Cancer Therapeutics* **8**, 2861-2871 (2009).
111. Tzafriri, A.R., Levin, A.D. & Edelman, E.R. Diffusion-limited binding explains binary dose response for local arterial and tumour drug delivery. *Cell Prolif* **42**, 348-363 (2009).
112. Su, D., Ma, R., Salloum, M. & Zhu, L. Multi-scale study of nanoparticle transport and deposition in tissues during an injection process. *Medical and Biological Engineering and Computing* **48**, 853-863 (2010).
113. Jain, R.K. Delivery of molecular and cellular medicine to solid tumors. *Adv Drug Deliv Rev* **46**, 149-168 (2001).
114. Zahnd, C. et al. Efficient Tumor Targeting with High-Affinity Designed Ankyrin Repeat Proteins: Effects of Affinity and Molecular Size. *Cancer Research* **70**, 1595-1605 (2010).
115. Bryce, N.S., Zhang, J.Z., Whan, R.M., Yamamoto, N. & Hambley, T.W. Accumulation of an anthraquinone and its platinum complexes in cancer cell spheroids: the effect of charge on drug distribution in solid tumour models. *Chemical Communications*, 2673-2675 (2009).
116. Bhise, N.S. et al. The relationship between terminal functionalization and molecular weight of a gene delivery polymer and transfection efficacy in mammary epithelial 2-D cultures and 3-D organotypic cultures. *Biomaterials* **31**, 8088-8096 (2010).
117. Sugahara, K.N. et al. Tissue-Penetrating Delivery of Compounds and Nanoparticles into Tumors. *Cancer cell* **16**, 510-520 (2009).
118. Sugahara, K.N. et al. Coadministration of a Tumor-Penetrating Peptide Enhances the Efficacy of Cancer Drugs. *Science* **328**, 1031-1035 (2010).
119. Fire, A. et al. Potent and specific genetic interference by double-stranded RNA in Caenorhabditis elegans. *Nature* **391**, 806-811 (1998).
120. Dufes, C., Uchegbu, I.F. & Schatzlein, A.G. Dendrimers in gene delivery. *Advanced Drug Delivery Reviews* **57**, 2177-2202 (2005).
121. Guillot-Nieckowski, M., Eisler, S. & Diederich, F. Dendritic vectors for gene transfection. *New Journal of Chemistry* **31**, 1111-1127 (2007).

122. Kang, H., DeLong, R., Fisher, M.H. & Juliano, R.L. Tat-conjugated PAMAM dendrimers as delivery agents for antisense and siRNA oligonucleotides. *Pharm Res* **22**, 2099-2106 (2005).
123. Zhou, J. et al. PAMAM dendrimers for efficient siRNA delivery and potent gene silencing. *Chem Commun (Camb)*, 2362-2364 (2006).
124. Luo, D., Haverstick, K., Belcheva, N., Han, E. & Saltzman, W.M. Poly(ethylene glycol)-Conjugated PAMAM Dendrimer for Biocompatible, High-Efficiency DNA Delivery. *Macromolecules* **35**, 3456-3462 (2002).
125. Jevprasesphant, R. et al. The influence of surface modification on the cytotoxicity of PAMAM dendrimers. *International Journal of Pharmaceutics* **252**, 263-266 (2003).
126. Kim, T.-i. et al. PAMAM-PEG-PAMAM: Novel Triblock Copolymer as a Biocompatible and Efficient Gene Delivery Carrier. *Biomacromolecules* **5**, 2487-2492 (2004).
127. Patil, M.L. et al. Surface-modified and internally cationic polyamidoamine dendrimers for efficient siRNA delivery. *Bioconjug Chem* **19**, 1396-1403 (2008).
128. Lee, J.H., Lim, Y.-b., Choi, M.-u., Yang, C.-h. & Park, J.-S. Quaternized Polyamidoamine Dendrimers as Novel Gene Delivery System: Relationship between Degree of Quaternization and Their Influences. *Bull. Korean Chem. Soc.* **24**, 1637-1640 (2003).
129. Kolhatkar, R.B., Kitchens, K.M., Swaan, P.W. & Ghandehari, H. Surface Acetylation of Polyamidoamine (PAMAM) Dendrimers Decreases Cytotoxicity while Maintaining Membrane Permeability. *Bioconjugate Chem.* **18**, 2054-2060 (2007).
130. Nam, H.Y. et al. Evaluation of generations 2, 3 and 4 arginine modified PAMAM dendrimers for gene delivery. *Int J Pharm* **363**, 199-205 (2008).
131. Lee, C.C., Liu, Y. & Reineke, T.M. General structure-activity relationship for poly(glycoamidoamine)s: the effect of amine density on cytotoxicity and DNA delivery efficiency. *Bioconjug Chem* **19**, 428-440 (2008).
132. Liu, Y. & Reineke, T.M. Poly(glycoamidoamine)s for Gene Delivery. Structural Effects on Cellular Internalization, Buffering Capacity, and Gene Expression. *Bioconjugate Chem.* **18**, 19-30 (2007).
133. Lin, C. et al. Bioreducible poly(amido amine)s with oligoamine side chains: Synthesis, characterization, and structural effects on gene delivery. *Journal of Controlled Release* **126**, 166-174 (2008).
134. Lee, L.K., Dunham, B.M., Li, Z. & Roth, C.M. Cellular Dynamics of Antisense Oligonucleotides and Short Interfering RNAs. *Annals of the New York Academy of Sciences* **1082**, 47-51 (2006).
135. Majoros, I.J., Keszler, B., Woehler, S., Bull, T. & Baker, J.R. Acetylation of Poly(amidoamine) Dendrimers. *Macromolecules* **36**, 5526-5529 (2003).
136. Sundaram, S., Lee, L.K. & Roth, C.M. Interplay of polyethyleneimine molecular weight and oligonucleotide backbone chemistry in the dynamics of antisense activity. *Nucl. Acids Res.* **35**, 4396-4408 (2007).
137. Hunter, R.J. Introduction to Modern Colloid Science. (Oxford University Press, New York; 1993).
138. Schaffer, D.V., Fidelman, N.A., Dan, N. & Lauffenburger, D.A. Vector unpacking as a potential barrier for receptor-mediated polyplex gene delivery. *Biotechnol Bioeng* **67**, 598-606 (2000).
139. Mao, S. et al. Influence of polyethylene glycol chain length on the physicochemical and biological properties of poly(ethylene imine)-graft-poly(ethylene glycol) block copolymer/SiRNA polyplexes. *Bioconjug Chem* **17**, 1209-1218 (2006).
140. Gartel, A.L. & Kandel, E.S. RNA interference in cancer. *Biomol Eng* **23**, 17-34 (2006).
141. Zhang, S., Zhao, B., Jiang, H., Wang, B. & Ma, B. Cationic lipids and polymers mediated vectors for delivery of siRNA. *J Control Release* **123**, 1-10 (2007).
142. Tsutsumi, T., Hirayama, F., Uekama, K. & Arima, H. Evaluation of polyamidoamine dendrimer/alpha-cyclodextrin conjugate (generation 3, G3) as a novel carrier for small interfering RNA (siRNA). *J Control Release* **119**, 349-359 (2007).
143. Patil, M.L. et al. Internally cationic polyamidoamine PAMAM-OH dendrimers for siRNA delivery: effect of the degree of quaternization and cancer targeting. *Biomacromolecules* **10**, 258-266 (2009).
144. Wolfenden, M.L. & Cloninger, M.J. Mannose/glucose-functionalized dendrimers to investigate the predictable tunability of multivalent interactions. *J Am Chem Soc* **127**, 12168-12169 (2005).

145. Woller, E.K., Walter, E.D., Morgan, J.R., Singel, D.J. & Cloninger, M.J. Altering the strength of lectin binding interactions and controlling the amount of lectin clustering using mannose/hydroxyl-functionalized dendrimers. *J Am Chem Soc* **125**, 8820-8826 (2003).
146. Boswell, C.A. et al. Synthesis, characterization, and biological evaluation of integrin alphavbeta3-targeted PAMAM dendrimers. *Mol Pharm* **5**, 527-539 (2008).
147. Hill, E., Shukla, R., Park, S.S. & Baker, J.R., Jr. Synthetic PAMAM-RGD conjugates target and bind to odontoblast-like MDPC 23 cells and the predentin in tooth organ cultures. *Bioconjug Chem* **18**, 1756-1762 (2007).
148. Yang, H. & Kao, W.J. Synthesis and characterization of nanoscale dendritic RGD clusters for potential applications in tissue engineering and drug delivery. *Int J Nanomedicine* **2**, 89-99 (2007).
149. Rasband, W.S. http://rsb.info.nih.gov/ij/ (National Institues of Health, Bethesda, MD, USA; 1997-2009).
150. Muller, R., Laschober, C., Szymanski, W.W. & Allmaier, G. Determination of molecular weight, particle size, and density of high number generation PAMAM dendrimers using MALDI-TOF-MS and nES-GEMMA. *Macromolecules* **40**, 5599-5605 (2007).
151. Shi, X.Y. et al. Comprehensive characterization of surface-functionalized poly (amidoamine) dendrimers with acetamide, hydroxyl, and carboxyl groups. *Colloids and Surfaces a-Physicochemical and Engineering Aspects* **272**, 139-150 (2006).
152. Marinelli, L., Lavecchia, A., Gottschalk, K.E., Novellino, E. & Kessler, H. Docking studies on alphavbeta3 integrin ligands: pharmacophore refinement and implications for drug design. *J Med Chem* **46**, 4393-4404 (2003).
153. Sun, Y.X. et al. The influence of RGD addition on the gene transfer characteristics of disulfide-containing polyethyleneimine/DNA complexes. *Biomaterials* **29**, 4356-4365 (2008).
154. Clements, B.A. et al. RGD conjugation to polyethyleneimine does not improve DNA delivery to bone marrow stromal cells. *Biomacromolecules* **7**, 1481-1488 (2006).
155. Mitra, A. et al. Targeting tumor angiogenic vasculature using polymer-RGD conjugates. *J Control Release* **102**, 191-201 (2005).
156. Fischbach, C. et al. Cancer cell angiogenic capability is regulated by 3D culture and integrin engagement. *Proc Natl Acad Sci U S A* **106**, 399-404 (2009).
157. Ng, Q.K. et al. Engineering clustered ligand binding into nonviral vectors: alphavbeta3 targeting as an example. *Mol Ther* **17**, 828-836 (2009).
158. Thurber, G.M., Schmidt, M.M. & Wittrup, K.D. Factors determining antibody distribution in tumors. *Trends Pharmacol Sci* **29**, 57-61 (2008).
159. Saltzman, W.M. Drug Delivery: Engineering Principles for Drug Therapy. (Oxford University Press, 2001).
160. Benedetto, S. et al. Quantification of the expression level of integrin receptor alpha(v)beta3 in cell lines and MR imaging with antibody-coated iron oxide particles. *Magn Reson Med* **56**, 711-716 (2006).
161. Wilhelm, C., Gazeau, F., Roger, J., Pons, J.N. & Bacri, J.C. Interaction of anionic superparamagnetic nanoparticles with cells: Kinetic analyses of membrane adsorption and subsequent internalization. *Langmuir* **18**, 8148-8155 (2002).
162. Lauffenburger, D. & Linderman, J. Receptors: Models for Binding, Trafficking, and Signaling. (Oxford University Press, Oxford; 1993).
163. Tassa, C. et al. Binding affinity and kinetic analysis of targeted small molecule-modified nanoparticles. *Bioconjug Chem* **21**, 14-19 (2010).
164. Garanger, E., Boturyn, D., Coll, J.L., Favrot, M.C. & Dumy, P. Multivalent RGD synthetic peptides as potent alphaVbeta3 integrin ligands. *Org Biomol Chem* **4**, 1958-1965 (2006).
165. Koo, L.Y., Irvine, D.J., Mayes, A.M., Lauffenburger, D.A. & Griffith, L.G. Co-regulation of cell adhesion by nanoscale RGD organization and mechanical stimulus. *J Cell Sci* **115**, 1423-1433 (2002).
166. Perumal, O.P., Inapagolla, R., Kannan, S. & Kannan, R.M. The effect of surface functionality on cellular trafficking of dendrimers. *Biomaterials* **29**, 3469-3476 (2008).
167. Fant, K. et al. Effects of PEGylation and Acetylation of PAMAM Dendrimers on DNA Binding, Cytotoxicity and in Vitro Transfection Efficiency. *Mol Pharm* (2010).

168. Patil, M.L., Zhang, M. & Minko, T. Multifunctional Triblock Nanocarrier (PAMAM-PEG-PLL) for the Efficient Intracellular siRNA Delivery and Gene Silencing. *ACS Nano* **5**, 1877-1887 (2011).
169. Huang, R., Ke, W., Liu, Y., Jiang, C. & Pei, Y. The use of lactoferrin as a ligand for targeting the polyamidoamine-based gene delivery system to the brain. *Biomaterials* **29**, 238-246 (2008).
170. Huang, R.Q. et al. Efficient gene delivery targeted to the brain using a transferrin-conjugated polyethyleneglycol-modified polyamidoamine dendrimer. *FASEB J* **21**, 1117-1125 (2007).
171. Tokatlian, T. & Segura, T. siRNA applications in nanomedicine. *Nanomedicine and Nanobiotechnology* **2**, 305-315 (2010).
172. Kataoka, K., Harada, A. & Nagasaki, Y. Block copolymer micelles for drug delivery: design, characterization and biological significance. *Advanced Drug Delivery Review* **47**, 113-131 (2001).
173. Nishiyama, N. & Kataoka, K. Current state, achievements, and future prospects of polymeric micelles as nanocarriers for drug and gene delivery. *Pharmacology & Therapeutics* **112**, 630-648 (2006).
174. Osada, K. & Kataoka, K. Drug and gene delivery based on supramolecular assemply of PEG-polypeptide hybrid block copolymers. *Advances in Polymer Science* **202**, 113-153 (2006).
175. Itaka, K. et al. Supramolecular nanocarrier of siRNA from PEG-based block catiomer carrying diamine side chain with distinctive pKa directed to enhance intracellular gene silencing. *Journal of the American Chemical Society* **126**, 13612-13613 (2005).
176. Xiong, X., Uludag, H. & Lavasanifar, A. Biodegradable amphiphilic poly(ethylene oxide)-block-polyesters with grafted polyamines as supramolecular nanocarriers for efficient siRNA delivery. *Biomaterials* **30**, 242-253 (2009).
177. Yokoyama, M. Polymeric micelles as a new drug carrier system and their required considerations for clinical trials. *Expert Opinion on Drug Delivery* **7**, 145-158 (2010).
178. KoreanBreastCancerStudyGroup in ClinicalTrials.gov [Internet], Vol. NCT00912639 (National Library of Medicine (US), 2009).
179. Samyang in ClinicalTrials.gov [Internet], Vol. NCT00876486 (National Library of Medicine (US), 2009).
180. Matsumoto, S. et al. Environment-responsive block copolymer micelles with a disulfide cross-linked core for enhanced siRNA delivery. *Biomacromolecules* **10**, 119-127 (2009).
181. Sun, T., Du, J., Yan, L., Mao, H. & Wang, J. Self-assembled biodegradable micellar nanoparticles of amphiphilic and cationic block copolymer for siRNA delivery. *Biomaterials* **29**, 4348-4355 (2008).
182. Beh, C. et al. Efficient delivery of Bcl-2-targeted siRNA using cationic polymer nanoparticles: downregulating mRNA expression level and sensitizing cancer cells to anticancer drug. *Biomacromolecules* **10**, 41-48 (2009).
183. Zhu, C. et al. Co-delivery of siRNA and paclitaxel into cancer cells by biodegradable cationic micelles based on PDMAEMA-PCL-PDMAEMA triblock copolymers. *Biomaterials* **31**, 2408-2416 (2010).
184. Kim, W. & Kim, S. Efficient siRNA delivery with non-viral polymeric vehicles. *Pharmaceutical Research* **26**, 657-666 (2009).
185. Chnari, E., Lari, H., Tian, L., Uhrich, K. & Moghe, P. Nanoscale anionic macromolecules for selective retention of low-density lipoproteins. *Biomaterials* **26**, 3749-3758 (2005).
186. Chnari, E., Nikitczuk, J., Uhrich, K. & Moghe, P. Nanoscale anionic macromolecules can inhibit cellular uptake of differentially
oxidized LDL. *Biomacromolecules* **7**, 597-603 (2006).
187. Chnari, E., Nikitczuk, J., Wang, J., Uhrich, K. & Moghe, P. Engineered polymeric nanoparticles for receptor-targeted blockage of oxidized low-density lipoprotein uptake and atherogenesis in macrophages. *Biomacromolecules* **7**, 1796-1805 (2006).
188. Djordjevic, J., Barch, M. & Uhrich, K. Polymeric micelles based on amphiphilic scorpion-like macromolecules: novel carriers for water-insoluble drugs. *Pharmaceutical Research* **22**, 24-32 (2005).
189. Djordjevic, J., Del Rosario, L., Wang, J. & Uhrich, K. Amphiphilic scorpion-like macromolecules as micellar nanocarriers. *Journal of Bioactive and Compatible Polymers* **23**, 532-551 (2008).
190. Iverson, N. et al. Bioactive polymers for multimodal inhibition of inflammation and atherogenesis in activated macrophages. *under review* (2010).

191. Iverson, N.M., Sparks, S.M., Demirdirek, B., Uhrich, K.E. & Moghe, P.V. Controllable inhibition of cellular uptake of oxidized low-density lipoprotein: Structure-function relationships for nanoscale amphiphilic polymers. *Acta Biomaterialia* **6**, 3081-3091 (2010).
192. Plourde, N., Kortagere, S., Welsh, W. & Moghe, P. Structure-activity relations of nanolipoblockers with the atherogenic domain of human macrophage scavenger receptor A. *Biomacromolecules* **10**, 1381-1391 (2009).
193. Tao, L. & Uhrich, K. Novel amphiphilic macromolecules and their in vitro characterization as stabilized micellar drug delivery systems. *Journal of Colloid and Interface Science* **298**, 102-110 (2006).
194. Tian, L., Yam, L., Zhou, N., Tat, H. & Uhrich, K. Amphiphilic scorpion-like macromolecules: design, synthesis, and characterization. *Macromolecules* **37**, 538-543 (2004).
195. Wang, J., Plourde, N., Iverson, N., Moghe, P. & Uhrich, K. Nanoscale amphiphilic macromolecules as lipoprotein inhibitors: the role of charge and architecture. *International Journal of Nanomedicine* **2**, 697-705 (2007).
196. Torchilin, V. Micellar Nanocarriers: Pharmaceutical Perspectives. *Pharmaceutical Research* **24**, 1-16 (2007).
197. Zintchenko, A., Philipp, A., Dehshahri, A. & Wagner, E. Simple modifications of branched PEI lead to highly efficient siRNA carriers with low toxicity. *Bioconjugate Chemistry* **19**, 1448-1455 (2008).
198. Brannon-Peppas, L. & Blanchette, J.O. Nanoparticle and targeted systems for cancer therapy. *Advance Drug Delivery Reviews* **56**, 1649-1659 (2004).
199. Davis, M.E., Chen, Z. & Shin, D.M. Nanoparticle therapeutics: an emerging treatment modality for cancer. *Nature Reviews Druge Discovery* **7**, 771-782 (2008).

APPENDIX

Appendix 1

Chapter 3: *PAMAM-RGD Conjugates Enhance siRNA Delivery Through a Multicellular Spheroid Model of Malignant Glioma*

The following are the MALDI TOF mass spectra obtained for the PAMAM-RGD conjugates formulated in this work:

G5 PAMAM

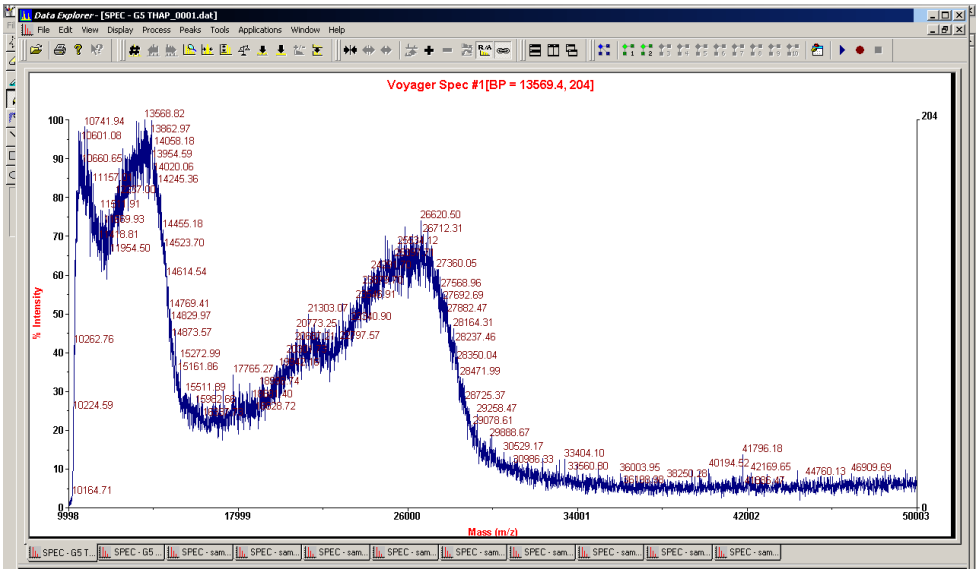

G5-2RGD

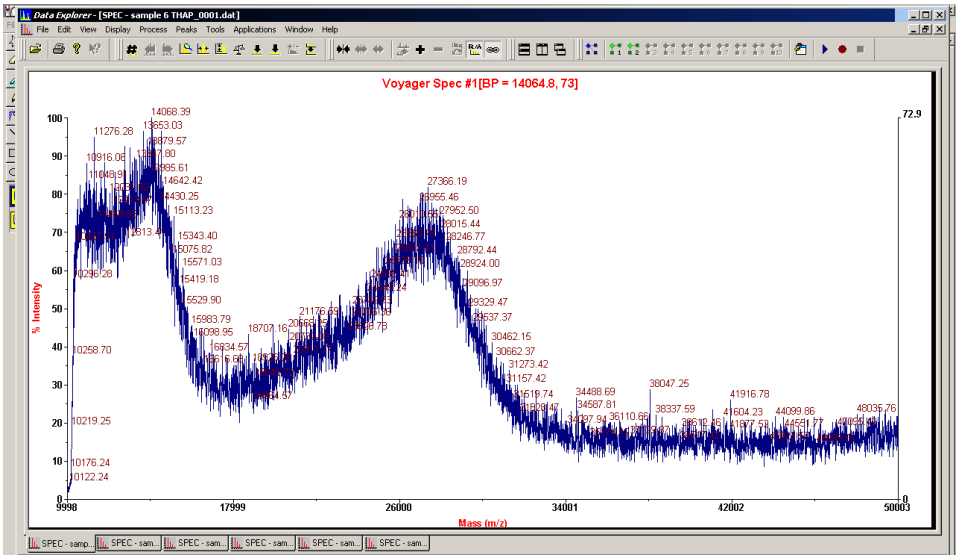

G5-3RGD

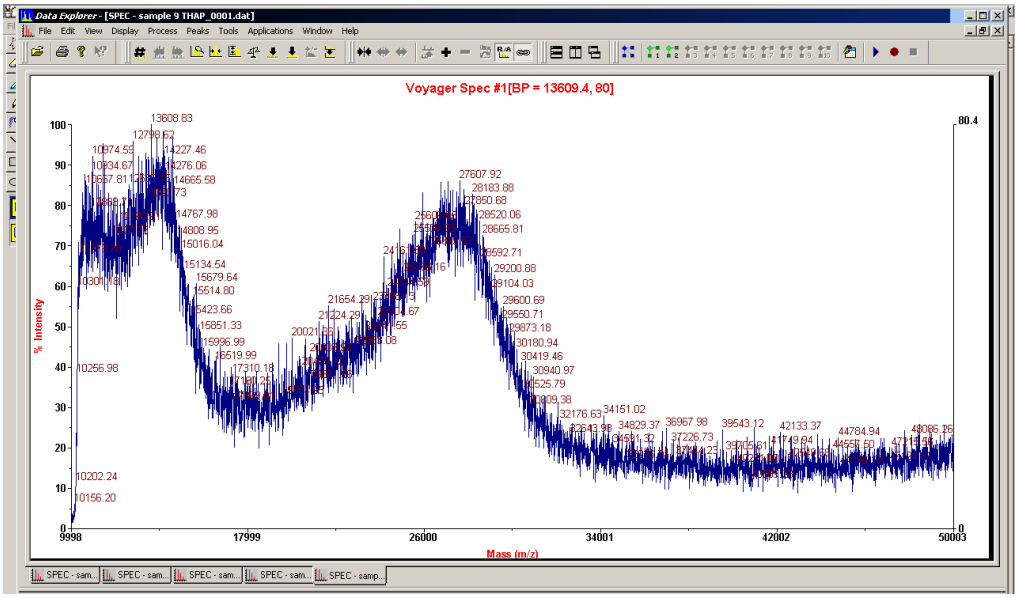

G5-7RGD

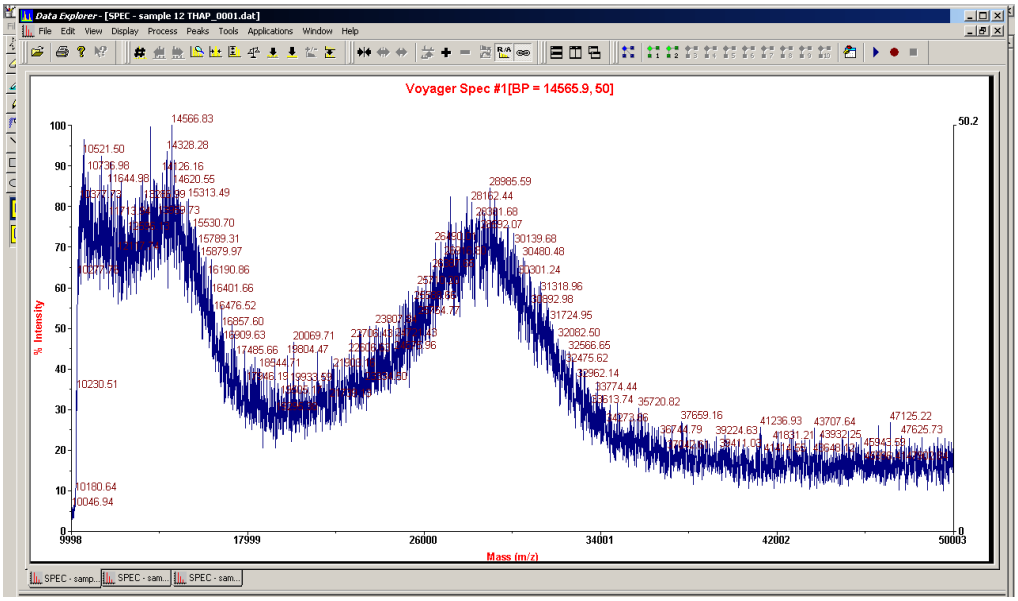

G5-10RGD

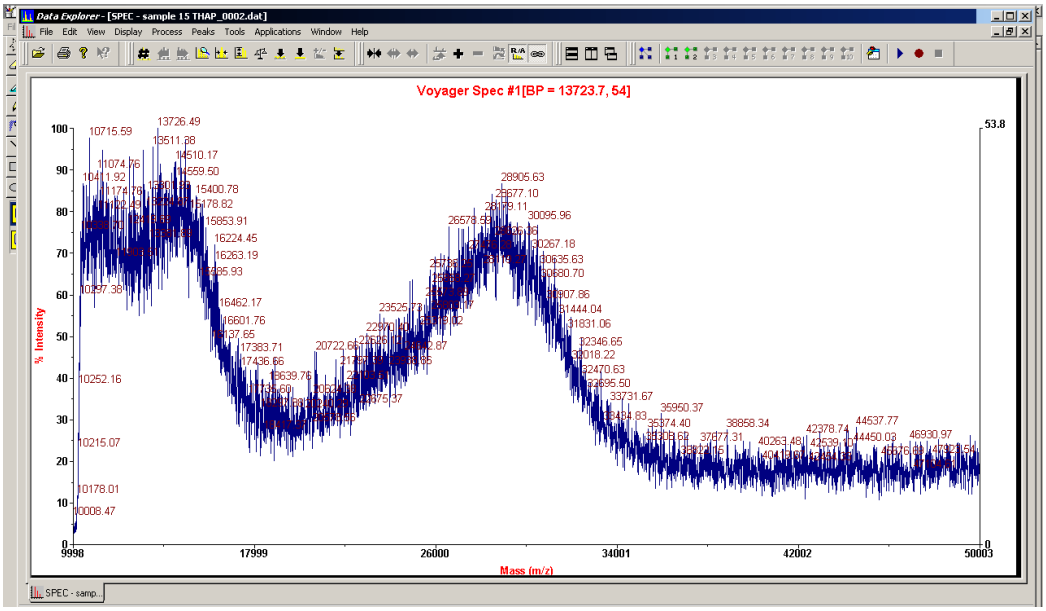
Data Explorer - [SPEC - sample 15 THAP_0002.dat]
File Edit View Display Process Peaks Tools Applications Window Help
Voyager Spec #1[BP = 13723.7, 54]
% Intensity
Mass (m/z)
9998
17999
26000
34001
42002
50003
53.8
SPEC - samp...

Appendix 2

Chapter 4: *Binding and Transport of PAMAM-RGD in a Tumor Spheroid model: The Effect of RGD Targeting Ligand Density*

Supplementary Data

1. Spheroid Architecture Analysis.

Methods. The porosity of spheroids formed from U87 cells was estimated from the analysis of high-magnification confocal images acquired of the spheroids. Spheroids were transferred from agarose-coated plates to the surface of a LabTek coverglass chamber immediately prior to imaging. A Leica LCSSB2 confocal microscope was used to acquire images of the spheroid structure at 63X magnification. Z-stack imaging was performed to capture images at 5 μm intervals for approximately 100 μm of depth into the spheroids. Confocal images were analyzed to estimate spheroid porosity using ImageJ software[149]. A pixel intensity threshold was selected that represented areas containing cells and was applied to each image. The fraction of surface area for each image that was not contained within the high-intensity threshold was considered void space. Average porosity throughout the spheroid volume was determined by averaging the void fraction determined from each image of the z-stack analysis.

Results. Images for each spheroid were acquired at different z-planes throughout the spheroid volume and were analyzed to estimate the fraction of surface area that represented void space for each spheroid (Figure S1). As the porosity profile of spheroids formed using the hanging drop method was found to be very heterogeneous and no consistent variation could be determined as a function of the z-distance throughout each spheroid, an average porosity estimate ($\bar{\varepsilon} = \sum_{j=1}^{N} \varepsilon_j = 0.09$) was taken

from the image analysis of four separate spheroids and used to represent the average spheroid architecture in the mathematical transport model.

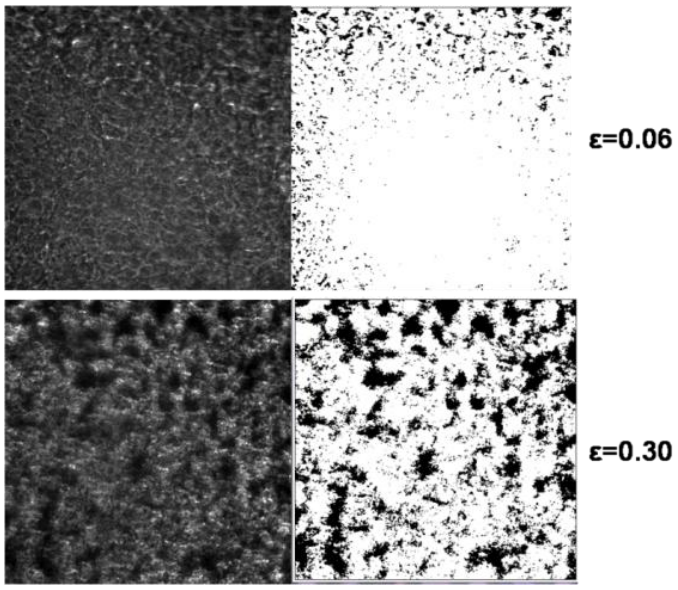

Figure S1. Representative images acquired from U87 spheroids (left column), and after applying thresholding to estimate spheroid porosity (right column). A pixel threshold was applied to each image where black regions represented voids and white regions represented cells. The surface area of each image with pixels contained within the threshold representing voids (black) was calculated, and an average void fraction, ε, was determined for each spheroid by averaging the void fraction calculated for each z-stack image.

2. Non-Specific Binding between PAMAM dendrimers and the SPR sensor chip

Unmodified G5 PAMAM dendrimers were injected as controls across the SPR sensorgram chip. A significant binding response was observed between cationic PAMAM and the anionic dextran on the SPR sensor chip (Figure S2). To confirm that this interaction was electrostatic in nature, injections were performed with PAMAM dendrimers containing 60 or 80% of surface amine neutralization by acetylation (Ac60 or Ac80, respectively). Acetylation of 60% of the amines resulted in a moderate decrease in

binding, while acetylation of 80% of the amines abolished binding (Figure S2). From these data, we infer that the nature of this interaction was electrostatic.

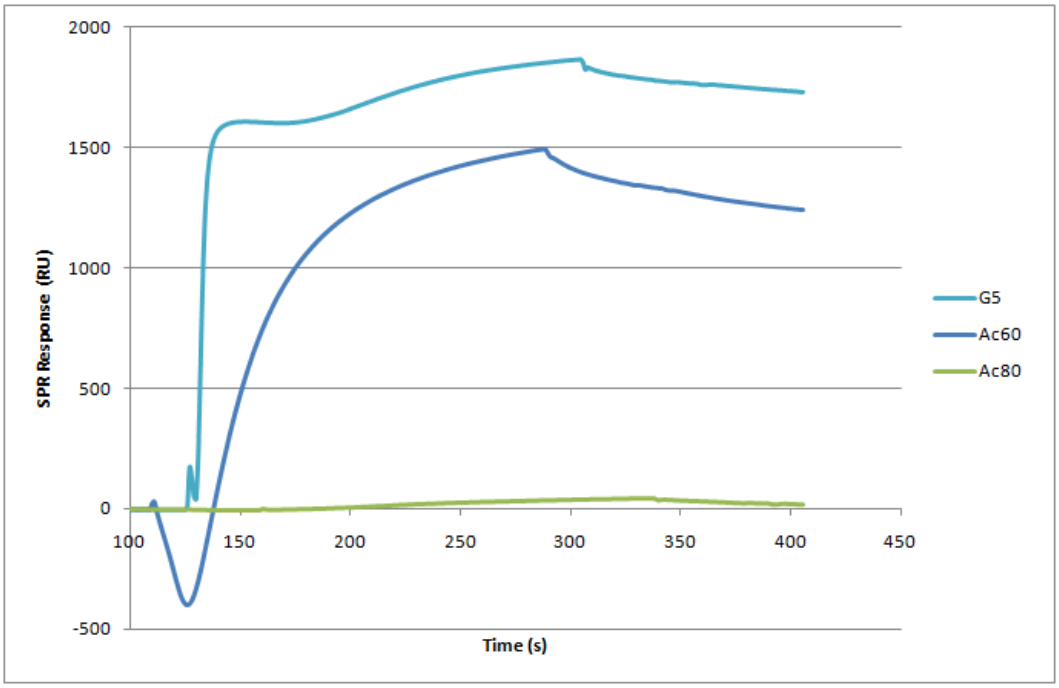

Figure S2. SPR sensorgrams showing injections of G5 PAMAM, and PAMAM with 60 or 80% of amine acetylation (Ac60 or Ac80) across a CM5 sensorgram chip. Dendrimers were injected at a concentration of 1 µM.

As it was not practical to acetylate 80% of the primary amines on the PAMAM-RGD conjugates used in this work (the amine groups are necessary to facilitate the cellular delivery of siRNA[18]), other steps were necessary to reduce the electrostatic binding between PAMAM and the SPR sensor chip. A sensor chip (CM4) was utilized that contains a lower concentration of the anionic dextran substrate, and soluble carboxymethyl dextran was added at a concentration of 1 mg/mL to minimize non-specific binding of cationic dendrimers to the anionic dextran substrate on the sensor chip surface. Nonetheless, some non-specific binding was still observed. However, it was possible to distinguish between the non-specific electrostatic interactions between G5 PAMAM and the sensor chip from the desired integrin-RGD interactions present when

injecting the PAMAM-RGD conjugates (Figure S3). The square shape of the sensorgram produced by the G5 PAMAM dendrimers suggests bulk non-specific binding, whereas the PAMAM-RGD conjugates produced sensorgrams with an association and dissociation shape typical of ligand-receptor binding. The differences in the shape and magnitude of these sensorgrams indicated that the non-specific electrostatic interactions elicited by cationic PAMAM dendrimers were reduced when using PAMAM-RGD conjugates, presumably because the strength of the integrin-RGD interaction was stronger than that of the electrostatic binding interactions. In addition, the RGD ligands may produce a steric barrier to increase the distance between the charged amines of PAMAM and the dextran substrate, thereby reducing the electrostatic interaction. Thus, we utilized this experimental procedure to generate the sensorgrams used to assess the binding kinetics and affinity between PAMAM-RGD and integrin proteins.

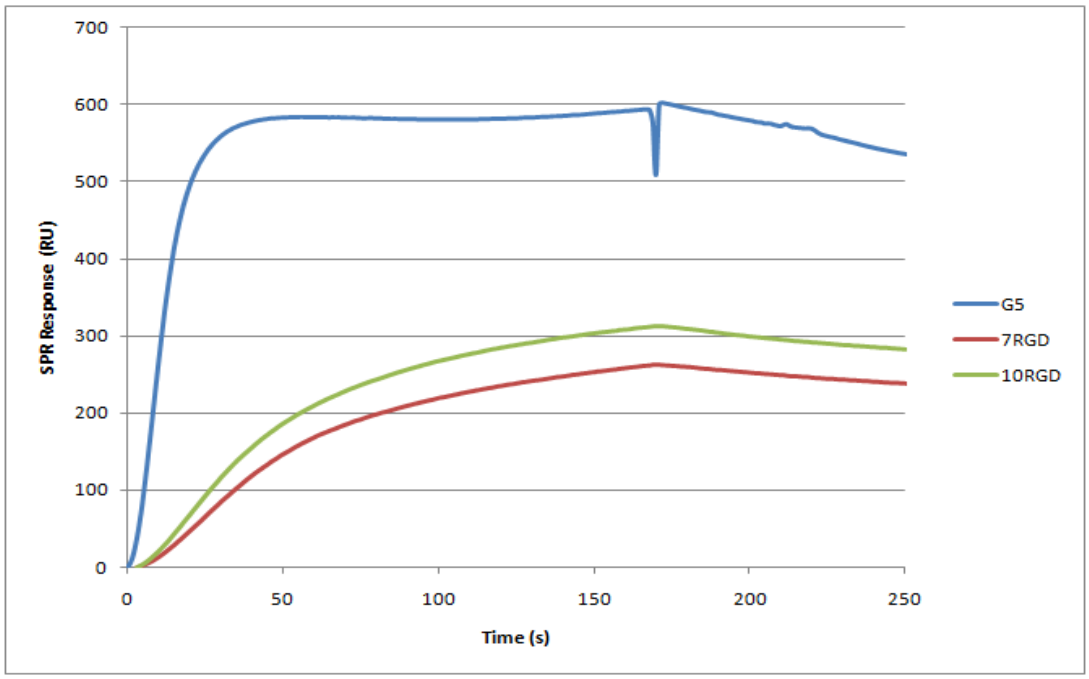

Figure S3. SPR sensorgrams of dendrimers injected over a CM4 sensor chip with 1 mg/mL of a soluble dextran non-specific binding reducing reagent. Unmodified PAMAM dendrimers (G5) elicited significant electrostatic binding with the sensor chips which was reduced when using PAMAM-RGD conjugates where the desired integrin-RGD interaction was captured by the sensorgrams.

Appendix 3

The following appendix shows work completed in conjunction with the work described in this dissertation. It has been accepted for publication in *Macromolecular Bioscience* in 2011. *(**Note**: The portions of this work completed by Carolyn L. Waite are italicized in the methods section)*

Efficient Intracellular siRNA Delivery by Ethyleneimine-Modified Amphiphilic Macromolecules

Sarah M. Sparks[a+], Carolyn L. Waite[b+], Alexander M. Harmon[a], Leora M. Nusblat[c], Charles M. Roth[b,c], and Kathryn E. Uhrich[a.c]*

[a]Department of Chemistry and Chemical Biology, [b]Department of Chemical and Biochemical Engineering, [c]Department of Biomedical Engineering, Rutgers University, Piscataway, NJ 08854, USA

[+]These authors contributed equally to this work

Summary

New materials that can bind and deliver oligonucleotides such as short interfering RNA (siRNA) without toxicity are greatly needed to fulfill the promise of therapeutic gene silencing. Amphiphilic macromolecules (AMs) that self-assemble to form nanoscale micelles were functionalized with linear ethyleneimines to create cationic AMs capable of complexing with siRNA. Structurally, the parent AM is formed of a mucic acid backbone whose tetra-hydroxy groups are alkylated with 12-carbon aliphatic chains to form the hydrophobic component of the macromolecule. This alkylated mucic acid is then mono-functionalized with poly(ethylene glycol) (PEG) to add hydrophilicity. The result is an AM with a free carboxylic acid within the hydrophobic domain of the unimer. In this work, linear ethyleneimines were conjugated to the free carboxylic acid to produce

an AM with one primary amine (**1N**) or one primary amine and four secondary amines (**5N**). Further, an AM with amine substitution both to the free carboxylic acid and between the PEG and the alkylated mucic acid was synthesized to produce a polymer with one primary amine and eight secondary amines (**9N**), four located on each side of the AM hydrophobic domain. All amine-functionalized AMs formed nanoscale micelles but only the **5N** and **9N** AMs had cationic zeta potentials, which increased with increasing number of amines. All AMs exhibited less inherent cytotoxicity than linear polyethyleneimine (L-PEI) at concentrations of 10 μM and above. By increasing the length of the cationic ethyleneimine chain and the total number of amines, successful siRNA complexation and cellular siRNA delivery was achieved in a malignant glioma cell line. In addition, siRNA-induced silencing of firefly luciferase was observed using complexes of siRNA with the **9N** AM and comparable to L-PEI, yet showed better cell viability at higher concentrations (above 10 μM). This work highlights the promise of cationic AMs as safe and efficient synthetic vectors for siRNA delivery. Specifically, a novel polymer (**9N**) was identified for efficient siRNA delivery to cancer cells and will be further evaluated.

Introduction

The use of short interfering RNA (siRNA) molecules for gene silencing has enormous clinical potential for treating human disease, particularly for anticancer applications[5, 140]. Recent advances in siRNA delivery technology have led to the initiation of several human clinical trials using therapeutic siRNA[4]. However, further development of safe, efficient siRNA delivery systems is required to advance siRNA therapeutics for routine clinical use and address diverse disease states. The delivery of siRNA and other

nucleic acid molecules to malignant cells has been attempted, for example, with varying degrees of success with numerous non-viral molecules including proteins, peptides, and synthetic polymers[171].

Self-assembled polymeric micelles have shown particular promise as drug and gene delivery vehicles due to their unique properties including steric stability, size suitable for passive tumor targeting, low cytotoxicity, high water solubility, and high drug encapsulation efficiency.[172,173, 174] Polymeric micelle systems are currently being investigated as drug delivery vehicles in several Phase I and II clinical trials in the United States[175-177], and are being evaluated in Phase III and IV studies internationally[178, 179]. More recently, several polymeric micelle systems have been evaluated for siRNA delivery[175, 176, 180, 181],or for the co-delivery of siRNA and hydrophobic anticancer drugs[182, 183]. However, further development is needed for a delivery system that possesses increased complex stability, lowered toxicity, biodegradability, as well as the versatility for treating multiple disease states and ease of modification (e.g., targeting moieties) to increase specificity. Specifically, for polymeric micelles, improvements on existing systems are necessary to improve their drug loading capacity, stability in the blood stream, and ability to penetrate the cell membrane to make these systems viable for widespread clinical use[184].

Nanoscale amphiphilic macromolecules (AMs) are novel, polymeric micelles developed by Uhrich and colleagues for treatment of cardiovascular disease and drug delivery[185-195]. The unimers are composed of a branched hydrophobic component formed by the tetra-alkylation of mucic acid, a biocompatible sugar, which is further derivatized with linear, hydrophilic poly(ethylene glycol) (PEG) – all of which are linked *via*

biodegradable bonds. In aqueous media, the unimers self-assemble to form nano-sized micelles at concentrations as low at 100 nM,[194] making them at least as stable as other polymeric micellar systems with CMC values on the order of 10^{-6} M[196]. Further, the polymers are biocompatible and capable of effectively delivering hydrophobic drugs intracellularly[188, 189, 191-193].

AMs are attractive for multiple applications due to their facile tunability, with multiple means of synthetic modification on both the hydrophilic and hydrophobic portions of the unimer. In this work, the hydrophobic functionality was exploited to create non-viral vectors for siRNA delivery. Specifically, linear, cationic ethyleneimine groups were conjugated to the unimer's hydrophobic backbone to facilitate electrostatic encapsulation and subsequent delivery of siRNA to malignant glioma cells. Ethyleneimines were chosen due to their similarity to the highly efficient non-viral vector, polyethyleneimine (PEI). However, PEI suffers from high cytotoxicity limiting its use for systemic in vivo applications where high polymer concentrations are required[184, 197]. The minimum number of amine groups necessary to efficiently deliver siRNA and elicit a gene-silencing response in malignant glioma cells, while maintaining the favorable structural properties and low cytotoxicity of the AM materials, was identified in this work. This proof-of-concept study outlines the rational design approach to siRNA delivery systems and identifies a promising new siRNA delivery system.

Experimental Part

Synthetic Materials

Unless otherwise stated, solvents and reagents were purchased from Fisher Scientific (Pittsburgh, PA) and Sigma-Aldrich (St. Louis, MO) and used as received. Poly(ethylene glycol) 5 kDa was purchased from Polysciences, Inc. (Warrington, PA) and dried by

azeotropic distillation from toluene before use. N-hydroxysuccinimide(NHS)-functionalized PEG, Methoxy-PEG-succinimidyl carboxymethyl (MW 5 kDa) (mPEG-SCM). was purchased from Laysan Bio, Inc (Arab, AL) and used as received**. 1**[188, 189, 193, 194]**, 2**[188], and **3**[189, 193]were prepared as previously published (See Scheme 1).

Polymer Characterization Methods

Proton nuclear magnetic resonance (^{1}H-NMR) spectra of the products were obtained using a Varian 400 MHz or 500 MHz spectrophotometer. Samples were dissolved in chloroform-d, with a few drops of dimethyl sulfoxide-d_6 if necessary, with tetramethylsilane as an internal reference. Molecular weights (Mw) and polydispersity indices (PDI) were determined using gel permeation chromatography (GPC) with respect to PEG (Sigma-Aldrich) on a Waters Stryagel® HR 3 THF column (7.8 x 300 mm). The Waters LC system (Milford, MA) was equipped with a 2414 refractive index detector, a 1515 isocratic HPLC pump, and 717plus autosampler. An IBM ThinkCentre computer with Waters Breeze Version 3.30 software installed was used for collection and processing of data. Samples were prepared at a concentration of 10 mg/mL in tetrahydrofuran, filtered using 0.45 μm pore size nylon or polytetrafluoroethylene syringe filters (Fisher Scientific) and placed in sample vials to be injected into the system. Melting points were determined by differential scanning calorimetry (DSC) on a TA DSC Q200. TA Universal Analysis 2000 software was used for data collection on a Dell Dimension 3000 computer. Samples (3-5 mg) were heated under dry nitrogen gas. Data were collected at heating and cooling rates of 10 °C /min with a two-cycle minimum.

Polymer Synthesis

1N Ethylenediamine (50 µL, 0.75 mmol) was dissolved in HPLC-grade CH_2Cl_2 (3 mL) and triethylamine (0.15 mL, 1.1 mmol). In a separate vessel, **2** (0.51 g, 0.085 mmol) was dissolved in HPLC-grade CH_2Cl_2 (9 mL) and subsequently added to the solution of ethylenediamine dropwise *via* syringe pump at a rate of 1.0 mL/hr. The reaction was stirred overnight (~ 18 hrs). The reaction solution was then diluted with CH_2Cl_2 and subsequently washed with 0.1 N HCl/brine (1x) and brine (2x). The combined aqueous portions were extracted with CH_2Cl_2 and the combined organics dried over $MgSO_4$, and concentrated to a yellow oil. The desired product was precipitated from the oil dissolved in CH_2Cl_2 (5 mL) by addition of 10-fold diethyl ether and cooling over dry ice for 1 hr. The solid was then collected by centrifugation at 3000 rpm for 5 min and the supernatant removed by decanting. The resulting white solid was dried under ambient atmosphere (12 hrs) and under high vacuum (12 hrs). Yield: 0.41 g, 80 %. ^{1}H-NMR ($CDCl_3$): δ 5.67 (m, 2H, CH), 5.14 (m, 2H, CH), 4.24 (m, 3H, CH_2), 3.60 (m, ~0.45 kH, CH_2O), 3.37 (s, 3H, OCH_3), 2.37 (m, 8H, CH_2), 2.29 (m, 4H, CH_2), 1.81 (b, 4H, CH_2), 1.60 (m, 8H, CH_2), 1.26 (m, 64H, CH_2), 0.87 (t, 12H, CH_3). T_m = 58 °C GPC: M_w: 6.3 kDa; PDI: 1.1.

5N Pentaethylenehexamine (0.15 mL, 0.64 mmol) was dissolved in HPLC-grade CH_2Cl_2 (10 mL) and triethylamine (0.33 mL, 2.4 mmol). In a separate vessel, **2** (0.48 g, 0.079 mmol) was dissolved in HPLC-grade CH_2Cl_2 (10 mL) and subsequently added to the solution of ethylenediamine dropwise *via* syringe pump at a rate of 1.0 mL/hr. The reaction was stirred overnight (~ 17 hrs). The bright yellow reaction solution was diluted with CH_2Cl_2 and subsequently washed with 0.1 N HCl/brine (1x) and brine (2x). The combined aqueous portions were extracted with CH_2Cl_2 and the combined organics dried

over $MgSO_4$, and concentrated to a cloudy yellow oil. The desired product was precipitated from the oil dissolved in CH_2Cl_2 (5 mL) by addition of 10-fold diethyl ether and cooling over dry ice for 1 hr. The solid was then collected by centrifugation at 3000 rpm for 5 min and the supernatant removed by decanting. The resulting white solid was dried under ambient atmosphere (12 hrs) and under high vacuum (12 hrs). Yield: 0.42 g, 86 %. ^{1}H-NMR (DMSO): δ 5.50 (m, 2H, CH), 5.11 (m, 2H, CH), 3.41 (m, ~0.45 kH, CH_2O), 3.24 (s, 3H, OCH_3), 2.89 (m, 13 H, CH_2), 2.80 (bs, 2H, CH_2), 2.76 (bs, 7H, CH_2), 2.64 (bs, 6H, CH_2), 1.49 (m, 8H, CH_2), 1.24 (m, 64H, CH_2), 0.84 (t, 12H, CH_3). T_m = 59 °C. GPC: M_w: 6.4 kDa; PDI: 1.1.

4 Product **3** (5.10 g, 5.43 mmol) and NHS (5.38 g, 46.8 mmol) were dissolved in anhydrous CH_2Cl_2 (100 mL) and anhydrous DMF (18 mL) under argon. Once a clear solution was obtained, N,N'-dicyclohexylcarbodiimide (17 mL, 17 mmol) was added and the reaction stirred at room temp under argon for 24 hours. The resulting solution with white suspension was stored at -4 °C overnight. The dicyclohexyl urea (DCU) byproduct was then removed by vacuum filtration and the filtrate washed with 0.1 N HCl and 50:50 brine/H_2O, dried over $MgSO_4$, and concentrated. The resulting white solid was then dissolved in a small amount of CH_2Cl_2 (5-10 mL) and stored at -4 °C for 2-3 hours. The resulting white suspension was filtered to remove residual DCU. The filtrate was then concentrated to dryness and the white solid dried under high vacuum overnight. Yield = 4.5 g, 73 %. ^{1}H-NMR ($CDCl_3$): δ = 5.96 (s, 2H, CH), 5.57 (s, 1H, CH), 2.81 (s, 8H, CH_2), 2.49 (m, 6H, CH_2), 2.37 (m, 2H, CH_2), 1.64 (m, 8H, CH_2), 1.27 (m, 64H, CH_2), 0.89 (t, 12H, CH_3).

9N Pentaethylenehexamine (0.05 mL, 0.2 mmol) was dissolved in CH_2Cl_2 (3 mL) and triethylamine (0.15 mL, 1.1 mmol). In a separate vessel, **4** (0.10 g, 0.090 mmol) was dissolved in HPLC-grade CH_2Cl_2 (3 mL) and subsequently added to the solution of ethylenediamine dropwise *via* syringe pump at a rate of 1.0 mL/hr. The reaction was stirred at room temperature a total of 8 hrs. mPEG-SCM (0.45 g, 0.090 mmol) dissolved in CH_2Cl_2 (7 mL) was then added to the yellow reaction solution dropwise *via* syringe pump at a rate of 1.0 mL/hr. The reaction was stirred at room temperature overnight (~ 17 hrs). The solvent was then removed from the reaction solution by rotary evaporation. The oil/solid was then redispersed in CH_2Cl_2 and filtered to remove the solid NHS-byproduct. The filtrate was concentrated to an oil and product precipitated from the oil dissolved in CH_2Cl_2 (5 mL) by addition of 10-fold diethyl ether. The solid was then collected by centrifugation at 3000 rpm for 5 min and the supernatant removed by decanting. The resulting white solid was washed with diethyl ether (1x) and dried under ambient atmosphere (12 hrs) and under high vacuum (12 hrs). Yield: 0.45 g, 87 %. ^{1}H-NMR ($CDCl_3$): δ 7.26 (s, 4H, CH), 3.69 (m, ~0.44 kH, CH_2O), 3.38 (s, 3H, OCH_3), 3.05 (bm, 15H, CH_2), 2.55 (bm, 16H, CH_2), 2.07 (bm, 40H, CH_2), 1.65 (bs, 7H, CH_2), 1.48 (t, 5H, CH_2), 1.26 (m, 37H, CH_2), 0.88 (t, 12H, CH_3). T_m = 59 °C. GPC: M_w: 5.5 kDa; PDI = 1.1.

Size and Zeta Potential of AMs and AM/siRNA complexes

Dynamic light scattering (DLS) and zeta potential analyses were performed using a Malvern Instruments Zetasizer Nano ZS-90 instrument (Southboro, MA). DLS measurements were performed at a 90° scattering angle at 25°C. Size distributions by volume of measurements were collected in triplicate, averaged and reported. Zeta

potential measurements were collected in triplicate, averaged and the Z-average charges reported. For all measurements, error bars represent peak widths of the average value.

Sample Preparation

AMs alone. *Polymer solutions at a concentration of 1.0 mg/mL were prepared using picopure water and filtered with a 0.45 µM Nylon syringe filter (Fischer Scientific, Pittsburgh, PA).*

AM/siRNA complexes. *Complexes were prepared in picopure water at various nitrogen/phosphate (N/P) ratios. For size and zeta potential measurements, 2mL of solutions containing AM/siRNA complexes were prepared at polymer concentrations sufficient for detection by the zetasizer instrument (1 mg/mL for **1** and **1N**, and 2 mg/mL for **5N** and **9N**). Solutions were briefly vortexed and incubated for at least 60 min at room temperature to allow for complex formation prior to size and zeta potential analysis.*

Gel Electrophoresis *Polymer/siRNA (Dharmacon, Lafayette, CO) complexes were first prepared at the desired nitrogen to phosphorous (N/P) ratios by mixing solutions of polymers (stocks maintained in DI water) and siRNA in PBS (final siRNA concentration of 12.5 µg/mL). Since polymer **1** does not contain primary amines, the mass of polymer **1** added for the gel electrophoresis experiments was equivalent to the mass of polymer **1N** added at the N/P ratios indicated in Figure 2. Solutions were briefly vortexed, and incubated for 60 min at room temperature to allow for complex formation. Polymer/siRNA complexes were loaded into 1% agarose gels run in an electrophoresis*

chamber at 70 V for 40 minutes. Following electrophoresis, gels were stained with SYBR Green II RNA gel stain (Invitrogen, Carlsbad, CA) for 30 minutes prior to imaging on a Bio-Rad Molecular Imager FX (Bio-Rad Laboratories, Hercules, CA) to visualize unbound siRNA. The fluorescence intensities of bands were quantified using Quantity One Quantitation software (Bio-Rad Laboratories, Hercules, CA).

Cell Culture *All cell culture products were obtained from Invitrogen (Carlsbad, CA). U87 MG cells (ATCC HTB-14) were maintained in DMEM medium supplemented with 10% fetal bovine serum (FBS), L-glutamine, and penicillin-streptomycin. A U87 cell line containing a stably integrated destabilized EGFP (d1EGFP) transgene (U87-GFP) was generated as described previously[18], and was maintained under constant selective pressure by G418 (500 μg/mL), and the growth medium was supplemented with sodium pyruvate and nonessential amino acids. U87-Luc, a human glioblastoma cell line with constitutive expression of firefly luciferase, was generously provided by Dr. Xu-Li Wang (Department of Pharmaceutics and Pharmaceutical Chemistry, University of Utah). U87-Luc cells were maintained in minimal essential medium supplemented with 10% FBS, penicillin-streptomycin, and maintained under selective pressure by G418.*

Cytotoxicity Assay *U87 glioma cells were seeded into 96 well plates (Corning, Corning, NY) at 10,000 cells per well in DMEM supplemented with 10% FBS and 1 % penicillin-streptomycin and incubated overnight at 37 ºC, with 5 % CO_2. The media was removed by aspiration and replaced with 200 μL aminated-AM or PEI dissolved in media at desired concentrations (n=4 per condition). Untreated control wells received media only. After 72 hours, cells were harvested by trypsinization (75 μL trypsin-EDTA*

followed with 75 μL complete media to neutralize trypsin) and 50 μL of staining solution (48:1:1 media:DMSO:Guava ViaCount Flex reagent (Guava Technologies, Hayward, CA) was added to each well. Cells were counted using a Guava EasyCyte Plus (Guava Technologies, Haywood CA) instrument with an original volume of 0.2 mL and a dilution factor of one.

siRNA Delivery Assay *U87-Luc cells were plated at a density of 5000 cells/well in 96-well plates approximately 20 hours prior to transfection. Immediately prior to transfection, polymer/siRNA complexes were prepared in 20 μL of PBS (N/P=50 for the AMs, and N/P=15 for linear PEI). Linear polyethyleneimine (Polysciences, Inc., Warrington, PA) commonly used polymeric transfection reagent, was used as a positive control. An irrelevant siRNA sequence not targeted against firefly luciferase was delivered as a negative control. The polyplexes were brought to a total volume of 100 μL in OptiMEM medium to obtain a final siRNA concentration of 100 nM. The serum-containing culture medium was aspirated from the cells, and each well treated with 100 μL of the polyplexes in OptiMEM medium. Each treatment was performed in triplicate. After a 4 hr incubation period, the transfection mixture was replaced with serum-containing growth medium and maintained under normal growth conditions until the cells were assayed for firefly luciferase expression 24 hours after the initial treatment.*

For fluorescence imaging, a similar transfection protocol was performed on U87-GFP cells seeded onto an 8-well LabTek coverglass chamber (Nalge Nunc, Naperville, IL) at a density of 5000 cells/well. U87-GFP cells were treated with a Cy5-labeled siRNA to facilitate imaging of cellular localization of siRNA.

Fluorescence Microscopy *Uptake of a fluorescently labeled siRNA (Dharmacon, Lafayette, CO) sequence into U87-GFP cells was evaluated using fluorescence microscopy. Imaging was performed 24 hours after siRNA transfection using an Olympus IX81 model fluorescent microscope (Olympus, Center Valley, PA). Imaging was performed at 20X magnification. The following excitation and emission wavelengths were used: GFP (excitation=482 nm, emission=536 nm) and Cy5 siRNA (excitation=628 nm, emission= 692 nm).*

Luciferase Detection Assay *Cells were prepared for firefly luciferase detection using the Luciferase Assay System (Promega, Madison, WI) according to the manufacturer's protocol. Firefly luciferase was quantified using The Reporter microplate luminometer (Turner Biosystems, Sunnyvale, CA). Following luciferase quantification, cell lysates were assayed for total protein content using the BCA Protein Assay kit (Pierce, Rockford, IL) according to the manufacturer's protocol.*

Statistics *Statistical comparisons for zeta potential measurements, luciferase silencing and polymer cytotoxicity were performed using a one-way ANOVA test with a Fisher's all-pairs post hoc comparison test.*

Results and Discussion

The goal of this study was to create novel synthetic vectors that exploit the structural properties of PEI beneficial for siRNA delivery while reducing the inherent cytotoxicity associated with PEI. AMs were modified with two different lengths of ethyleneimine chains to yield three novel polymer systems: ethylenediamine to yield **1N**, or pentaethylenehexamine to yield **5N** and **9N** polymers. The polymers were synthesized

as shown in **Scheme 1** from the amine-specific N-hydroxysuccinimide (NHS)-activated polymer **1**, which has been the focus of a previous publication[189].

The parent compound, **3**, served as the basic building block for the polymer modifications. Specifically, the carboxylic acid on the mucic acid backbone was activated with N-hydroxysuccinimide to functionalize the polymers with linear ethyleneimines, systematically increasing the total number of amines in the final polymers from one, **1N**, up to nine, **9N**. For **1N** and **5N**, an excess of the diamines coupled with their slow addition to the polymer solution *via* syringe pump were utilized to control for the disubstitution of polymer to both primary amines. For **9N**, a 2:1 molar ratio of compound **4** to pentaethylene hexamine coupled with the slow addition of **4** to the diamine *via* syringe pump were used to limit the formation of undesired oligomers. Subsequently, a 1:1 molar ratio of the NHS-PEG with respect to **4** coupled with its slow addition to the diaminated **4** *via* syringe pump were utilized to limit the coupling of PEG to both sides of the 4. For all aminated polymers, Isolation of cationic AMs with amines conjugated to, rather than associated with, the polymer was insured by precipitation from diethyl ether; this process precipitates the AM products but not the ethyleneimine starting materials. Amine conjugation was further verified by ^{1}H NMR spectroscopy. In addition to monitoring ^{1}H NMR spectra for the disappearance of protons associated with the NHS activating group (~ 2.8 ppm), new peaks assigned to the ethyleneamine protons were observed resonating at 1.3 and 1.8 ppm for **1N** and from 2.5-3.0 ppm for **5N** and **9N**. For all cationic AMs, the integrations of the ^{1}H NMR are consistent with mono PEG substitution to produce the desired, cationic AMs. The molecular weights of the cationic AMs were determined by GPC relative to PEG standards. As shown in **Table 1**, **1N** and

5N have similar molecular weights while the molecular weight of **9N** is approximately 1 kDa less. This difference can be attributed to the use of different PEG starting materials from different vendors that may have varying peak molecular weights. In addition, due to the incorporation of amines between the hydrophobic and hydrophilic component in the structure of **9N**, the polymer may associate more with the column than the other cationic polymers, thereby making the molecular weight appear lower than it actually is. For all cationic AMs, the absence of a high molecular weight peak in the GPC corresponding to ~ 10 kDa suggests there was little-to-no PEG di-substitution in any of the resulting polymers.

The toxicity of the aminated-AMs compared to linear PEI 25 kDa (L-PEI) was assessed in U87 glioma cells. A dose response curve was generated for all samples by counting viable cells remaining after a 72-hour exposure to the polymers (**Figure 1**). A significant decrease in cytotoxicity ($p<0.05$) was observed for all AMs compared to L-PEI at the highest concentrations tested (10^{-5} and 10^{-4} M). Interestingly, when comparing the AMs, the **9N** material exhibited the lowest cytotoxicity compared to the AMs containing fewer amine groups. One explanation for this observation is that the surface charge density of the **9N** micelles is lower as their hydrodynamic diameter (shown in **Figure 2c**) has increased by a factor of approximately five and, therefore, their area is increased by a factor of about 25 compared to the **1N** and **5N** micelles.

The ability of cationic AMs to complex anionic siRNA was evaluated using gel electrophoresis. Complexes were formed at a range of N/P ratios and run on an electrophoresis gel to separate un-complexed siRNA from the AM/siRNA complexes. The decrease in fluorescence intensity of the band corresponding to un-complexed

siRNA verifies the siRNA complexation efficiency of the cationic AMs. Polymers containing zero or one cationic amine group (i.e., **1** and **1N**) displayed no complexation of siRNA at charge ratios tested up to nitrogen/phosphorus (N/P) 80 (**Figure 2b**). By increasing the number of amine groups to five (**5N**), a modest extent of siRNA complexation (approximately 20%) was observed at N/P ratios of 60 and higher. Significantly improved siRNA complexation efficiency was observed by using the AM containing nine amine groups, **9N**, where most of the siRNA was encapsulated by N/P=50. The ability of AMs to complex siRNA was compared to L-PEI, where nearly complete siRNA complexation was observed by gel electrophoresis at N/P$\geq$15. Hence, for subsequent physical and biological characterization studies, AM/siRNA complexes were formed at N/P$\geq$50.

All cationic AMs formed micelles in the nanoscale size range as determined by dynamic light scattering (**Figure 2c**). **1N** and **5N** formed micelles of approximately the same size as polymer, **1**, while micelles formed from **9N** were much larger (~125 nm), presumably due to charge repulsion of the highly cationic ethyleneimine units. Once complexed with siRNA (**Figure 2c**, N/P=50 and 100), all cationic AMs maintained the nanoscale size of the AMs alone. Self-assembled polymeric micelles are known to have stable sizes that are dictated primarily by the architecture of the amphiphilic polymer segments[172]. Especially at high N/P ratios, the size of polymer micelles often remains unchanged in the presence of nucleic acids as the presence of relatively small amounts of siRNA does not change the properties of the stable polymer micelles[172, 180]. Maintaining sizes of less than ~100 nm is desirable for improved circulation time, passive tumor

targeting by the enhanced permeation and retention (EPR) effect, and optimal cellular uptake[198, 199].

Successful conjugation of the amines was shown by the disappearance of N-hydroxysuccinimide in the ^{1}H NMR as well as the increase in the zeta potential from negative (for polymer **1)**, to less negative (polymer **1N)**, and positive (polymers **5N** and **9N)**, as shown in **Figure 2d (**micelles only**)**. The zeta potential increased with increasing ethyleneimine length, further indicating the successful incorporation of amine groups. When siRNA was complexed with the cationic AMs at N/P ratios of 50 and 100, the zeta potentials for the aminated polymers **5N** and **9N** significantly changed compared to the native polymer in the absence of siRNA ($p<0.05$). Specifically, at N/P 50, the zeta potentials for complexes of siRNA and **5N** decreased from 12.7 mV of the **5N** alone to 5.3 mV when complexed with siRNA. Likewise, the zeta potential of **9N** decreased from 33.1 mV alone to 7.89 mV when complexed with siRNA. The zeta potentials for both AMs increased at N/P 100 – back to that for the vehicle alone for **5N** but only to 22.2 mV for **9N**. This data suggests that **9N** complexed most efficiently with siRNA at the N/P ratios evaluated in this study, as the decrease in zeta potential is a result of charge neutralization when the negatively charged siRNA complexes with the cationic AMs. These results are in agreement with the gel electrophoresis data. Based on the physical characterization of AM/siRNA complexes by gel electrophoresis, dynamic light scattering, and zeta potential, **9N** was expected to be the most effective siRNA delivery vehicle.

The ability of AMs to facilitate cellular delivery of siRNA and elicit silencing of the reporter gene, firefly luciferase, in U87 cells was evaluated. Polyplexes of AMs and

anti-luciferase siRNA were formed (siRNA concentration: 100 nM, N/P=50, AM concentration: ~10^{-5} M) and delivered to U87-Luc cells which were subsequently assayed for luciferase expression. To visually evaluate the cellular uptake of siRNA, a fluorescently labeled siRNA sequence was delivered separately to U87-GFP cells which were then imaged using fluorescent microscopy.

Successful cellular association of siRNA delivered by **5N** and **9N** was observed using fluorescent microscopy and was qualitatively comparable to siRNA delivered by L-PEI (**Figure 3A**). Significant luciferase silencing (p <0.05) was observed using the AMs containing five or nine amines (**5N** and **9N**), but not observed using the AMs containing just one amine group (**1N**) (**Figure 3B**). A similar luciferase silencing response was observed between the **9N** and L-PEI, a widely-studied polymeric system for nucleic acid delivery (**Figure 3B**). Delivering a scrambled siRNA sequence did not elicit luciferase silencing, demonstrating that the AMs alone do not induce off-target silencing effects.

To study the dynamics and dose-dependence of luciferase silencing by **9N**, the most promising aminated-AM, siRNA transfection experiments were performed at various time points, polymer concentrations (**Figure 3C**) and siRNA concentrations (**Figure 3D**). The minimum N/P ratio required for a maximum luciferase silencing response was N/P=25 (siRNA concentration: 100 nM, AM concentration: 1.2x10^{-5} M), (**Figure 3C**), and the minimum siRNA concentration required for optimal silencing response was 50 nM (**Figure 3D**).

Studying the dose response and dynamics of siRNA delivery by AMs provides insights into the mechanisms governing siRNA delivery by these novel molecules. Our results suggest that using polymer **9N** at N/P>25 is not biologically beneficial as similar

extents of gene silencing were observed using **9N** at N/P=25 and N/P=50. It is desirable to identify the lowest possible polymer concentration that can achieve optimal siRNA delivery, as having excessively high polymer concentrations can elicit undesirable cytotoxicity and may result in insolubility of polymers in aqueous media. Further, we observed that using siRNA concentrations of 50 nM was sufficient to achieve maximal luciferase gene silencing with **9N**. Presumably, having siRNA in excess of the minimum effective concentrations is unnecessary as the number of target mRNAs present in the cell is limited, and can be sufficiently targeted by siRNA present at 50 nM.

We also observed trends in siRNA silencing as a function of time, where maximum siRNA silencing was observed at 48 hours, and decreased after 72 hours. This trend in gene silencing dynamics is consistent with previous work evaluating the gene silencing dynamics of antisense oligonucleotides delivered by branched PEIs where the silencing of green fluorescent protein (GFP) became less pronounced after 24 hours[136]. This decrease in gene silencing activity after 48 hours can likely be attributed to intracellular degradation of siRNA molecules by nucleases over time.

Interestingly, the trends observed in the quantitative luciferase silencing assay differed somewhat from the qualitative observations of cellular association of a fluorescently labeled siRNA sequence into U87GFP cells. It appeared that **9N** delivered more siRNA to the cells than L-PEI in the fluorescent images, however, this trend was not observed in the luciferase silencing assay where both **9N** and L-PEI elicited similar extents of luciferase silencing. This observation suggests that while **9N** may be capable of delivering siRNA to cells, other intracellular barriers such as siRNA unpackaging or

endosomal escape may be affecting gene silencing activity by **9N**. This phenomenon will be investigated further in subsequent work.

Conclusions

Amphiphilic macromolecules that self-assemble to form nanoscale micellar assemblies were functionalized with linear ethyleneimines to render them positively charged for improved siRNA complexation. By increasing the number of secondary amines from one up to nine (i.e., from **1N** to **9N**, respectively), increased zeta potential and stable complexation with siRNA was achieved. All cationic AMs were less cytotoxic to U87 cells than L-PEI at polymer concentrations of 10 μM or greater. The cationic AM with nine total amines, **9N**, successfully delivered siRNA molecules to U87 cells and elicited silencing of the reporter gene, firefly luciferase. This work highlights the promise of AMs for siRNA delivery and specifically identified a novel AM molecule, **9N**, that displays low cytotoxicity compared to L-PEI, stable complexes with siRNA while maintaining a nanoscale size, and efficiently delivers siRNA delivery to malignant glioma cells.

Acknowledgements: We acknowledge the gift of U87-Luc cells from *Xu-Li Wang* at the *University of Utah* and financial support from *Rutgers University*, the *NIH* (2R01EB008278-07, P.I. CR), a *Schering-Plough* fellowship (SMS), and an *NSF* IGERT (DGE-0504497) fellowship (CLW).

Figures

Scheme 1

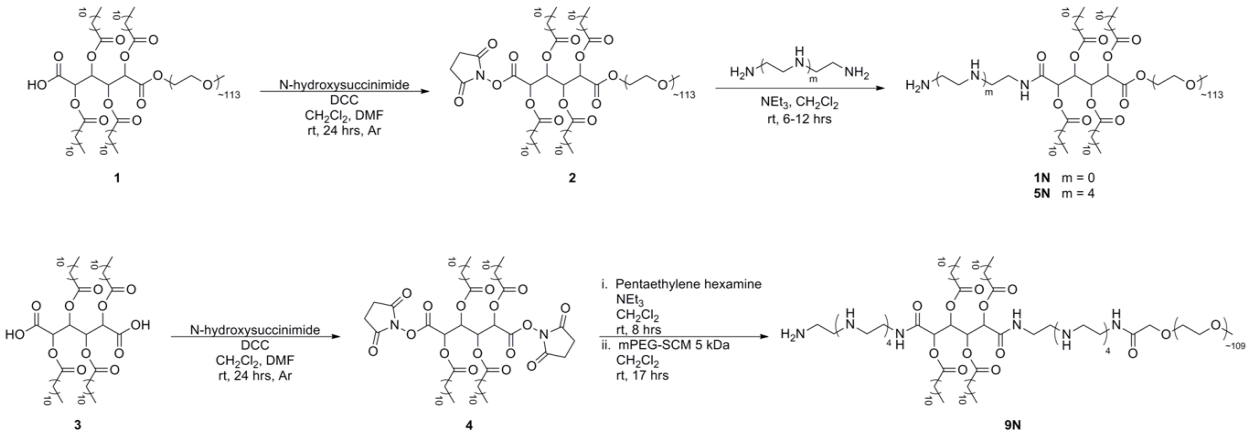

Synthesis of cationic-AMs; (top) synthesis of **1N** and **5N** from NHS-activation of **1** to yield **2** [21], (bottom) synthesis of **9N** *via* di-activation of **3** with NHS to yield **4**.

Table 1

Cationic AM	M_W (kDa)	PDI	T_m (° C)
1N	6.3	1.1	58
5N	6.4	1.1	59
9N	5.5	1.1	59

Molecular weights, poydispercity indices (PDI), and melting temperature (T_m) ethyleneimine-modified AMs.

Figure 1

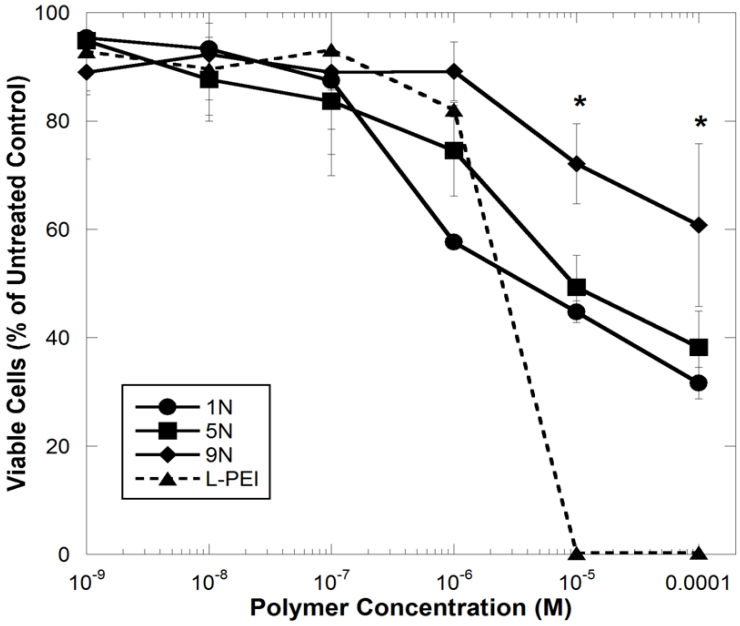

Cytotoxicity of cationic-AMs and L-PEI to U87 glioma cells after 72 hours of exposure. Data represent mean $\pm$ standard deviation (n=4). Astericks represent concentrations at which cationic-AMs elicited a significantly lower cytotoxicity than L-PEI ($p < 0.05$).

Figure 2

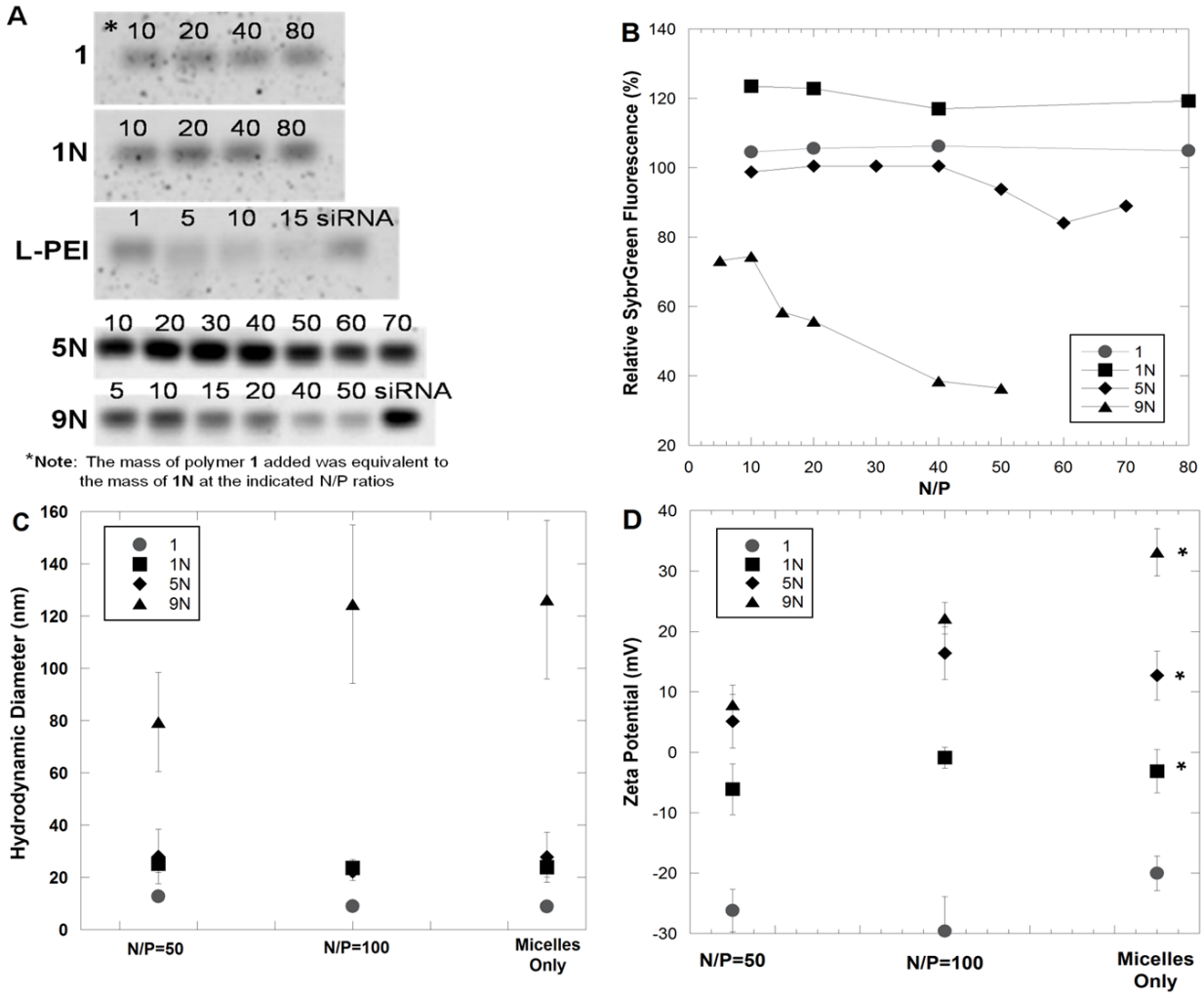

Characterization of AM/siRNA complexes by gel electrophoresis (A and B), dynamic light scattering (C), and zeta potential (D). Relative SybrGreen fluorescence corresponds to unbound siRNA detected in an electrophoresis band normalized by a band of free siRNA (B). Images of gel electrophoresis bands are shown with the N/P ratio for each band denoted above the band, where the mass of polymer **1** added was equivalent to **1N** at the indicated N/P ratios (A). Gel electrophoresis siRNA complexation studies were performed at least three times for each polymer, and one representative gel image and band quantification is shown here. The zeta potential measurements of each polymer

were compared to each other at varying N/P ratios, and astericks in **D** indicate polymers whose zeta potentials differed as a function of N/P ratio ($p<0.05$).

Figure 3

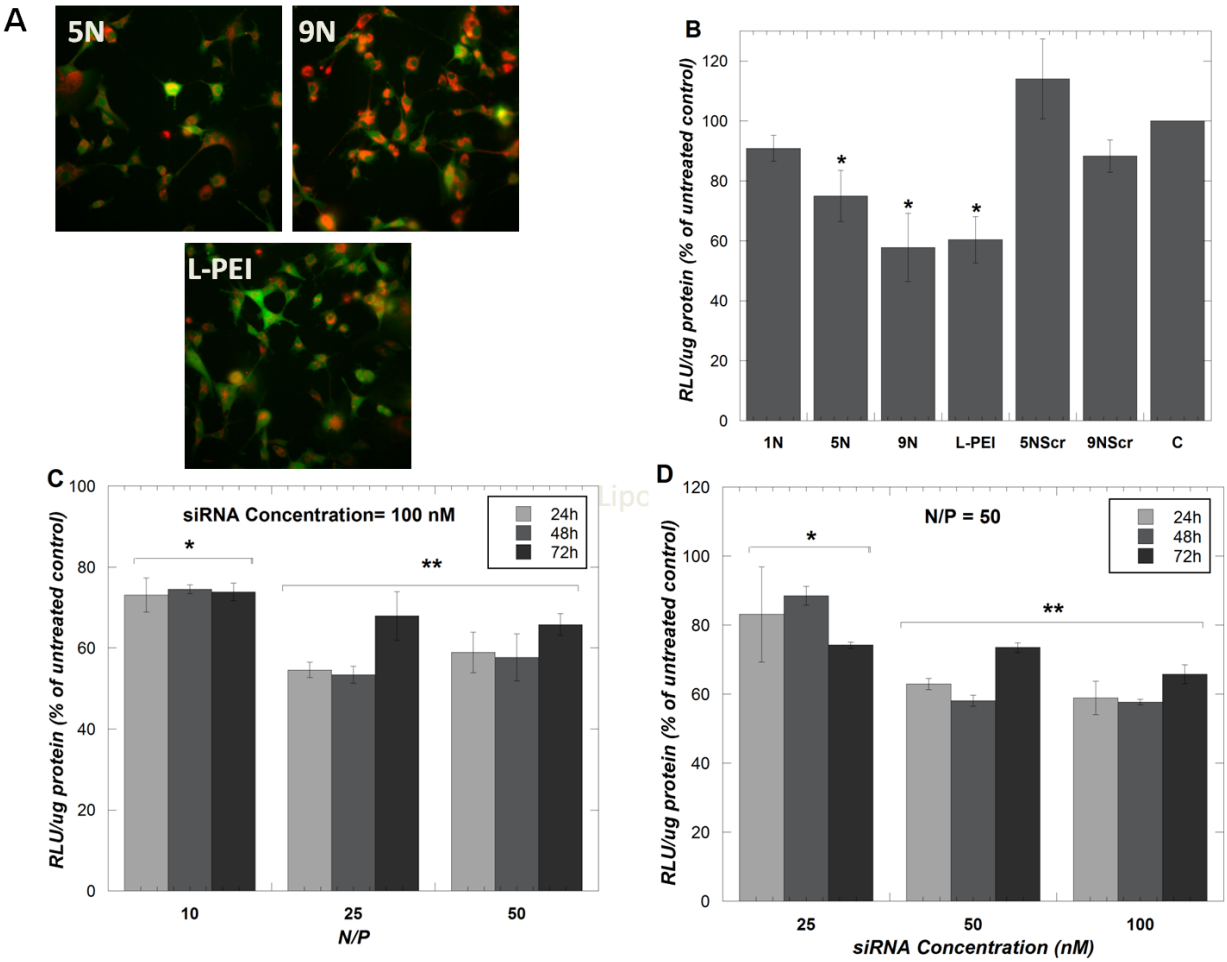

Fluorescent microscope images of siRNA distribution (red) in U87-d1EGFP cells (green) when delivered by the indicated polymers (A) and luciferase silencing in U87-Luc cells 24 hours post-transfection (B). L-PEI was used at N/P=15. The samples **5N**Scr and **9N**Scr indicate treatments with a scrambled siRNA sequence. Time-course and dose titrations were performed of **9N** /siRNA complexes to U87-Luc cells (C and D). Data represent mean ± standard deviation (*n*=3). Asterisks indicate treatments that elicited

statistically significant luciferase silencing compared to the untreated control, C (B) or treatments that elicited statistically different luciferase silencing compared to the other treatment groups in the experiment (C and D) ($p<0.05$).

CURRICULUM VITAE

CAROLYN LEIGH WAITE

Education

2006-2011: Ph.D. Chemical and Biochemical Engineering (Expected October 2011), Rutgers University, Piscataway, NJ
2006-2009: M.S. Chemical and Biochemical Engineering (May 2009), Rutgers University, Piscataway, NJ
2002-2006: B.S. Chemical Engineering (May 2006), Lafayette College, Easton, PA

Principal Positions

2006-2011: Graduate Research Assistant, Rutgers University, Piscataway, NJ
June- December 2010: Bioprocess Development Intern, Johnson&Johnson, Spring House, PA
June-August 2009: Visiting Researcher, Institute for Research in Biomedicine, Barcelona, Spain

Journal Publications

1. **Waite CL**, Sparks SM, Uhrich KE, and Roth CM. "Acetylation of PAMAM dendrimers for cellular delivery of siRNA." *BMC Biotechnology*, **2009**, 9:38.
2. **Waite CL** and Roth CM. "PAMAM-RGD conjugates enhance siRNA delivery through a multicellular spheroid model of malignant glioma" *Bioconjugate Chem.* **2009**, 20 (10), 1908-1916.
3. Sparks SM, **Waite CL**, Harmon AH, Nusblat LM, Roth CM, Uhrich KE "Efficient intracellular siRNA delivery by ethyleneimine-modified nanoscale amphiphilic macromolecules" *Macromolecular Bioscience*. **2011**, In Press.
4. **Waite CL** and Roth CM. "Binding and transport of PAMAM-RGD in a tumor spheroid model: The effect of RGD targeting ligand density" (*Manuscript submitted for publication: March, 2011*)
5. **Waite CL** and Roth CM. "Nanoscale drug delivery systems for enhanced drug penetration into solid tumors: Current progress and opportunities"(*Invited for submission to Critical Reviews in Biomedical Engineering in summer 2011*)